
Theses and Dissertations

Fall 2010

Use of direct-reading instruments for measuring airborne nanoparticles in the workplace

Donna Jean Holzer Vosburgh
University of Iowa

Copyright 2010 Donna Jean Holzer Vosburgh

This dissertation is available at Iowa Research Online: <http://ir.uiowa.edu/etd/901>

Recommended Citation

Vosburgh, Donna Jean Holzer. "Use of direct-reading instruments for measuring airborne nanoparticles in the workplace." PhD (Doctor of Philosophy) thesis, University of Iowa, 2010.
<http://ir.uiowa.edu/etd/901>.

Follow this and additional works at: <http://ir.uiowa.edu/etd>

 Part of the [Occupational Health and Industrial Hygiene Commons](#)

USE OF DIRECT-READING INSTRUMENTS FOR MEASURING AIRBORNE
NANOPARTICLES IN THE WORKPLACE

by

Donna Jean Holzer Vosburgh

An Abstract

Of a thesis submitted in partial fulfillment of the requirements
for the Doctor of Philosophy degree
in Occupational and Environmental Health (Industrial Hygiene)
in the Graduate College of
The University of Iowa

December 2010

Thesis Supervisor: Associate Professor Thomas M. Peters

ABSTRACT

This work strived to increase knowledge of assessing airborne nanoparticles in the workplace by characterizing nanoparticle concentrations in a workplace using direct-reading instruments, evaluating a DC2000CE diffusion charger, and the creation of a personal diffusion battery (pDB).

Direct-reading instruments were used with aerosol mapping and task monitoring to evaluate airborne nanoparticle concentrations in an apparel company that produces waterproof jackets composed of polytetrafluoroethylene membrane laminated fabric. Jacket production required that sewn seams be sealed with waterproof tape applied with hot air (600°C). Particle number concentrations were greater in the sewing and sealing areas than the office area while respirable mass was negligible throughout the facility. The breathing zone particle number concentrations of the workers who sealed the sewn seams were highly variable and significantly greater when sealing seams than when conducting other tasks ($p < 0.0001$). The effectiveness of the canopy hoods used to ventilate sealing operations was poor. These measurements support the idea that work places where hot processes are conducted may have substantially greater concentrations of airborne nanoparticles than background measurements even with control measures in place.

Laboratory tests were conducted to evaluate a commercially available diffusion charger, the DC2000CE, that measures nanoparticle surface area concentration. The surface area concentrations of unimodal and multimodal polydispersed aerosols measured by the DC2000CE were less than the surface area concentrations measured by the reference instruments. The differences in results were attributed to a difference of measuring active versus geometric surface area concentration and the design of the DC2000CE. The maximum measurable active surface area concentration ($2,500 \text{ mm}^2 \text{ m}^{-3}$) was found to be greater than the manufacturer stated maximum ($1000 \text{ mm}^2 \text{ m}^{-3}$). Moving or vibrating a DC2000CE while taking measurements can cause

the appearance of increased surface area concentration results. The DC2000CE has limitations that must be acknowledged when using the DC2000CE to measure airborne nanoparticle surface area concentrations in a workplace.

A four stage pDB (3.2 kg) composed of a screen-type diffusion battery, solenoid valve system, and an electronic controller was developed. The pDB was combined with a CPC and a data inversion was created that could be used to solve for the number median diameter, geometric standard deviation, and particle number concentration of a unimodal distribution. The pDB+CPC with inversion was evaluated using unimodal propylene torch exhaust and incense exhaust. For particle number concentration of particles with diameters less than 100 nm, the pDB+CPC with inversion results were between 86% to 109% of reference instrument results when the inversion did not solve to an inversion constraint and between 6% to 198% for results that solved to an inversion constraint. When coupled with a direct-reading instrument, the pDB with an inversion was able to measure the size distribution of particles with a NMD smaller than 286 nm.

Abstract Approved:

Thesis Supervisor

Title and Department

Date

USE OF DIRECT-READING INSTRUMENTS FOR MEASURING AIRBORNE
NANOPARTICLES IN THE WORKPLACE

by

Donna Jean Holzer Vosburgh

A thesis submitted in partial fulfillment of the requirements
for the Doctor of Philosophy degree
in Occupational and Environmental Health (Industrial Hygiene)
in the Graduate College of
The University of Iowa

December 2010

Thesis Supervisor: Associate Professor Thomas M. Peters

Graduate College
The University of Iowa
Iowa City, Iowa

CERTIFICATE OF APPROVAL

PH.D. THESIS

This is to certify that the Ph.D. thesis of

Donna Jean Holzer Vosburgh

has been approved by the Examining Committee
for the thesis requirement for the Doctor of Philosophy
degree in Occupational and Environmental Health (Industrial Hygiene) at the
December 2010 graduation.

Thesis Committee: _____
Thomas M. Peters, Thesis Supervisor

T. Renee Anthony

Patrick O'Shaughnessy

Jacob Oleson

Wayne Sanderson

To David, thank you for your unwavering faith

It's only the difference between looking and seeing.
Look long enough and if you're doing it right you get to see.

Nicholas Evans
The Horse Whisperer

ACKNOWLEDGMENTS

I would like to offer my sincere thanks my advisor, Tom Peters, for his guidance and advice. Without his patience, eagerness to share his knowledge, and interest in his students, I could not have accomplished this endeavor.

The people I have had the opportunity to work with over the course of this dissertation have been brilliant. I would like to thank Dr. Bon-Ki Ku from NIOSH, Dr. Maura Sheehan from West Chester University of Pennsylvania, and Timothy Klein from TAK Industries, LLC. Their willingness to collaborate despite the obstacle of distance was greatly appreciated. My dissertation committee was wonderful to work with and I would like to thank them for their time and expertise. Their advice allowed me to conduct meaningful research. I would like to thank Lauren Gant for volunteering her vibration expertise and assistance with conducting measurements. I am very grateful to Adele Bonney for her rather large role in helping me improve my writing.

I would like to thank the organizations that provided funding for this research: NIOSH Heartland Center for Occupational Health and Safety pilot grant (T420H008491), and a University of Iowa Executive Council of Graduate and Professional Students Research Grant, and a NIOSH KO1 Award (OH009255). I would also like to thank the Heartland Center for Occupational Safety and Health for their financial support and training.

Without the support of my lab mates (Will Cyrs, Lorenzo Cena, Eric Sawvel, Dane Boysen, Sabah Saleh, Barry Hill, Javier Santalla, and Michael Humann), graduate student support group (Dr. Kathleen Staley, and the other students), weekly dissertation group (Alysha Myers and Michael Humann), friends, and family, I would never have been able to complete this degree. I cannot thank you enough.

ABSTRACT

This work strived to increase knowledge of assessing airborne nanoparticles in the workplace by characterizing nanoparticle concentrations in a workplace using direct-reading instruments, evaluating a DC2000CE diffusion charger, and the creation of a personal diffusion battery (pDB).

Direct-reading instruments were used with aerosol mapping and task monitoring to evaluate airborne nanoparticle concentrations in an apparel company that produces waterproof jackets composed of polytetrafluoroethylene membrane laminated fabric. Jacket production required that sewn seams be sealed with waterproof tape applied with hot air (600°C). Particle number concentrations were greater in the sewing and sealing areas than the office area while respirable mass was negligible throughout the facility. The breathing zone particle number concentrations of the workers who sealed the sewn seams were highly variable and significantly greater when sealing seams than when conducting other tasks ($p < 0.0001$). The effectiveness of the canopy hoods used to ventilate sealing operations was poor. These measurements support the idea that work places where hot processes are conducted may have substantially greater concentrations of airborne nanoparticles than background measurements even with control measures in place.

Laboratory tests were conducted to evaluate a commercially available diffusion charger, the DC2000CE, that measures nanoparticle surface area concentration. The surface area concentrations of unimodal and multimodal polydispersed aerosols measured by the DC2000CE were less than the surface area concentrations measured by the reference instruments. The differences in results were attributed to a difference of measuring active versus geometric surface area concentration and the design of the DC2000CE. The maximum measurable active surface area concentration ($2,500 \text{ mm}^2 \text{ m}^{-3}$) was found to be greater than the manufacturer stated maximum

(1000 mm² m⁻³). Moving or vibrating a DC2000CE while taking measurements can cause the appearance of increased surface area concentration results. The DC2000CE has limitations that must be acknowledged when using the DC2000CE to measure airborne nanoparticle surface area concentrations in a workplace.

A four stage pDB (3.2 kg) composed of a screen-type diffusion battery, solenoid valve system, and an electronic controller was developed. The pDB was combined with a CPC and a data inversion was created that could be used to solve for the number median diameter, geometric standard deviation, and particle number concentration of a unimodal distribution. The pDB+CPC with inversion was evaluated using unimodal propylene torch exhaust and incense exhaust. For particle number concentration of particles with diameters less than 100 nm, the pDB+CPC with inversion results were between 86% to 109% of reference instrument results when the inversion did not solve to an inversion constraint and between 6% to 198% for results that solved to an inversion constraint. When coupled with a direct-reading instrument, the pDB with an inversion was able to measure the size distribution of particles with a NMD smaller than 290 nm.

TABLE OF CONTENTS

LIST OF TABLES	ix
LIST OF FIGURES	x
CHAPTER I INTRODUCTION.....	1
Nanoparticles	1
Toxicity of Nanoparticles	1
Deposition of Airborne Nanoparticles in Humans.....	2
Nanoparticle Exposure and Worker Health.....	2
Workplace Nanoparticle Regulation.....	3
Aerosol Measurement Metrics	3
Measuring Airborne Nanoparticles with Direct-Reading Instruments	4
Size Segregating Nanoparticles	5
Direct-Reading Instruments to Measure Airborne Nanoparticles	6
Unforeseen Results	8
Shortcomings of Literature	8
Specific Aims.....	9
CHAPTER II AIRBORNE NANOPARTICLE CONCENTRATIONS IN THE MANUFACTURING OF POLYTETRAFLUOROETHYLENE (PTFE) APPAREL.....	11
Abstract.....	11
Introduction.....	12
Methods	13
Aerosol Mapping	14
Breathing Zone Concentrations	15
Evaluation of Hood Used to Capture Particles at Sealing Stations	16
Statistical Analyses.....	17
Results.....	19
Aerosol Mapping	19
Breathing Zone Concentrations	19
Evaluation of Hood Used to Capture Particles at Sealing Stations	20
Discussion.....	20
Conclusions	25
Recommendations	25
CHAPTER III EVALUATION OF A DIFFUSION CHARGER FOR ITS EFFECTIVENESS IN MEASURING WORKPLACE AEROSOLS	36
Abstract.....	36
Introduction.....	37
Methods	39
DC2000CE	39
Comparison to Reference Instruments	40
Comparison of Two DC2000CE Responses	42
Assessment of Maximum Measurable Active Surface Area Concentration	42
Assessment of Physical Limitations.....	42

Statistical Analysis	43
Results.....	44
Comparison to Reference Instruments	44
Comparison of Two DC2000CE Responses	45
Assessment of Maximum Measurable Active Surface Area Concentration	45
Assessment of Physical Limitations.....	45
Discussion.....	46
Conclusions	50
 CHAPTER VI DESIGN AND EVALUATION OF A PERSONAL DIFFUSION BATTERY	61
Abstract.....	61
Introduction.....	61
Methods	64
Personal Diffusion Battery (pDB) Design.....	64
Theoretical pDB Stage Pressure Drop and Penetration.....	65
Measured pDB Stage Pressure Drop and Penetration	66
Detection Efficiency.....	67
Inversion Spreadsheet.....	69
pDB+CPC Inversion Spreadsheet Limitations.....	70
Polydispersed Aerosols	71
Results.....	72
pDB Stage Pressure Drop and Penetration.....	72
Detection Efficiency.....	73
pDB+CPC Inversion Spreadsheet Limitations.....	73
Polydispersed Aerosols	74
Discussion.....	75
Conclusions	79
 CHAPTER V CONCLUSIONS	94
Future Studies	95
 APPENDIX A: CALCULATION OF NANOPARTICLE NUMBER CONCENTRATION AND RESPIRABLE MASS USING A CONDENSATION PARTICLE COUNTER (CPC) AND OPTICAL PARTICLE COUNTER (OPC).....	97
 APPENDIX B: CREATING THE INVERSION SPREADSHEET.....	98
Steps to create the inversion spreadsheet.....	98
 APPENDIX C: INPUT INTO THE INVERSION SPREADSHEET	105
 REFERENCES	107

LIST OF TABLES

Table	
I.	Particle number and respirable mass concentrations found during aerosol mapping by area.....26
II.	Sealing worker breathing zone geometric mean (GM) number concentrations, geometric standard deviation (GSD), and number of 1-second measurements for each worker.....27
III.	Seam responsibility group geometric mean (GM) number concentrations, geometric standard deviation (GSD), number of workers in each seam responsibility group, and workers that comprise each group28
IV.	Percent time sealing seams versus conducting other tasks geometric mean (GM) number concentrations, geometric standard deviation (GSD), number of workers in each percent time sealing group, and workers that comprise each group.....29
V.	Breathing zone and in-duct particle number concentrations.30
VI.	Active surface area concentrations measured by the DC2000CE compared to geometric and active surface area concentration measured by reference instruments for polydispersed aerosols.....52
VII.	Comparison of the response of two DC2000CEs measuring incense.53
VIII.	Response of the DC2000CE with increasing diesel exhaust concentrations.....54
IX.	Theoretical pressure drops across only screens and observed pressure drops across each stage of pDB at 0.7 L min^{-1}81
X.	Original distributions and inversion distribution results to determine lower and upper NMD that could be distinguished with the pDB+CPC inversion.....82
XI.	Inversion distribution results for varying number of pDB+CPC stages to determine minimum number of stages required for the NMD particle size range of 17 nm to 290 nm.....83
XII.	Polydispersed aerosol distributions measured with the SMPS and pDB+CPC with inversion.84
XIII.	Comparison of pDB+CPC with inversion to SMPS with regard to particle number concentrations between 9.4 nm and 100 nm for polydispersed aerosol distributions measured with the SMPS and pDB+CPC with inversion.....85
C1.	Input number concentrations and inversion spreadsheet output.....106

LIST OF FIGURES

Figure

1.	Layout of the facility showing three major areas: office area; sewing area; and sealing area.	31
2.	Schematic diagram of sealing station, showing the local exhaust ventilation hood: (A) front view; and (B) side view.....	32
3.	Map of particle number concentrations in the sewing and sealing areas. Crosses indicate sample locations and shaded work stations indicated that they were in use during mapping.....	33
4.	Particle number concentrations measured in the breathing zone of a sealing worker during the transition from lunch break to the afternoon shift.....	34
5.	Particle number concentration by size measured at the final discharge of the local exhaust ventilation system.	35
6.	Set up for measuring polydispersed aerosols.....	55
7.	Particle number (A.) and surface area concentrations (B.) by size measured for unimodal polydispersed aerosols.	56
8.	Particle number (A.) and surface area concentrations (B.) by size measured for multimodal polydispersed aerosols.....	57
9.	Influence of concentration on DC2000CE response measuring diesel exhaust when concentrations were less and greater than the maximum active surface area concentration stated by the manufacturer.	58
10.	The influence of orientation and movement on DC2000CE measurements. The dotted line is the minimum active surface area concentration stated by the manufacturer of the DC2000CE ($10 \text{ mm}^2 \text{ m}^{-3}$).....	59
11.	The influence of placing a DC2000CE on a vibrating surface. The dotted line is the minimum active surface area concentration stated by the manufacturer of the DC2000CE ($10 \text{ mm}^2 \text{ m}^{-3}$).....	60
12.	Personal diffusion battery (pDB) (A.) Schematic of the pDB (B.) Airflow through each stage of pDB.....	86
13.	Experimental set ups to (A.) Determine particle penetration across the pDB at 0.7 L min^{-1} (B.) Test pDB+CPC with inversion using combustion aerosols (C.) Determine detection efficiency of CPC to SMPS.	87
14.	Representation of the inversion spreadsheet specifying the input, output, and required parts of the spreadsheet	88

15.	pDB observed and inversion penetrations for airflow of 0.7 L min^{-1}	89
16.	Iterated DE values with the fit regression line.....	90
17.	Ratios of CPC number concentration to the product of SMPS number concentration and DE_d when DE_d values equaled 1 and when they equaled the regression line	91
18.	Comparison of the mean propylene torch measured by the SMPS and the results of the three pDB+CPC with inversion runs for the 240-second measurements (A) and 80-second measurements (B).....	92
19.	Comparison of the mean incense measured by the SMPS and the results of the three pDB+CPC with inversion runs for the 240-second measurements (A) and 80-second measurements (B).	93
B1.	Screenshot of the top of the spreadsheet.....	102
B2.	Screenshot of the bottom of the spreadsheet	103
B3.	Screenshot of the “Solver” window.....	104

CHAPTER I

INTRODUCTION

Nanoparticles

Nanoparticles—particles with at least one dimension less than 100 nm (ASTM Standard E2456, 2006)—are present in many workplaces. Incidental nanoparticles are a result of workplace processes involving high heat (Elihn & Berg, 2009). Engineered nanoparticles are intentionally created for use in a variety of products such as epoxy (Bekyarova et al., 2007) and pharmaceuticals (Teli, Mutalik, & Rajanikant, 2010).

Toxicity of Nanoparticles

Toxicological studies have found nanoparticles of certain compositions to be more toxic than larger particles of the same composition (Johnston et al., 2000; Karlsson, Gustafsson, Cronholm, & Möller, 2009; Oberdorster, Celein, Ferin, & Weiss, 1995). Nanoparticle composition influences toxicity (Bastian et al., 2009; Fujita et al., 2009; Nygaard et al., 2009) and different cell types differently (Lai et al., 2008). The crystalline structure of some nanoparticles, such as TiO₂, influences toxicity (Braydich-Stolle et al., 2009).

Nanoparticles can cause damage in many ways. Inhalation of nanoparticles has been shown to trigger immune responses in rats (Samuelsen, Nygaard, & Lovik, 2009) causing lung inflammation (Alessandrini et al., 2009) and cell death (Fujita et al., 2009). Nanoparticles can be taken up by cells (Braydich-Stolle et al., 2009), enter systemic circulation (Li et al., 2008; Zhu et al., 2009), and cause damage in areas other than the respiratory system such as the brain (Wang et al., 2009; J. Wang et al., 2008) and kidneys (Y. S. Kim et al., 2008). Maternal exposure to anatase TiO₂ has caused cell death, changed in the expression of genes associated with brain development, and influenced the development and function of the central nervous system in mice pups (Shimizu et al., 2009).

Deposition of Airborne Nanoparticles in Humans

In humans, nanoparticles have high rates of respiratory deposition (Daigle et al., 2003) and deposit throughout the respiratory system (ICRP, 1994). As nanoparticle size decreases there is an increase in particle deposition for people of all ages regardless of breathing pattern (Daigle et al., 2003; C. S. Kim & Jaques, 2005). Slower breathing allows for increased nanoparticle deposition due to the dependence of nanoparticle deposition by diffusion (C. S. Kim & Jaques, 2005).

Nanoparticle Exposure and Worker Health

Chronic or acute exposures to nanoparticles have been found to cause negative health effects. For example chronic exposures to diesel exhaust, which contains nanoparticles (Figler, Sahle, Krantz, & Ulfvarson, 1996), has been associated with increased risks of lung cancer in men (Boffetta et al., 2001; Neumeyer-Gromen, Razum, Kersten, Seidler, & Zeeb, 2009). Fume generated from welding contains high number concentrations of nanoparticles (Jenkins, Pierce, & Eagar, 2005; Stephenson, Seshadri, & Veranth, 2003). Chronic exposure to welding fume has been associated with metal fume fever, increased incidence of bronchitis and pneumonia, and may be a risk factor for Parkinsonism syndrome (Korczyński, 2000; Racette et al., 2001). High, acute occupational exposure to incidental polytetrafluoroethylene nanoparticles led to cases of polymer fume fever (Harris, 1951; Lewis & Kerby, 1965) and in extreme exposure, pulmonary edema (Brubaker, 1977; E. A. Evans, 1973; Tsai, Guo, Chen, & Shieh, 2000), with one case resulting in death (Tsai et al., 2000).

The influence of engineered nanoparticles on worker health is not well known. A worker that inhaled an estimated gram of nickel nanoparticles over an approximate 90 minute period died from adult respiratory distress syndrome (Phillips, Green, Davies, & Murray, 2010). When compared to the OSHA permissible exposure limit for nickel of 1 mg m^{-3} over an eight hour period, the worker's exposure was large regardless of if the nickel was composed of nanoparticles. In 2007 and 2008 seven workers that worked in

the same room of a plant where they sprayed paste onto polystyrene boards were admitted to the hospital with clinical findings of pleural effusion and pericardial effusion. After the workers became ill, the paste was found to contain 30 nm polyacrylic ester particles. 30 nm polyacrylic ester particles were discovered in the chest fluid and lung biopsies of the workers. Two of the seven workers later died from respiratory failure (Song, Li, & Du, 2009).

Workplace Nanoparticle Regulation

There are no specific occupational exposure limits for nanoparticles in place to protect worker health. There are occupational exposure limits for nanoparticles composed of materials that are regulated under permissible exposure limits, such as nickel which has a limit of 1 mg m^{-3} . If the nanoparticles are not of a composition to be regulated by a permissible exposure limit, then they fall under Particles Not Otherwise Regulated (PNOR). The code of federal regulations 1910.1000 Table Z-1 specifies the PNOR limit as a time-weighted average of 5 mg m^{-3} respirable fraction over an eight hour period and it is determined gravimetrically (National Institute of Occupational Safety and Health, 2003).

Gravimetric analysis does not allow for adequate quantification of nanoparticle exposure. The mass of nanoparticles is small. To collect a sample that could be detected gravimetrically, the sample would most likely require a longer sampling time than an 8-hour work sample. If larger particles were also collected, the mass of the larger particles would mask any increase from the nanoparticles.

Aerosol Measurement Metrics

There are three metrics that are used to quantify aerosols are mass, number, and surface area. They can be expressed in terms of particle mass concentration, number concentration, and surface area concentration. Particle mass concentration—the mass of particulate matter in a unit volume of aerosol (Hinds, 1999)—is the metric that has been used most often in the past and is the most common metric used for regulation, such as

PNOR (National Institute of Occupational Safety and Health, 2003). Particle number concentration—the number of particles in a unit volume of aerosol (Hinds, 1999)—has been used to represent amounts of bioaerosols, fibers (Hinds, 1999), and nanoparticles (Pui, Qi, Stanley, Oberdörster, & Maynard, 2008). The metric of surface area has been used less often than the metrics of mass or number. But particle surface area concentration may be the most relevant physical measurement of nanoparticle exposure due to the high surface area to volume ratio (Maynard & Maynard, 2002; Moshhammer & Neuberger, 2003; Oberdoerster, Oberdoerster & Oberdoerster, 2005).

Measuring Airborne Nanoparticles with Direct-Reading Instruments

Direct-reading instruments are useful to measure airborne nanoparticle concentrations in the workplace. Direct-reading instruments that use particle electrical properties or condensation as a way to increase particle size are needed to measure airborne nanoparticles (Mohr, Lehmann, & Rutter, 2005). A direct-reading instrument that can measure airborne nanoparticles is needed since work shift averaged concentrations have been found to misrepresent airborne nanoparticle concentrations in the workplace (Ramachandran, Paulsen, Watts, & Kittelson, 2005). A direct-reading instrument with a short averaging time allows for identification of peaks in airborne nanoparticle concentrations (D. E. Evans, Ku, Birch, & Dunn, 2010; Imhof et al., 2005; Mohr et al., 2005; Ramachandran et al., 2005). Peak identification combined with activity monitoring (Peters et al., 2009) or facility mapping (Peters, Heitbrink, Evans, Slavin, & Maynard, 2006) allow for nanoparticle source identification.

To measure a worker's exposure to nanoparticles, a breathing zone measurement of airborne nanoparticle concentration is needed. Nanoparticles coagulate rapidly causing measurements farther from a source to be composed of less, larger particles than were at the source (Hinds, 1999). Depending on the worker's proximity to the source and the direct-reading instrument, the worker's exposure may be different from the airborne

nanoparticle concentration measured. A personal, direct-reading instrument would allow for measurements of worker nanoparticle exposure by taking airborne nanoparticle concentration measurements in a worker's breathing zone. To be personal, the direct-reading instrument would need to be small and able to withstand movements so that it could be worn by a worker while conducting all of their tasks. There is no commercially available, personal, direct-reading instrument that can measure airborne nanoparticles in a worker's breathing zone.

Size Segregating Nanoparticles

Size segregating an aerosol is useful because it allows for only certain particle sizes to be measured at a time. The segregated measurement can then be combined with other segregated measurements to create a distribution (Barron & Willeke, 2001) or the segregated measurement can be used independently, for example with regard to compliance with the respirable fraction of PNOR (National Institute of Occupational Safety and Health, 2003). Due to their lack of mass, traditional means of separating particles by size are not effective for separating airborne nanoparticles from the rest of an aerosol. Cyclones and impactors are traditional devices to separate particles by size. They use inertia to remove large particles from the aerosol so what remains is the particle size of interest (Barron & Willeke, 2001; Hinds, 1999). Nanoparticles require devices that rely on a property other than inertia to separate particles by size. A diffusion battery is a device that uses diffusion to separate submicron particles, including nanoparticles. There are multiply types of diffusion batteries—collimated hole, parallel plate, and screen type—and they all function the same in that the small particles in an aerosol diffuse to the sides or fibers of the diffusion battery and are removed from the aerosol.

Direct-Reading Instruments to Measure Airborne Nanoparticles

There are currently four categories of direct reading instruments that have been used in various combinations with each other to characterize the presence of airborne

nanoparticles in workplaces; condensation particle counter (CPC), scanning mobility particle sizer (SMPS), diffusion charger (DC), and electrical low pressure impactor (ELPI). A CPC is used to measure number concentration of particles between approximately 10 nm to 1000 nm. To count the particles the CPC increases the size of submicron particles by vapor supersaturation so the enlarged particles can then be detected by a laser. An alcohol or water soaked wick is needed to create the supersaturation environment. Depending on the model, particle counts can be logged every second. The size of CPC varies depending on the model. Many models are handheld, but due to the liquid needed to create the supersaturation environment, the CPC cannot be tipped. If tipped, the liquid will drip off the wick and flood the area in front of the laser interrupting measurements. The CPC does not provide information with regard to the size of the aerosol being measured so there is no way to distinguish the nanoparticles in their results (Baron & Willeke, 2001).

A SMPS measures the number concentration, by size, of particles between approximately 10 to 800 nm. A SMPS is composed of a differential mobility analyzer and a CPC. As the submicron aerosol enters the differential mobility analyzer, the particle obtains a bipolar charge and is then sent through a column that contains a charged electrode. The charge on the electrode causes particles of only certain electrical mobilities to pass through the column and into the CPC where it is counted. The charge of the electrode is cycled through a range of charges during the SMPS measurement to obtain the number concentrations for all the particle sizes covered by the instrument (Baron & Willeke, 2001). Depending on the model, a SMPS requires at least two minutes to conduct a measurement which may be too slow to use to identify nanoparticle sources. The size of a SMPS is large enough to require that it be placed on a cart to be moved.

A DC is used to measure the surface area concentration of particles less than 1000 nm. Diffusion charging occurs when particles come in contact with unipolar ions and the charge is transferred to the particle. Diffusion causes the particles to come in contact with

the ions. The particles are collected on an electrometer to measure the amount of charge on the particles (Hinds, 1999). The amount of charge a particle can hold is dependent on the particle's active surface area, defined as the portion of the particle that interacts with the surrounding gas, as opposed to the physical surface area of the particle (Keller, Fierz, Siegmann, Siegmann, & Filippov, 2001). In the DC, an ion trap collects the ions that did not come in contact with a particle. Some DCs have the ion trap voltage set such that only particles representative of sizes that deposit in the lung are measured by the electrometer (Fissan, Neumann, Trampe, Pui, & Shin, 2007). Depending on the model, measurements can be logged every ten seconds. DCs vary in size with some small enough to be carried by a worker. A DC does not provide information with regard to the size of the particles being measured so there is no way to distinguish the nanoparticles in their results. DCs have potential limitations that need to be evaluated with respect to measuring workplace aerosols (Asbach, Fissan, Stahlmecke, Kuhlbusch, & Pui, 2009).

An ELPI uses diffusion charging and impaction to measure particle number concentration by size for particles between 30 nm to 10,000 nm. Aerosols enter the ELPI where diffusion charging occurs and an ion trap is used to remove excess ions. Then the charged particles enter a low pressure cascade impactor where the charged particles collect on the respective stages based on their aerodynamic diameter. Each stage has an electrometer that measures the amount of charged particles that collect on the stage (Baron & Willeke, 2001). Depending on the model, measurements can be logged every five seconds. The size of an ELPI is large enough to require that it be placed on a cart to be moved.

Out of necessity, the instruments characterized the presence of airborne nanoparticles by either measuring areas other than worker breathing zones or breathing zone measurements that interfered with worker tasks (Elihn & Berg, 2009; D. E. Evans, Heitbrink, Slavin, & Peters, 2007; D. E. Evans et al., 2010; Fujitani, Kobayashi,

Arashidani, Kunugita, & Suemura, 2008; Methner, Hodson, & Geraci, 2010; Peters et al., 2006; Ramachandran et al., 2005).

Unforeseen Results

Studies of airborne nanoparticles in workplaces have found unforeseen results. Studies have shown that exposure to incidental nanoparticles can be due to sources other than plant processes, such as heating units (Peters et al., 2006). Studies have also shown that workers processing engineered nanoparticles are not necessarily exposed to the engineered nanoparticles. The handling of bulk amounts of material in processes have been found to cause exposure to larger agglomerates of the nanoparticles, instead of the nanoparticles themselves (D. E. Evans et al., 2010; Peters et al., 2009).

Exposures to engineered nanoparticles may also occur in areas other than where engineered nanoparticles are produced or handled. Engineered nanoparticles can be transferred from the production or laboratory areas to other areas on worker's clothing or shoes (Methner, Birch, Evans, Ku, Crouch, & Hoover, 2007). Nanoparticles can be aerosolized anywhere in a facility by using vacuums that have previously been used to clean nanoparticle production or laboratory areas. When the vacuums collected the nanoparticles, the nanoparticles were not trapped. Then when the vacuums were turned on again, the nanoparticles were aerosolized in the exhaust (Maynard, Baron, Foley, Shvedova, Kisin, & Castronova, 2004).

Shortcomings of Literature

There are key issues that need to be researched with regard to nanoparticle exposures in the workplace. First, the work environments in which exposure assessments have been conducted needs to be expanded. Most nanoparticle exposure assessments have been conducted in facilities that use engineered nanoparticles or heavy industrial settings that conduct hot processes that have been known to produce incidental nanoparticles, such as welding. Many manufacturing operations use hot processes, not just the traditional heavy industrial settings. Identifying and characterizing exposure to

nanoparticles created by hot processes in industries that have not been previously considered, such as the apparel industry, is necessary to identify dangerous work environments.

Second, more studies are needed to evaluate commercially available instruments used in nanoparticle exposure assessments, specifically DCs. The direct-reading instruments that are currently available all have limitations with regard to the data they provide, but the limitations of DCs are not well known. Evaluating the DCs to identify and understand their limitations is essential in understanding the results they provide.

Third, work is needed to develop a direct-reading instrument that can be used to measure personal exposures specifically for nanoparticles. Use of multiple instruments in the workplace to measure airborne nanoparticle concentrations is prohibitive for use within an industrial hygiene framework. Direct-reading instruments are expensive and most companies cannot afford to own multiple instruments. Even with multiple instruments, it is not possible to measure personal exposures unless the worker is stationary while they conduct their tasks. A personal, direct-reading instrument is needed to expand the worker exposures that can be measured.

Specific Aims

This dissertation strives to reduce some of the shortcomings in the literature by increasing knowledge with regard to nanoparticle exposure in the workplace. The long term goal of this dissertation is to determine a way to accurately measure personal nanoparticle exposure in a wide variety of work environments without biasing the results by interfering with the workers' tasks. Once that has been accomplished, actual exposure risks can be determined and control measures could be appropriately applied.

This research works towards achieving that goal by having accomplished the following aims:

1. Available direct-reading instruments were used to characterize incidental nanoparticle exposures during the sealing of sewn seams on breathable,

waterproof garments. The airborne nanoparticle concentrations at the facility were characterized using existing equipment to determine worker breathing zone concentrations to incidental nanoparticles.

2. A DC was evaluated for use to assess workplace nanoparticle exposure. Limitations of the DC that prevent it from being used to quantify personal nanoparticle exposures were identified.
3. A personal screen-type diffusion battery was designed and evaluated as a way to assess personal exposures to nanoparticles. A personal screen-type diffusion battery was designed so that, with a detector, it could be used to determine the geometric mean, geometric standard deviation, and number concentration of a unimodal aerosol distribution. The laboratory evaluation compared the results measured by the personal diffusion battery and detector to a SMPS.

CHAPTER II
AIRBORNE NANOPARTICLE CONCENTRATIONS IN THE
MANUFACTURING OF POLYTETRAFLUOROETHYLENE (PTFE)
APPAREL

Abstract

One form of waterproof, breathable apparel is manufactured from polytetrafluoroethylene (PTFE) membrane laminated fabric, using a specific process to seal seams that have been sewn with traditional techniques. The sealing process involves applying waterproof tape to the seam by feeding the seam through two rollers while applying hot air (600°C). This study addressed the potential for exposure to particulate matter from this sealing process, by characterizing airborne particles in a facility that produces over 1,000 lightweight PTFE rain jackets per day. Aerosol concentrations throughout the facility were mapped, breathing zone concentrations were measured, and hoods used to ventilate the seam sealing operation were evaluated. The geometric mean (GM) particle number concentrations were substantially greater in the sewing and sealing areas (67,000 and 188,000 particles cm⁻³) compared to that measured in the office area (12,100 particles cm⁻³). Respirable mass concentrations were negligible throughout the facility (GM=0.002 mg m⁻³ in the sewing and sealing areas). The particles exiting the final discharge of the facility's ventilation system were dominated by nanoparticles (number median diameter = 25 nm; geometric standard deviation of 1.39). The breathing zone particle number concentrations of the workers who sealed the sewn seams were highly variable and significantly greater when sealing seams than when conducting other tasks ($p < 0.0001$). The sealing workers' breathing zone concentrations ranged from 147,000 particles cm⁻³ to 798,000 particles cm⁻³, and their seam responsibility significantly influenced their breathing zone concentrations ($p = 0.03$). The finding that particle number concentrations were approximately equal outside the hood and inside the

local exhaust duct indicated poor effectiveness of the canopy hoods used to ventilate sealing operations.

Introduction

Waterproof, breathable apparel, which is impermeable to liquids but allows vapor such as perspiration to pass through (Holmes, 2000), is commonly produced from polytetrafluoroethylene (PTFE) membrane laminated material (Mukhopadhyay & Midha, 2008). This type of apparel is used by a variety of professions, such as gowns for surgeons and nurses, foul weather survival clothing for military personnel, or protective gear for firefighters (Mukhopadhyay & Midha, 2008).

Depending on the fabric used to make apparel, workers may have a wide variety of exposures (e.g., cotton dust (LeVan et al., 2006), latex (Weytjens, Labrecque, Malo, & Cartier, 1999), formaldehyde (Pinkerton, Hein, & Stayner, 2004)). The PTFE fabric and processes used to produce waterproof, breathable apparel may cause specific and unique particulate hazards. In the manufacturing process, pieces of fabric are joined using traditional sewing techniques. Then sealing tape, also containing PTFE, is applied to ensure that the sewn seam is waterproof (Jeong & An, 2004). During the traditional sewing of the PTFE fabric there is a low potential for airborne particle production. However, during the sealing of the sewn seams, there is a possibility of exposure to incidental nanoparticles. The sealing process involves feeding the apparel through two rollers that compress the sealing tape onto the seam while hot air (600 °C) is blown onto the sealing tape. Places where two seams overlap are reheated by placing the overlapping section between two heated plates to ensure they do not leak. The high temperature of the process may cause some of the tape or material to evaporate which could lead to incidental nanoparticles as it cools.

Toxicological studies in rodents have found exposure to nanoparticles of PTFE to be toxic (Oberdorster et al., 1995) and that PTFE nanoparticles had greater pulmonary toxicity than larger particles of PTFE (Johnston et al., 2000). In humans, very high

exposure to PTFE nanoparticles has led to cases of polymer fume fever (Harris, 1951; Lewis & Kerby, 1965) and in extreme exposure, pulmonary edema, with one case resulting in death (Tsai et al., 2000).

The purpose of this work was to characterize airborne particle concentrations in a facility that makes two styles of light-weight, waterproof, breathable rain jackets made of PTFE fabric, at a production rate of 1,000 jackets per day. Aerosol concentrations throughout the facility were mapped, breathing zone concentrations were measured, and the hoods used to ventilate the sealing operation were evaluated. In addition worker characteristics that may have had a potential association with breathing zone concentrations were identified.

Methods

The facility was divided into three main areas (Figure 1): office area, sewing area, and sealing area. The office area housed management, administration, and engineering staff and was physically partitioned from the other areas. Jobs performed in the sewing and sealing areas to create a rain jacket included: 1) traditional sewing of cut pieces of fabric (sewing area); 2) sealing of sewn seams (sealing area); 3) quality control (sealing area) 4) reheating overlapping seams (sealing area); and 5) bundling jackets for shipping (sewing area.) In the sealing area there were 41 sealing stations (work stations to seal seams) and 20 overlap stations (work stations where overlapping sealed seams are reheated).

As depicted in Figure 2, each sealing station was fitted with a local exhaust ventilation hood intended to remove contaminants that were generated by the sealing process. The hood consisted of a transparent canopy (the hood manufacturer requested to remain anonymous) with a design airflow of $11.3 \text{ m}^3 \text{ min}^{-1}$ ($400 \text{ ft}^3 \text{ min}^{-1}$). The hood had sloping front and back sides and a flat top (Figure 2B). The hood was positioned approximately 20 cm over the work table and was held by a support on the right side. The sealing workers viewed their work through a window on the front of the hood. The hood

was connected to a ventilation duct (diameter = 15.2 cm; 6 in.) on the right front corner. The duct opening was positioned away from the sealing tape rollers to avoid cooling of the hot air required to produce a high-quality seal. The hood contained gaps where the sealing tape holder extended up through the hood top. The hood (68 cm by 53 cm) covered only a portion of the entire work table (100 cm by 66 cm).

Aerosol Mapping

On a morning when 15 workers were actively sealing seams, particle number and respirable mass concentrations were mapped at multiple locations in the sewing and sealing areas and at one location in the office area. As described by Peters, Heitbrink, Evans, Slavin, and Maynard (2006), two real-time aerosol instruments were placed on a mobile sampling cart—condensation particle counter (CPC) (Model 3007, TSI Incorporated, Shoreview, MN) and an optical particle counter (OPC) (PDM-1108, Grimm, Ainring, Germany)—and measurements were taken at 34 locations throughout the sewing and sealing areas. At each location over a period of one minute, the CPC was used to measure the number concentration of particles between 10 nm to 1 μm in diameter, and the OPC was used to measure the number concentrations of particles between 0.3 μm to 20 μm in diameter in 15 size channels. These data were then used to estimate nanoparticle number and respirable mass concentrations (Peters et al., 2006). The calculations are shown in appendix A.

Initial number concentrations measured with the CPC were found to exceed the maximum concentration range for the instrument. Therefore to dilute the particle concentration, a filter (6702-7500 Whatman Inc. Kent, United Kingdom) with a 0.16 cm (1/16 in.) hole drilled into its end cap was connected to the inlet of the CPC as described by Peters et al. (2006). In the office area, one-minute mean particle number concentrations were measured using the CPC with (W) the filter present and without (WO) the filter present in the following configuration: WO-W-WO-W-WO-W. The dilution factor was then estimated by dividing the mean number concentration measured

without the filter by that measured with the filter. Mapping software (Surfer, Golden Software, Golden, CO) was used to perform Kriging—a geostatistical method that produce regularly spaced data from irregularly spaced data—of the particle number concentrations measured at the 34 locations. The regularly-spaced data was then used to construct a map of the facility with contours of equal particle number concentration. Respirable mass concentrations were summarized in tabular format.

Breathing Zone Concentrations

Number concentrations were measured in the breathing zone of nine sealing workers. A 0.64 cm inner diameter electrically conductive tube was used to transport air from outside of the exhaust hood, directly above the window, to a CPC (Model 3007, TSI Incorporated, Shoreview, MN) that was set up to log concentrations once per second. The inlet of the transport tube was positioned in the breathing zone of the sealing workers when they were sealing seams (DiNardi, 2003). Although a representation of personal exposure, this measurement is not a true personal sample because the inlet of the transport tube was affixed to the window of the canopy hood on the workstation instead of on the sealing worker. Aerosol entering the CPC was diluted as described above for the aerosol mapping.

Measurement duration for each worker varied from 9 to 26 minutes to cover all of the tasks that composed the job of sealing seams. Measurements of all workers were taken on the same day. Sealing seams involved four tasks. First, the sealing worker collected a bundle of jackets from a storage shelf in the sewing area and brought it back to their sealing station. The sealing worker then filled out paperwork associated with the bundle. Next, the worker sealed a number of seams on each jacket. Each jacket required the sealing of over 20 seams, but each worker was assigned only a specific set up seams to seal on the jacket. Multiple workers had similar seam responsibilities. When finished, the jackets were re-bundled and placed on a different shelf in the sewing area for the next

sealing worker to collect. One jacket from every third bundle was taken to a quality control station by the sealing worker.

Sealing worker tasks and characteristics were video recorded to allow identification and coding of tasks and characteristics that may have influenced breathing zone concentrations. The task information from the video included the specific time when a worker was sealing seams and when they conducted other tasks (e.g., paperwork). Percent time sealing seams versus conducting other tasks was calculated and each worker was placed in one of three groups: greater than 70% time, 61 to 69% time and less than 60% time. The characteristic information from the video included the worker's seam responsibility, jacket style, and worker movement while feeding material into the rollers. Worker movement (determined by personal preference) was categorized as either a smooth, fluid motion or a choppy motion, quickly and repeatedly moving the material slightly up and down.

The video was also used to place sealing workers into one of four seam responsibility groups, based on seam length, position, and number of seams. The groups were: "long" - two long seams (the length of the jacket) with or without two additional short seams (less than one fourth the length of the jacket); "middle" - 10 or more long (at least one half the length of the jacket) and short (less than one fourth the length of the jacket) seams located in the middle of the jacket; "short" - four or fewer short seams (less than one fourth the length of the jacket); and "mixture" - five long (length of the jacket) and short (less than one fourth the length of the jacket) seams throughout the jacket.

Evaluation of Hood Used to Capture Particles at Sealing

Stations

The effectiveness of the hood used to capture particles was evaluated at three sealing stations. The hoods were required to be on during the entire shift so following was done to evaluate the effectiveness of the hoods. At each station, the airflow was

measured 80 cm downstream of the hood-duct connection by Pitot tube traverse using a Series 400 Air Velocity Meter (Dwyer Instruments, Inc., Michigan City, IN).

Particle number concentrations were measured simultaneously in the breathing zone of the sealing worker and inside the exhaust duct immediately downstream of the hoods. Breathing zone concentrations were measured with one CPC as described above, and a second CPC was used to measure in-duct concentrations. A 0.64 cm conductive tube, with the opening placed in the center of the duct, was used to transport aerosol to the second CPC. The aerosols entering both instruments were diluted as described above. Both CPCs were set up to record concentrations once per second and the measurement duration for each station varied from 28 to 38 minutes. Hood concentration reduction factor was estimated as the GM number concentration measured in the duct divided by the sum of that measured in the duct and in the breathing zone times 100%.

The number concentration by size of the airborne particles was measured at the final discharge of the facility's local exhaust ventilation system. An electrically conductive tube with a 0.64 cm inner diameter was used to transport the aerosol to a 20 L holding chamber from the final discharge duct. A scanning mobility particle sizer (SMPS) (SMPS+C model 5.4, Grimm, Ainring, Germany) was used to measure the particle size distribution of aerosol in the holding chamber. The holding chamber dampened fluctuations in aerosol concentration that would otherwise have rendered the size distribution measured with the SMPS invalid.

Statistical Analyses

The number concentrations measured in the workers' breathing zones and in the local exhaust ducts were log-transformed. Repeated measurements obtained on the same individual typically exhibit a positive correlation that must be accounted for. Linear mixed-effects model account for the correlation of the repeated measures on a person by fitting a correlation structure with few parameters while distinguishing between-subject and within-subject sources of variation (Fitzmaurice, Laird, & Ware, 2004). To address

correlation associated with repeated measures, a linear mixed-effects model was used to analyze the repeated 1-second measurements taken on each sealing worker. A linear mixed-effects model was fit to determine if there was a statistically significant difference in the breathing zone concentrations when the sealing workers sealed seams compared to when they conducted other tasks (e.g. paperwork) and to determine if the sealing workers' breathing zone concentrations were equal across workers to test if the sealing workers were a homogenous exposure group. Many variance/covariance structures were tested to specify the within-subject correlation in the model and compound symmetry was chosen because had the lowest Akaike information criterion (AIC) value. A post-hoc Tukey-Kramer multiple comparison test identified which workers' breathing zone concentrations were statistically different. The geometric mean (GM) and geometric standard deviation (GSD) of the particle number concentrations for each worker was determined.

The GM particle number concentration for each worker was calculated from their repeated 1-second measurements. These GM values were used to represent the sealing workers breathing zone concentrations when determining which worker characteristics of seam responsibility, movement, and jacket style significantly influenced breathing zone concentrations. One-way Analysis of Variance (ANOVA) was used to test whether breathing zone concentrations were equal across the four seam responsibility groups with a post hoc Duncan's multiple comparisons test to identify which groups had different concentrations. Independent sample t-tests were used to determine if worker movement or jacket style were associated with breathing zone concentrations. A one-way ANOVA was used to determine if GM breathing zone number concentration was equal across the three groups of percent time sealing seams versus conducting other tasks. Statistical significance for all tests was evaluated at the 95% confidence level. Analyses were carried out using the statistical software SAS version 9.2.

Results

Aerosol Mapping

Particle number concentrations were greater in the sealing area than in the sewing area (Figure 3; Table I). The GM of the particle number concentrations in the sewing area (67,000 particles cm^{-3}) was over three times greater than that in the office area (12,100 particles cm^{-3}). The GM of the particle number concentrations in the sealing area (188,000 particles cm^{-3}) was more than a magnitude greater than the office area. Respirable mass concentrations in the sewing and sealing areas ranged from 0.001-0.007 mg m^{-3} with the GM concentration (0.002 mg m^{-3}) in the sealing area slightly greater than that in the sewing area (0.001 mg m^{-3}).

Breathing Zone Concentrations

The GM of 1-second particle number concentrations measured in the breathing zone of the sealing workers ranged from 147,000 particles cm^{-3} to 798,000 particles cm^{-3} (Table II). The concentrations were highly variable with GSDs ranging from 1.16 to 2.27. The GM concentrations were not equal across workers ($p < 0.0001$). Thus, the sealing workers were not a homogeneous exposure group with respect to breathing zone number concentration. Five breathing zone concentration worker groups were found to be statistically significantly different. Breathing zone number concentrations were significantly different ($p < 0.0001$) when the workers were sealing seams (GM = 394,000 particles cm^{-3} , GSD = 2.18) compared to when they were conducting other tasks (GM = 266,000 particles cm^{-3} , GSD = 1.77).

The results from the analysis of tasks and characteristics using each worker's calculated GM particle number concentrations are summarized in Table III and Table IV. The GM number concentrations of the four seam responsibility groups ranged from 192,000 particles cm^{-3} ("short" group) to 688,000 particles cm^{-3} ("middle" group) and the GM concentrations were not equal across seam responsibility groups ($p = 0.03$; Table III). The GM concentration of the "middle" group was significantly greater than that of

the “short” and “mixture” groups. The GM concentration of the “long” group was not statistically different from that of any other group. The GM concentrations of the three percentage time sealing seams versus conducting other task groups were also not statistically different ($p = 0.22$; Table IV). The GM concentrations were not statistically significantly different for workers using different movements ($p = 0.82$) or sealing seams on different jacket styles ($p = 0.36$).

Figure 4 shows breathing zone particle number concentrations as a worker transitioned from lunch break to the beginning of the afternoon shift. Breathing zone concentrations were relatively low and constant during the end of the lunch break (GM = 117,000 particles cm^{-3} , GSD = 1.21) but increased dramatically and became more variable when the afternoon shift began (GM = 240,000 particles cm^{-3} , GSD = 1.79). Breathing zone concentrations during lunch break did not reach levels of the office area due to other sealing workers working through the lunch break.

Evaluation of Hood Used to Capture Particles at Sealing Stations

Particle number concentrations measured in the breathing zone and inside the exhaust ducts of the local exhaust ventilation system are shown in Table V. Although some of the particles were captured the concentration reduction factor of the hood was 56% or less. Airflow through the local exhaust ventilation system ranged from 11.5-12.3 $\text{m}^3 \text{min}^{-1}$ (405-436 $\text{ft}^3 \text{min}^{-1}$) and met vendor specifications for airflow.

The particle number concentration by size of the aerosol captured by the local exhaust ventilation measured at the final discharge of the system (Figure 5) was composed almost entirely of nanoparticles. The size distribution had a number median diameter of 25 nm with GSD of 1.39.

Discussion

Nanoparticle number concentrations were elevated in a facility that produces apparel composed of PTFE fabric. The airborne particles were dominated by

nanoparticles (NMD = 25 nm, GSD = 1.39) with the greatest concentrations observed in the breathing zone of sealing workers (GM ranged from 147,000 to 798,000 particles cm^{-3}). Number concentrations in both sealing and sewing areas were very high compared to those found in the office area. There are no regulatory standards for particle number concentration. However, number concentrations found at this facility were similar to or greater than those observed in heavy industrial settings, such as an automotive foundry (D. E. Evans et al., 2007) and plants where smelting and grinding occurred (Elihn & Berg, 2009). Actual breathing zone concentrations may in fact be greater than measured because, even with the filter to dilute the particle number concentrations, the CPC readings were at times above the upper limit of the CPC (100,000 particles cm^{-3}). At concentrations above the upper limit coincidence may cause the CPC to underestimate the particle concentration (Hämeri, Koponen, Aalto, & Kulmala, 2002).

In contrast, particle mass concentrations were low throughout the facility (GM < 0.020 mg m^{-3}). These values are substantially lower than the OSHA permissible exposure limit for particles not otherwise regulated with time-weighted average exposure limit of 15 mg m^{-3} for respirable mass concentration. This finding is expected given that the aerosol was composed almost entirely of nanoparticles that contribute little to mass concentration despite their high number concentrations.

The source of the nanoparticles is attributed to the hot process of sealing seams. Breathing zone number concentrations were significantly greater when the sealing workers were sealing seams compared to when they were conducting other tasks. They also increased dramatically at the start of a work shift (Figure 4). The single mode observed in the particle size distribution (Figure 5) is typical of a single aerosol source, and the aerosol mapping provided further evidence that the source was located within the sewing and sealing areas. Lastly, the fact that breathing zone number concentrations were substantially greater than those observed during aerosol mapping was consistent with the heated sealing process being the dominant aerosol source.

The canopy hoods of the local exhaust ventilation system do not adequately capture the nanoparticles generated by the sealing process. Breathing zone concentrations were very high for all sealing workers. The concentration reduction factor was poor and ranged from 36% to 56%.

Certain characteristics of canopy hoods combined with their application for sealing may explain the poor capture efficiencies. First, canopy hoods function best when they are used to control hot contaminants which have thermal buoyancy to aid in their collection (McDermott, 2001). Although sealing involves high heat, nanoparticles may have been created and then trapped underneath the jacket during sealing. Those particles would then tend to mix with cool air and would no longer be carried by thermal buoyancy up into the hood. Second, canopy hoods are known to produce a limited capture zone even with a high exhaust airflow rate (McDermott, 2001). When removing the jacket from underneath the hood, the worker may have released the nanoparticles that were trapped under the jacket outside the canopy hood's capture zone. Lastly, capture efficiency of a canopy hood is diminished by objects located below the hood (Goodfellow & Bender, 1980) and sealing required the workers' arms and the jacket to be below the hood. The importance of the combination of canopy hood characteristics is illustrated by the association among seam responsibilities and breathing zone concentrations. The breathing zone concentrations for the "short" or "mixture" groups were lower than those in the "middle" group (Table III). Workers in "short" or "mixture" groups had at least one seam that ended at a jacket edge, so they lifted the jacket when it was still underneath the hood before starting another seam. With this lifting action, nanoparticles would have a fair likelihood of capture. In contrast the "middle" group was responsible for a combination of more than ten long and short seams located in the middle of the jacket. The location of those seams required the worker to slide and drape the jacket over the work table as they moved from seam to seam. Sliding the jacket may have drawn the nanoparticles outside the canopy hood's capture zone.

A redesigned hood may improve nanoparticle capture and reduce the number concentrations in the breathing zone. However, a new design must balance the need to provide sufficient workspace to access all seams of a jacket, maintain the temperature at the seam to create a high quality seal, and adequately capture the nanoparticles. Although providing adequate workspace and proper sealing temperature, the current design does not have appropriate concentration reduction factor. A hood with a partial enclosure may address these competing issues more effectively than a canopy hood, but may also reduce the workspace to an unacceptable size. Further work under controlled laboratory conditions is needed to evaluate the effectiveness of different hood designs.

There are several issues that may limit the applicability of our findings. The measurements for this study were taken at one facility and may not be representative of other facilities that seal sewn seams. Aerosol mapping was conducted during one morning only and consequently may not be representative of different days or times of day. The particle size distribution measured in the exhaust air was assumed to represent the particulate inside the facility. This assumption enabled measurement despite constraints of sampling with the SMPS (requires stable aerosol concentrations over ~6 min sampling time) near aerosol sources with highly fluctuating generation rates (i.e., sealing sewn seams). It is possible that larger particles within the facility were not captured or conveyed through the ductwork, thereby biasing the measured distribution to smaller sizes. However, the results of aerosol mapping (Table I; high number concentrations and low mass concentrations) are consistent with the fact that the aerosol burden within the facility is dominated by nanoparticles and with the particle size distribution measured in the exhaust air.

Breathing zone concentrations were not measured when workers were away from their work station conducting tasks other than sealing because the tube was affixed to the canopy hood. However, these tasks (picking up and dropping off bundles of jackets) took the worker away from the measurement location for a short time (<10%) compared to the

tasks that were conducted at the work station (filling out paperwork and sealing sewn seams). Particle mapping results suggest that these tasks were conducted in areas of the facility where particle concentrations were likely to be substantially lower than at the workstation. Thus, particle number concentrations for these tasks were likely overestimated. Despite this fact, breathing zone concentrations during sealing sewn seams were found to be significantly and substantially greater than those observed during other tasks. Sampling was conducted in this way because of the limitation that there were no direct-read instruments to measure personal exposure to nanoparticles at the time of this work.

Some seemingly conflicting results arose from our inability to apply linear mixed-effects models throughout the statistical analysis. The use of a mixed model enabled us to determine that the nine workers studied were not part of a single homogenous exposure group, although the differences among the GM of workers were sometimes small (see Table II; Group A is different from Group B). The ability of the mixed model to take advantage of the numerous 1-second measurements on each worker ($n > 485$) allowed these differences to be detected. The limited number of subjects prevented our use of mixed-effects models to investigate the influence of characteristics on breathing zone concentrations. Instead, we used ANOVA and t-tests to determine whether characteristics were associated with breathing zone concentrations. These analyses require that measurements are independent. The GM of 1-second measurements for each worker ($n=9$) were used to avoid the issue that 1-second measurements were highly correlated temporally. The low number of samples limited our ability to detect differences between groups. Consequently, the characteristics of time sealing seams, movement of sealing worker, and style of jacket sealed were not found to be statistically significant, although there were sometimes substantial differences in the group GMs (see Table IV) compared to those observed in Table II. The characteristics may be significant when tested with a larger sample size.

Conclusions

Nanoparticle number concentrations were identified to be very high in a facility that produces apparel composed of PTFE fabric. The greatest concentrations were found in the breathing zone of workers responsible for sealing sewn seams. These nanoparticles were identified to be incidental to the hot process of sealing seams. Canopy hoods used to ventilate the sealing workstations were found to have poor concentration reduction factor. Several limitations of canopy hoods when applied to this particular application may explain this poor concentration reduction factor.

Recommendations

Determination of the composition of the particles in the facility was outside the scope of this work. However, it is an important subject of future work.

A redesigned hood is likely to improve nanoparticle capture and reduce the number concentrations in the breathing zone. A hood with a partial enclosure may reconcile the need to provide sufficient workspace, obtain high concentration reduction factor, and to maintain adequate temperature of sealing. Further work under controlled laboratory conditions are needed to develop different hood designs and evaluate their effectiveness.

Table I: Particle number and respirable mass concentrations found during aerosol mapping by area.

Particle Number Concentrations				
Area	n	GM (particles cm⁻³)	Range (particles cm⁻³)	GSD
Office	1	12,100	11,600-12,500	1.02
Sewing	11	67,000	39,000-136,000	1.63
Sealing	23	188,000	78,000-445,000	1.59
Respirable Mass Concentrations				
Area	n	GM (mg m⁻³)	Range (mg m⁻³)	GSD
Sewing	11	0.001	0.001-0.002	1.36
Sealing	23	0.002	0.001-0.007	1.5

Table II. Sealing worker breathing zone geometric mean (GM) number concentrations, geometric standard deviation (GSD), and number of 1-second measurements for each worker.

Worker	Number of 1-Second Measurements	GM (particles cm⁻³)	GSD	Tukey-Kramer Grouping Levels*
8	485	147,000	1.75	A
1	1,312	240,000	1.79	B
2	1,465	248,000	1.16	C
3	1,275	250,000	1.21	C
4	1,211	291,000	1.48	D
5	1,316	321,000	1.96	D
7	865	591,000	1.75	E
9	592	603,000	2.10	E
6	1,599	798,000	2.27	E

* Means with the same letter are not statistically different.

Table III. Seam responsibility group geometric mean (GM) number concentrations, geometric standard deviation (GSD), number of workers in each seam responsibility group, and workers that comprise each group.

Group	Worker ID	Number of Workers in Group (n=)	GM (particles cm⁻³)	GSD	Duncan Grouping Levels*
Long	4, 5, 9	3	383,000	1.48	A, B
Middle	6, 7	2	688,000	1.24	A
Short	2, 8	2	192,000	1.44	B
Mixture	1, 3	2	245,000	1.03	B

*Means with the same letter are not statistically different.

Table IV. Percent time sealing seams versus conducting other tasks geometric mean (GM) number concentrations, geometric standard deviation (GSD), number of workers in each percent time sealing group, and workers that comprise each group.

Group	Worker ID	Number of Workers in Group (n=)	GM (particles cm⁻³)	GSD	Duncan Grouping Levels*
Greater than 70%	1, 6, 7	3	484,000	1.87	A
61% to 69%	3, 5, 9	3	364,000	1.57	A
Less than 60%	4, 2, 8	3	220,000	1.42	A

* Means with the same letter are not statistically different.

Table V. Breathing zone and in-duct particle number concentrations

Station	Number of 1-Second Measurements	Air Flow (m ³ min ⁻¹)	Breathing Zone		In-Duct		Concentration Reduction Factor (%)
			GM (particles cm ⁻³)	GSD	GM (particles cm ⁻³)	GSD	
1	2,440	12.3	6.03 x 10 ⁵	2.60	7.75 x 10 ⁵	2.57	56
2	1,761	11.5	2.57 x 10 ⁶	2.44	1.45 x 10 ⁶	1.90	36
3	2,318	12.3	3.77 x 10 ⁵	1.41	2.31 x 10 ⁵	3.30	38

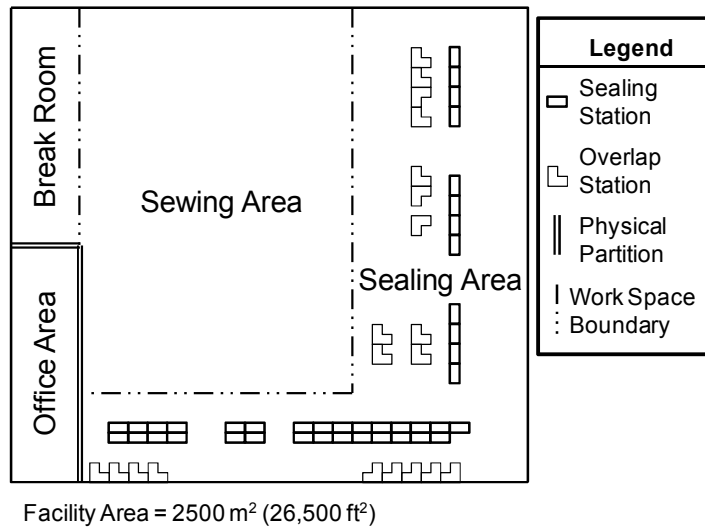


Figure 1. Layout of the facility showing three major areas: office area; sewing area; and sealing area.

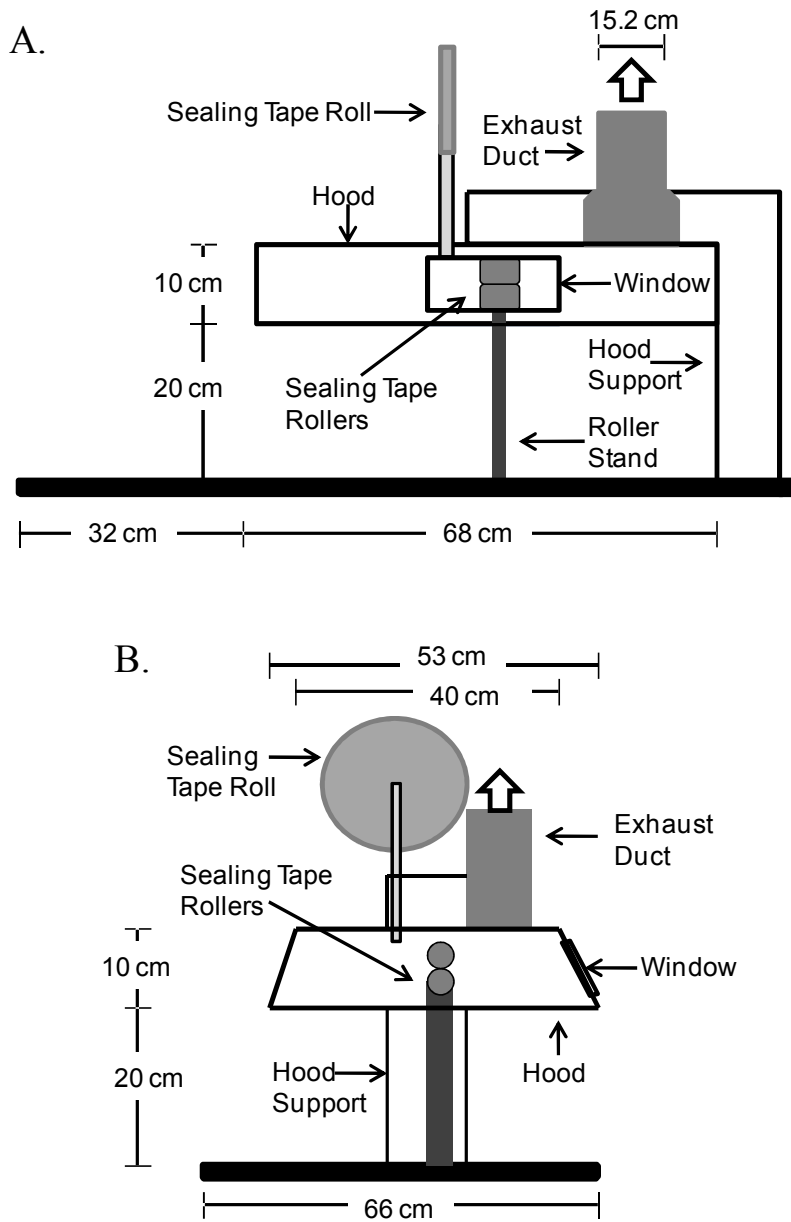


Figure 2. Schematic diagram of sealing station, showing the local exhaust ventilation hood: (A) front view; and (B) side view.

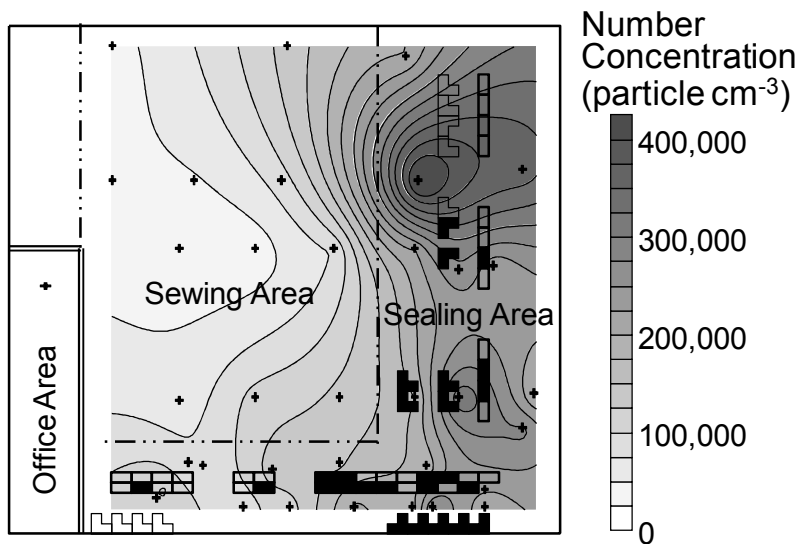


Figure 3. Map of particle number concentrations in the sewing and sealing areas. Crosses indicate sample locations and shaded work stations indicate stations that they were in use during mapping.

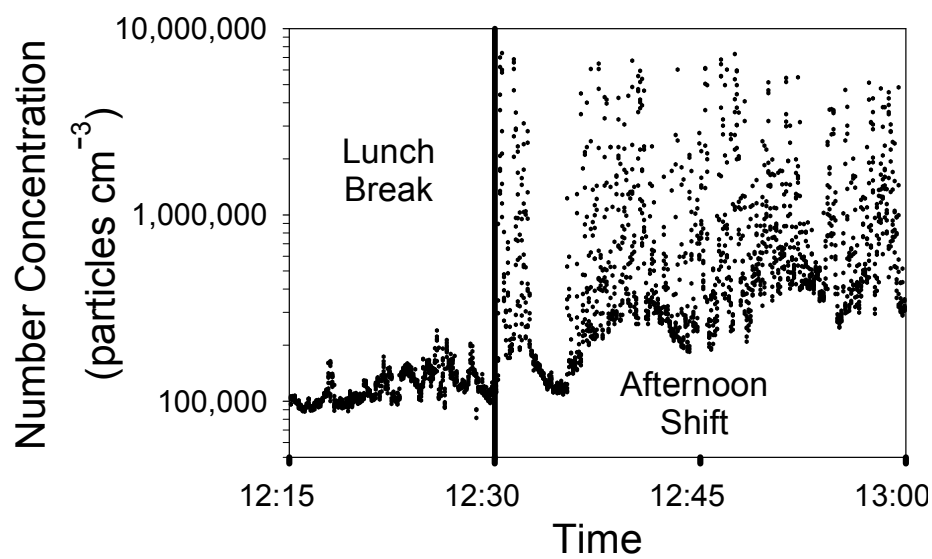


Figure 4. Particle number concentrations measured in the breathing zone of a sealing worker during the transition from lunch break to the afternoon shift.

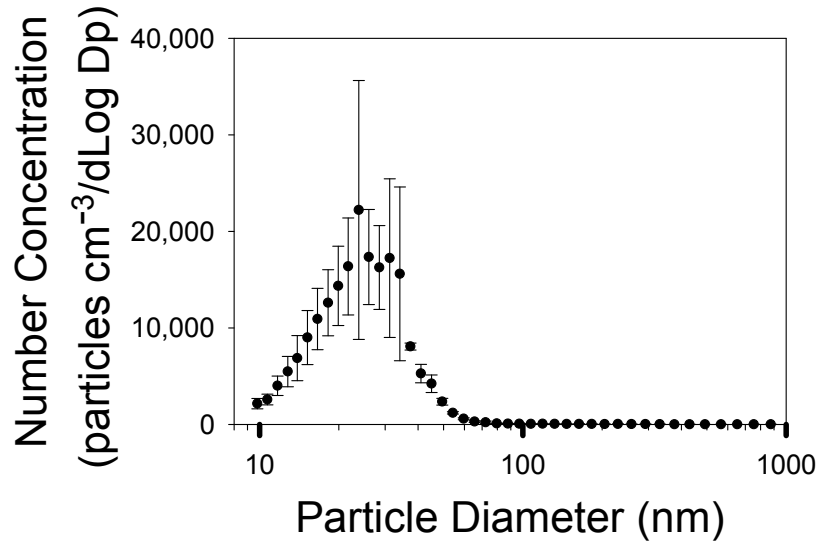


Figure 5. Particle number concentration by size measured at the final discharge of the local exhaust ventilation system.

CHAPTER III
EVALUATION OF A DIFFUSION CHARGER FOR ITS
EFFECTIVENESS IN MEASURING WORKPLACE AEROSOLS

Abstract

This study evaluated a portable diffusion charger (DC) for its effectiveness to measure airborne nanoparticle concentrations in a workplace. Particle surface area concentrations measured with the DC were compared to reference instruments for unimodal aerosols and mixes of aerosols. Tests were also conducted to determine the maximum measurable surface area concentration over which the DC response retained a linear response with the reference instruments. The effect of orientation and movement on the DC performance was also addressed. The active surface area concentration measured by the DC did not equal the geometric surface area concentration measured by the reference instruments for unimodal or multimodal aerosols. The greatest ratio of active surface area concentration measured by the DC to geometric surface area concentration of the reference instruments (R_{DC/ref_g}) was 0.54 for the smallest test aerosol, propylene torch exhaust with a number median diameter (NMD) of 22 nm. This ratio decreased as the NMD of the test aerosol increased. The DC underestimating surface area concentration compared to the reference instruments was attributed to the difference between measuring active versus geometric surface area concentration and the design of the DC. There was a statistically significant difference ($p < 0.0001$) in results between individual DCs measuring the same aerosol. One DC reported 13% less surface area concentration than the other DC. The maximum measurable active surface area concentration was $2,500 \text{ mm}^2 \text{ m}^{-3}$, which was greater than that stated by the manufacturer ($1000 \text{ mm}^2 \text{ m}^{-3}$). Moving or vibrating a DC while taking measurements caused increased surface area concentration and should be avoided when using the DC2000CE in a workplace.

Introduction

Nanoparticles are particles with a diameter smaller than 100nm (ASTM Standard E2456, 2006) and they occur in many workplaces. Regardless of age or breathing pattern, diffusion causes nanoparticles to have high rates of deposition (Daigle et al., 2003; C. S. Kim & Jaques, 2005) throughout the respiratory system (ICRP, 1994; C. S. Kim & Jaques, 2005). Toxicological studies have found that some nanoparticles increase their toxicity in comparison to larger particles of the same composition (Johnston et al., 2000; Karlsson et al., 2009; Oberdorster et al., 1995). Surface area concentration may be the most relevant physical measurement of nanoparticle exposure (Maynard & Maynard, 2002; Moshhammer & Neuberger, 2003; Oberdoerster et al., 2005). Direct-reading instruments that measure number or surface area concentration are more sensitive to nanoparticles than gravimetric methods (Mohr et al., 2005). Direct-reading instruments are needed to identify tasks and sources related to nanoparticle exposure (Peters et al., 2009; Ramachandran et al., 2005) because they address the issues of high temporal and spatial variability caused by the tendency of nanoparticles to coagulate rapidly and create concentration gradients (Hinds, 1999; Imhof et al., 2005).

A diffusion charger (DC) is a direct-reading instrument that measures the active surface area concentration of an aerosol. The active surface area concentration is that portion of the aerosol that interacts with the surrounding gas, as opposed to the geometric surface area of the particles (Keller et al., 2001). The DC creates unipolar ions with a corona discharge. Those ions then come in contact with the particles by diffusion and transfer their charge to the particle. An electrometer is used to measure the amount of charge that a particle can hold, which is dependent on the active surface area of the particle (Hinds, 1999). As particle size increases the active surface area will increasingly underestimate the geometric surface area of the particle (Jung & Kittelson, 2005; Ku & Maynard, 2005).

The S_p ratio (equation 1), a dimensionless ratio of active to geometric surface area, has been theorized to represent the accuracy with which the DC measures the geometric surface area of aerosols

$$S_p = 3\lambda / (C\delta d_p) \quad \text{equation 1}$$

Where λ is the mean free path, C is the Cunningham slip correction, δ is the scattering parameter that expresses the tendency of a gas molecule to bounce from the surface of the particle, which for air is 0.905, and d_p is the particle diameter (Heitbrink et al., 2009). This relationship suggests that S_p ratio is theoretically dependent only on particle size and gas parameters, not particle shape or composition. For the S_p ratio to accurately represent the active surface area of particles measured by the DC, the particles must first be charged to 100% of their capacity. The physical construction of the DC, which determines the time the particles are in the charging region of the DC; this influences the efficiency of the particle charging (Pui, 1976).

There are conflicting reports relating particle composition and morphology to a DC response. Several studies have hypothesized that particle composition or morphology influence the DC measurements (Jung & Kittelson, 2005; Kittelson, Watts, Savstrom, & Johnson, 2005; Mohr et al., 2005). However, Ku and Maynard (2005) found that the particle shape does not influence the DC measurement for silver particles smaller than 100 nm.

DCs may be used to measure airborne concentrations of nanoparticle in the expanding field of nanotechnology. For nanoparticles, the active surface area concentration measured by a DC is close to the geometric surface area concentration of the particle (Heitbrink et al., 2009). A DC has been shown to provide direct-reading output with a response time such that it could identify peaks in particle concentration (Mohr et al., 2005). The direct-reading output has allowed DCs to be useful in the identification of exposure sources by utilizing a data time stamp (Imhof et al., 2005; Ntziachristos, 2007; Ramachandran et al., 2005). In studies monitoring nanoparticle

exposures, DCs have been used in conjunction with other equipment to obtain qualitative information with regard to airborne nanoparticles (D. E. Evans et al., 2010; Heitbrink et al., 2009; Imhof et al., 2005; Ramachandran et al., 2005).

Prior to the independent use of a DC to quantify airborne concentrations of nanoparticle, each brand of DC should be evaluated. Brands of DCs have different flow rates and aerosol charging chamber dimensions, which will influence the charging efficiency of particles and the measurement accuracy (Asbach et al., 2009).

This study evaluation DC (Model DC2000CE, EcoChem Analytics, League City, TX) which has been used, with other instruments, to measure airborne concentrations of nanoparticles in work environments (D. E. Evans et al., 2010; Heitbrink et al., 2009; Ramachandran et al., 2005) because it is small (17.1 cm by 6.3 cm by 12.7 cm), lightweight (1.6 kg), logs data, and battery powered. This study compares concentrations from the DC2000CE compared to reference instruments. The DC was also evaluated to determine whether it could be used at surface area concentrations greater than the maximum active surface area concentration stated by the manufacturer. Finally, the influence of DC2000CE orientation and movement on results while taking measurements was also addressed to determine whether this unit would be useful in a personal, nanoparticle exposure assessment.

Methods

DC2000CE

The DC2000CE user guide (EcoChem Analytics, 2005) specifies that the DC2000CE is able to measure aerosol active surface area concentrations from $10 \text{ mm}^2 \text{ m}^{-3}$ to $1000 \text{ mm}^2 \text{ m}^{-3}$. The minimum active surface area concentration is dependent on the sensitivity of the electrometer in the DC (Asbach et al., 2009). The number of particles that define the active surface area concentration range varies depending on the size of particles being measured. The number of particles that can be detected in the range of the DC2000CE decreases as particle size increases due to the diameter-squared relationship

with surface area. The output from the DC2000CE does not provide size-specific information for the aerosol being measured. The user guide does not specify a particle size range over which the DC2000CE responds and it recommends creating a calibration factor for the DC2000CE by comparing it to other particle measuring instruments but it does not provide guidance on how to accomplish the comparison.

Comparison to Reference Instruments

The accuracy of the DC2000CE compared to reference instruments was tested using the set up shown in Figure 6. Polydispersed aerosols were generated and then injected into the 450 L mixing chamber. The polydispersed aerosol concentrations were measured by a DC2000CE (serial number 213), scanning mobility particle sizer (SMPS) (SMPS+C model 5.4, Grimm, Ainring, Germany), and an aerodynamic particle sizer (APS) (Model 3321, TSI Inc., Shoreview, MN) from an 8 L sampling chamber. The number concentration by size was measured with the SMPS from 9 nm to 460 nm and with the APS from 461 nm to 20 μm . Data from these instruments served as the reference. It was assumed that electrical mobility diameter reported by the SMPS was equal to the aerodynamic particle diameter reported by the APS. A pump (Model Omni, BGI Incorporated, Waltham, MA) was attached to the sampling chamber to provide extra airflow into the sampling chamber.

One nano-sized aerosol, two fine aerosols, and one coarse aerosol were used in this study to cover the potential range of the DC2000CE. The nano-sized aerosol was exhaust from a propylene torch (Model MAP-Pro, Worthington Cylinders, Columbus, OH). The fine aerosols were exhaust from a burning incense stick, and a diesel electric generator (Model DG6LE, RedHawk Equipment, Columbus, OH). The diesel generator was operated with ultra-low-sulfur highway diesel (15 ppm sulfur max.). The coarse aerosol composed of Arizona Road Dust (ARD) (ISO Medium, Powder Technology Incorporated, Burnsville, MN) aerosolized with a fluidized bed aerosol generator (Model 3400, TSI Inc., Shoreview, MN). Tests were conducted with one source (unimodal,

polydispersed aerosols) as well as multiple sources (multimodal, polydispersed aerosols.) The mixtures of the aerosols to create multimodal polydispersed aerosols are listed in Table VI.

Three runs were measured without aerosol and then three runs of each aerosol were measured. Each run was six minutes in length, the time needed for one SMPS run. The APS was set to average particle concentration over the six minutes. The DC2000CE was set to log measurements every 10 seconds. The DC2000CE results were averaged over the six minute time period of the SMPS and APS runs.

The ratio of active surface area concentration measured by the DC2000CE to the geometric surface area concentration calculated by the reference instruments (R_{DC/ref_g}) (equation 3) and the ratio of the active surface area concentration measured by the DC2000CE to the active surface area concentration measured by the reference instruments (R_{DC/ref_a}) (equation 5) were determined for all generated polydispersed aerosols. Particles were assumed to be spherical, thus to calculate the geometric surface area concentration measured by the reference instrument (SA_{ref_g})

$$SA_{ref_g} = \sum_{i=9.8}^{19,810} N_i(\pi d_i^2) \quad \text{equation 2}$$

where N_i was the number concentration in each of the i bins of the reference instruments, and d_i was the midpoint diameter of the bin. R_{DC/ref_g} was calculated by

$$R_{DC/ref_g} = SA_{DC}/SA_{ref_g} \quad \text{equation 3}$$

The active surface area concentration measured by the reference instruments (SA_{ref_a})

$$SA_{ref_a} = \sum_{i=9.8}^{19,810} N_i(\pi d_i^2) Sp_i \quad \text{equation 4}$$

where Sp_i was the computed Sp ratio value for the i th bin. R_{DC/ref_a} was calculated by

$$R_{DC/ref_a} = SA_{DC}/SA_{ref_a} \quad \text{equation 5}$$

Comparison of Two DC2000CE Responses

Two DC2000CEs were used to measure the active surface area concentration of incense simultaneously. The SMPS and pump were removed from the polydispersed aerosol set up (Figure 6) and replaced with a second DC2000CE (serial number 181). Both DC2000CE serial number 213 and serial number 181 were then used to measure surface area concentration of incense exhaust for 16, 10-second measurements.

Assessment of Maximum Measurable Active Surface Area Concentration

A separate experiment was conducted to evaluate the maximum active surface area concentration that a DC2000CE is able to measure while maintaining a linear output with respect to the reference instruments. Using the set up shown in Figure 6, diesel exhaust was injected into the mixing chamber to produce aerosols with similar size distributions but varying concentrations that ranged from 2 to 1,344,348 particle cm^{-3} . Three runs of ten concentrations were measured using DC2000CE serial number 213. Each run was six minutes in length (the time needed for one SMPS run) with the APS set to average particle concentration over six minutes. The logged 10-second measurements of the DC2000CE were averaged over the six minute time period of the SMPS and APS runs.

Assessment of Physical Limitations

The influence of motion on DC2000CE response was evaluated by placing the DC2000CE serial number 213 in five different orientations with a zero filter (8016245, TSI Inc., Shoreview, MN) placed on the inlet. The zero filter filters out all particulate matter so no particles reach the DC2000CE thus the DC2000CE response should be below the minimum response of $10 \text{ mm}^2 \text{ m}^{-3}$. The DC2000CE was set to log every 10 seconds and placed in its normal operation position (on feet) for one minute to allow the response to zero. Then every two minutes the DC2000CE was moved to a different orientation randomly determined: the instrument on its 1) feet; 2) back where the mode

switches are located; 3) top (unit upside down); 4) feet; 5) right (inlet) side; and 6) left (window) side. The orientation was changed with two movements: a gentle rolling motion without the DC2000CE losing contact with the table surface; and an abrupt motion with the DC2000CE picked up approximately 5 cm off the table and then quickly placed back on the table in a new orientation. All tests were conducted in triplicate.

The influence of vibration on instrument response was tested by placing the DC2000CE on a vibrating surface; again with a zero filter (8016245, TSI Inc., Shoreview, MN) on the inlet. The vibrating surface used for these tests was a blower (Model 4C129, Dayton, Chicago, IL) that was set to 20% of motor RPM. The DC2000CE was set to log every 10 seconds throughout the following sequence: one minute for zeroing period; blower on for two minutes; blower off for one minute. This sequence was repeated in triplicate. The vibration in the x, y, and z plane were measured using a human vibration monitor (Model HVM100, Larson Davis, Depew, NY) placed on the blower.

Statistical Analysis

Spearman rank order correlation coefficients were computed and tested for the unimodal polydispersed combustion results and for the multimodal polydispersed results that included ARD to determine if there was a statistically significant relationship between SA_{DC} and SA_{ref_g} . The coefficients were computed using the three runs of each aerosol type and the three runs without aerosol ($n = 12$ for unimodal aerosols, $n = 12$ for multimodal aerosols).

A Wilcoxon Rank Sum test was used to determine if the DC2000CE serial number 213 and serial number 181 had statistically different results while measuring incense. The statistical tests were evaluated at the 95% confidence level. All statistical analysis was carried out using the statistical package SAS version 9.2.

Results

Comparison to Reference Instruments

The comparison of the response of the DC2000CE to the reference instruments for polydispersed unimodal and multimodal aerosols are provided in Table VI. If the DC2000CE measured active surface area concentration was similar to the reference instruments calculated geometric surface area concentrations then R_{DC/ref_g} should approach unity. R_{DC/ref_a} should approach unity if the DC2000CE measured active surface area concentration and the calculated active surface area concentration of the reference instruments was similar. Aerosol number and surface area concentrations measured with the reference instruments are provided in Figure 7 for unimodal polydispersed aerosols and in Figure 8 for multimodal polydispersed aerosols. The geometric surface area concentrations of the unimodal polydispersed aerosols (Figure 7) was a function of the distribution number median diameter (NMD) and number concentration. For the multimodal polydispersed aerosols shown in Figure 8, the geometric surface area concentrations appear almost unimodal with the surface area concentration peak influenced by the aerosol mixture component that provided the greatest surface area concentration.

The ratios of R_{DC/ref_g} and R_{DC/ref_a} were substantially less than unity for all aerosols. As shown in Table VI, R_{DC/ref_g} ranged from 0.02 to 0.54 and R_{DC/ref_a} ranged from 0.13 to 0.61 for unimodal polydispersed aerosols. For propylene torch, diesel, and incense the number concentration decreased as the NMD, SA_{DC} , and SA_{ref_g} increase. The R_{DC/ref_g} for the multimodal distributions ranged from 0.03 to 0.15 and the R_{DC/ref_a} ranged from 0.20 to 0.25.

Spearman rank order correlation coefficient computed for the unimodal polydispersed aerosols of propylene torch, diesel, and incense was 0.95 and there was a statistically significant relationship between SA_{DC} and SA_{ref_g} ($p < 0.0001$). Spearman rank order correlation coefficient computed for the multimodal polydispersed aerosols

that contained ARD was 0.88 and there was a statistically significant relationship between the SA_{DC} and SA_{ref_g} ($p=0.0002$).

Comparison of Two DC2000CE Responses

As shown in Table VII, the active surface area concentration measured by two different DC2000CEs was statistically different while measuring incense. DC2000CE 181 ($942 \text{ mm}^2 \text{ m}^{-3}$) measured 13% less SA_{DC} than DC2000CE 213 ($1087 \text{ mm}^2 \text{ m}^{-3}$), which was a statistically significant difference ($p<0.0001$). The SA_{DC} difference in terms of number concentration for particles with a diameter of 128 nm, the NMD of incense (Table VI), would equate to $2,817 \text{ particle cm}^{-3}$. The SA_{DC} difference in terms of number concentration measured by the reference instruments would equate to 18,780 particles cm^{-3} ($2,817 \text{ particle cm}^{-3}$ with a diameter of 128 nm multiplied by the incense R_{DC/ref_g} of 0.13).

Assessment of Maximum Measurable Active Surface Area Concentration

The DC2000CE was able to measure concentrations with similar R_{DC/ref_g} compared to the reference instruments to approximately $2,500 \text{ mm}^2 \text{ m}^{-3}$ (Figure 9) or 2.5 times the maximum active surface area concentration stated by the manufacturer ($1000 \text{ mm}^2 \text{ m}^{-3}$). The relationship between the DC2000CE response and the surface area concentration measured with the reference instruments was linear ($SA_{DC}=0.15SA_{ref_g} + 1.74$; $R^2 = 0.99$) for concentrations below $2,500 \text{ mm}^2 \text{ m}^{-3}$. As shown in Table VIII, the particle size distribution of the aerosol for different concentrations was relatively constant with the GM varying from 95 nm to 127 nm and the GSD varying from 1.48 to 1.53.

Assessment of Physical Limitations

The influence of instrument movement on DC2000CE response is shown in Figure 10. Surface area concentrations were observed above the minimum active surface area concentration stated by the manufacturer ($10 \text{ mm}^2 \text{ m}^{-3}$) 30 seconds after a movement occurred and then return to near zero values (Figure 10). The greatest values occurred for

the rolling movement window side, which was over four times the value for the other orientations and over forty times the minimum active surface area concentration stated by the manufacturer. The greatest mean surface area concentrations for the abrupt movements were observed when the instrument was moved to the window and feet orientations. Those values were approximately 20 times the concentrations of the other orientations and the minimum active surface area concentration stated by the manufacturer.

The influence of vibration on the DC2000CE response is shown in Figure 11. The average root mean square vibration was 2.82 m s^{-2} in the x-direction, 3.25 m s^{-2} in the y-direction, and 1.87 m s^{-2} in the z direction. When the DC2000CE was vibrating, the results were greater than two times the minimum active surface area concentration stated by the manufacturer ($10 \text{ mm}^2 \text{ m}^{-3}$).

Discussion

The DC2000CE measures airborne nanoparticles and larger submicron particles. There were statistically significant correlations between the SA_{DC} and SA_{ref_g} for both the unimodal polydispersed combustion aerosols and the multimodal polydispersed aerosols containing ARD. The unimodal aerosols were composed of particles below 400 nm. In contrast, the multimodal aerosols that contained ARD included particles larger than 1 μm , although the concentrations of particles greater than 1 μm were less than 100 particle cm^{-3} . Although the Spearman correlation coefficients were high for the unimodal and multimodal aerosols, the unimodal aerosols coefficient was larger than the multimodal aerosols coefficient. The results of the coefficient for aerosols containing particles less than 400 nm being greater than the coefficient for aerosols containing particles larger than 1 μm agreed with a study conducted in an automotive manufacturing plant by Heitbrink et al. (2009). Heitbrink et al. (2009) found the DC2000CE response to be more closely related to particle number concentration of particles between 10 to 300 nm than to

respirable mass concentrations, which would have included particles with diameters greater than 1 μm .

Although there was a statistically significant relationship between SA_{DC} and SA_{ref_g} , the active surface area concentration measured by the DC2000CE did not equal the geometric surface area concentration measured by the reference instruments for unimodal, or multimodal particle distributions (Table VI). The DC2000CE results were expected to be less than the reference instruments results because the DC2000CE measures active surface area and the reference instruments were used to calculate geometric surface area. The differences between the DC2000CE and the reference instruments were great with the least difference being for propylene torch with a R_{DC/ref_g} of 0.54. When compared to the concentration accuracy of a TSI 3007 portable CPC, an instrument used in exposure assessments (Methner et al., 2007; Peters et al., 2006; Pui et al., 2008) which has a reported concentration accuracy of 0.8 to 1.2 (TSI Incorporated, 2004) the R_{DC/ref_g} was much smaller.

Particle size had the greatest influence on R_{DC/ref_g} . R_{DC/ref_g} values for the unimodal polydispersed aerosols show a relationship of decreasing R_{DC/ref_g} as distribution NMD increases. The relationship also appeared in the R_{DC/ref_g} of the multimodal polydispersed aerosols. The component of the mixture that provided the greater part of the surface area concentration (Figure 8) had greater influence on the mixture R_{DC/ref_g} (Table VI). The mixture R_{DC/ref_g} was closest to the R_{DC/ref_g} of the mixture component that provided the main surface area concentration. Ku (2010) also found that the ratio of DC2000CE to reference instruments decreased as particle size increased for spherical particles between 100 to 900 nm.

The design of the DC2000CE caused greater differences in results than can be accounted for with the Sp ratio alone. The Sp ratio is dependent on particle size as was the R_{DC/ref_g} . If the difference between the DC2000CE results and the reference instrument results were only a matter of active versus geometric surface area then the Sp

ratio could be used as a calibration factor. R_{DC/ref_a} would have equaled 1 for the differences to be only a matter of active versus geometric surface area but the closest R_{DC/ref_a} to 1 was 0.61 for propylene torch. The DC2000CE would have had to charge the particles to 100% of their capacity for the differences in results to have been only a matter of active versus geometric surface area. The charging efficiency of a unipolar diffusion charger is less than 100% due to the design of DCs (where the needle is placed in the DC, the size of the charging zone, and airflow through the charging zone, etc.) (Intra & Tippayawong, 2009).

This study found statistically significant differences between different DC2000CEs in terms of SA_{DC} but it is unknown if the difference is substantial. The difference between DC2000CE serial number 213 and serial number 181 active surface area concentrations (Table VII) was 13%, which equates to a $18,780 \text{ particle cm}^{-3}$ difference in terms of the reference instruments. In a study comparing differences between two models of portable CPCs, the differences were found between +/- 17% (Matson, Ekberg, & Afshari, 2004). Differences between DC2000CE of the same model were less than the differences between the two different models of CPCs.

Over-ranging a DC2000CE while measuring nanoparticles in a workplace would be less of a concern compared to other direct-reading instruments. The DC2000CE maximum measureable active surface area concentration ($2,500 \text{ mm}^2 \text{ m}^{-3}$) was greater than the maximum active surface area concentration stated by the manufacturer ($1000 \text{ mm}^2 \text{ m}^{-3}$) (Figure 9). Direct-reading instruments have over-ranged in the field while measuring nanoparticle concentrations requiring nanoparticle concentrations to be diluted by various means, such as using a high efficiency particle filter with a hole (Heitbrink et al., 2009; Peters et al., 2006). Taking into account the R_{DC/ref_g} of incense (0.15), $2,500 \text{ mm}^2 \text{ m}^{-3}$ equates to $323,813 \text{ particle cm}^{-3}$ of 128 nm diameter particles in terms of reference instrument number concentration. The number concentration is over three times

the reported maximum number concentration of a TSI 3007 CPC (TSI Incorporated, 2004) for a 128 nm particle and would be larger for smaller particles.

Moving the DC2000CE while it is running may cause substantial errors in the active surface area concentrations measured with the amount of error varying depending on how the DC2000CE was moved. Placing the DC2000CE on a vibrating surface would also cause measurement errors (Figure 11) but the measurement error variation associated with vibrating was less than with moving the DC2000CE (Figure 10). Care should be taken to either not move the DC2000CE while it is sampling or to determine ahead of time if the movement is the type that would cause a measurement error. Until it is known where the error stems from, care should be taken with all instruments that use diffusion charging to determine if there are similar physical considerations associated with their use.

The reference instruments chosen for this study limit the comparison of these results to other studies. R_{DC/ref_g} and R_{DC/ref_a} are dependent on the reference instruments so different reference instruments may have different results.

More work must be done before a DC2000CE can be used independently to measure airborne nanoparticle concentrations in a workplace. Calibrating the DC2000CE by particle size compared to the geometric surface area measured by a reference instrument is needed to account for the differences caused by measuring active versus geometric surface area and instrument design. The maximum particle size that generates a response from the DC2000CE must be part of the calibration factor. The DC2000CE ARD response ($4 \text{ mm}^2 \text{ m}^3$) was less than the lower minimum active surface area concentration, thus the maximum particles size that generates a response is somewhere below 978 nm. The error associated with measuring the geometric surface area concentration of particles greater than 500 nm when it is assumed that the DC2000CE is only measuring particles less than 300 nm may cause great error due to the diameter squared nature of surface area measurements (Asbach et al., 2009). Once a calibration

factor by size has been determined, such as the correction found by Ku (2010), the calibration factor must be tested with multiple DC2000CEs. It is unknown whether the statistically significant different results of two DC2000CEs found in this study are of a magnitude that would disallow a single calibration factor by size to be valid for multiple DC2000CEs. Also, many work environments are composed of a mixture of particle sizes (Elihn & Berg, 2009; D. E. Evans et al., 2007; Heitbrink et al., 2009) and the addition of a particle size selection device to the front of a DC2000CE would address the issue of environments with unknown particle sizes.

Conclusions

This study evaluated a DC2000CE for its effectiveness to measure airborne nanoparticle concentrations in a workplace. The DC2000CE has limitations that currently restrict its ability to measure airborne nanoparticle concentrations in the workplace. The active surface area concentration measured by the DC2000CE did not equal the geometric surface area concentration measured by the reference instruments and the ratio of the two decreased as particle size increased which was to be expected. The active surface area concentration measured by the DC2000CE also did not equal the calculated active surface area of the reference instruments. A calibration factor by size is needed because the DC2000CE measured the surface area of all of the aerosols used in this study with accuracies less than 0.54. Thus, there is no particle size range larger than 22 nm where the DC2000CE has accuracies compared to the reference instruments similar to those of other portable direct-reading instruments. A general calibration factor by size should be validated with multiple DC2000CEs. The maximum measurable active surface area of a DC2000CE was substantially greater than the maximum active surface area concentration stated by the manufacturer, which equates to number concentrations greater than some handheld CPCs. There are physical considerations that must be taken into account when using the DC2000CE in a workplace. Care should be taken not to move or vibrate a

DC2000CE while it is measuring aerosols, as errors are introduced and persist for as long as 30 seconds after motion has stopped.

Table VI. Active surface area concentrations measured by the DC2000CE compared to geometric and active surface area concentration measured by reference instruments for polydispersed aerosols.

Unimodal								
Aerosol	NMD (nm)	GSD	Number Concentration (particle cm⁻³)	DC Mean SA_{DC} (mm² m⁻³)	Reference Mean SA_{ref_g} (mm² m⁻³)	R_{DC/ref_g}	Reference Mean SA_{ref_a} (mm² m⁻³)	R_{DC/ref_a}
Propylene Torch	22	1.53	144,171	133	249	0.54	220	0.61
Diesel	122	1.48	62,491	560	3,772	0.15	2,426	0.23
Incense	128	1.69	46,366	581	4,439	0.13	2,358	0.25
ARD	978	1.50	108	4	177	0.02	30	0.13
Multimodal								
Aerosol			Number Concentration (particle cm⁻³)	DC Mean SA_{DC} (mm² m⁻³)	Reference Mean SA_{ref_g} (mm² m⁻³)	R_{DC/ref_g}	Reference Mean SA_{ref_a} (mm² m⁻³)	R_{DC/ref_a}
Propylene Torch, ARD			41,026	105	3,146	0.03	430	0.25
Incense, ARD			42,321	339	3,150	0.11	1,731	0.20
Propylene Torch, Incense			116,533	553	3,741	0.15	2,174	0.24
Propylene Torch, Incense, ARD			107,122	673	5,317	0.16	2,706	0.25

Table VII. Comparison of the response of two DC2000CEs measuring incense.

Diffusion Charger	Number of 10 sec measurements (n=)	Mean SA_{DC} (mm² m⁻³)	Standard Deviation (mm² m⁻³)	Wilcoxon Rank Sum p-value
181	16	942	35	<0.0001
213	16	1,087	29	
181 and 213 Difference				
SA_{DC} (mm² m⁻³)	Number Concentration (particle cm⁻³)		Number Concentration x Incense R_{DC/ref_g} (particle cm⁻³)	
145	2,817		18,780	

Table VIII. Response of the DC2000CE with increasing diesel exhaust concentrations.

Mean DC2000CE Surface Area Concentration (mm² m⁻³)	Mean Reference Number Concentration (particles cm⁻³)	Mean GM (nm)	Mean GSD
1	2	-	-
162	14,631	127	1.49
560	62,491	122	1.48
766	80,574	123	1.50
1,056	131,045	108	1.53
1,516	185,833	110	1.51
2,360	282,859	112	1.49
2,532	401,369	100	1.51
3,028	728,676	98	1.50
3,530	1,344,348	95	1.51

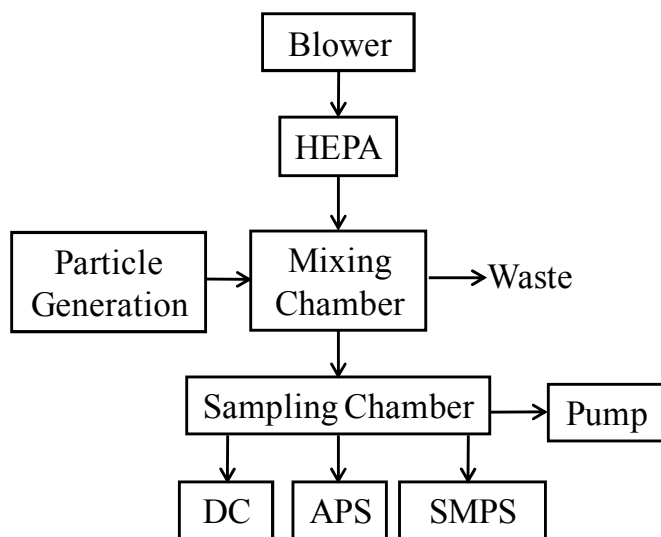
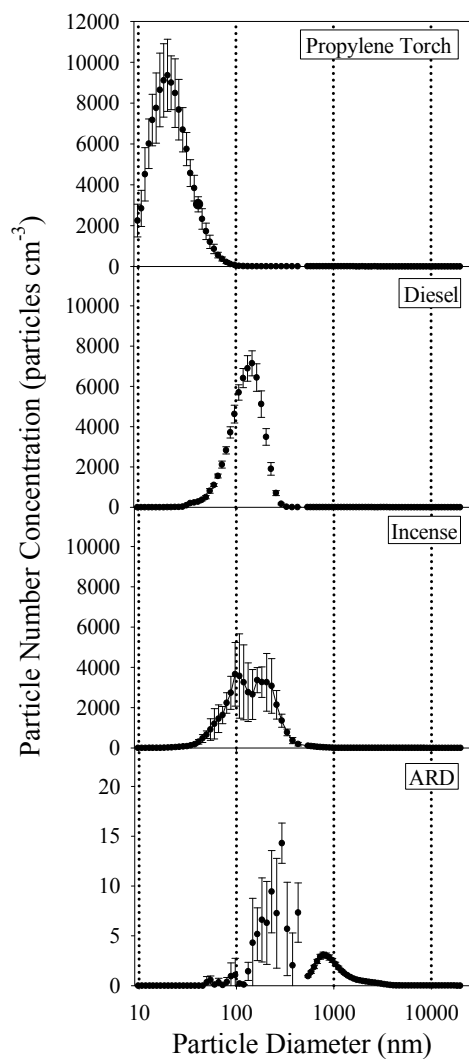


Figure 6. Set up for measuring polydispersed aerosols.

A.



B.

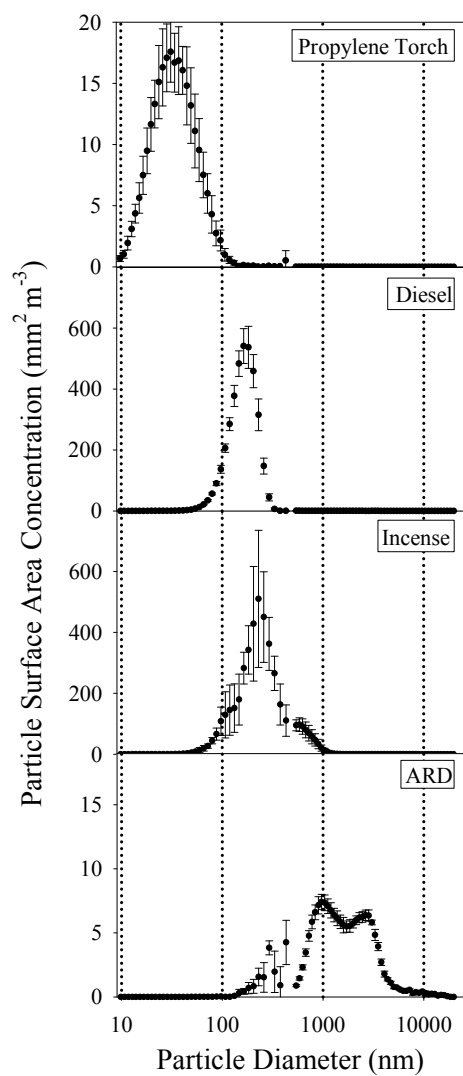


Figure 7. Particle number (A.) and surface area concentrations (B.) by size measured for unimodal polydispersed aerosols.

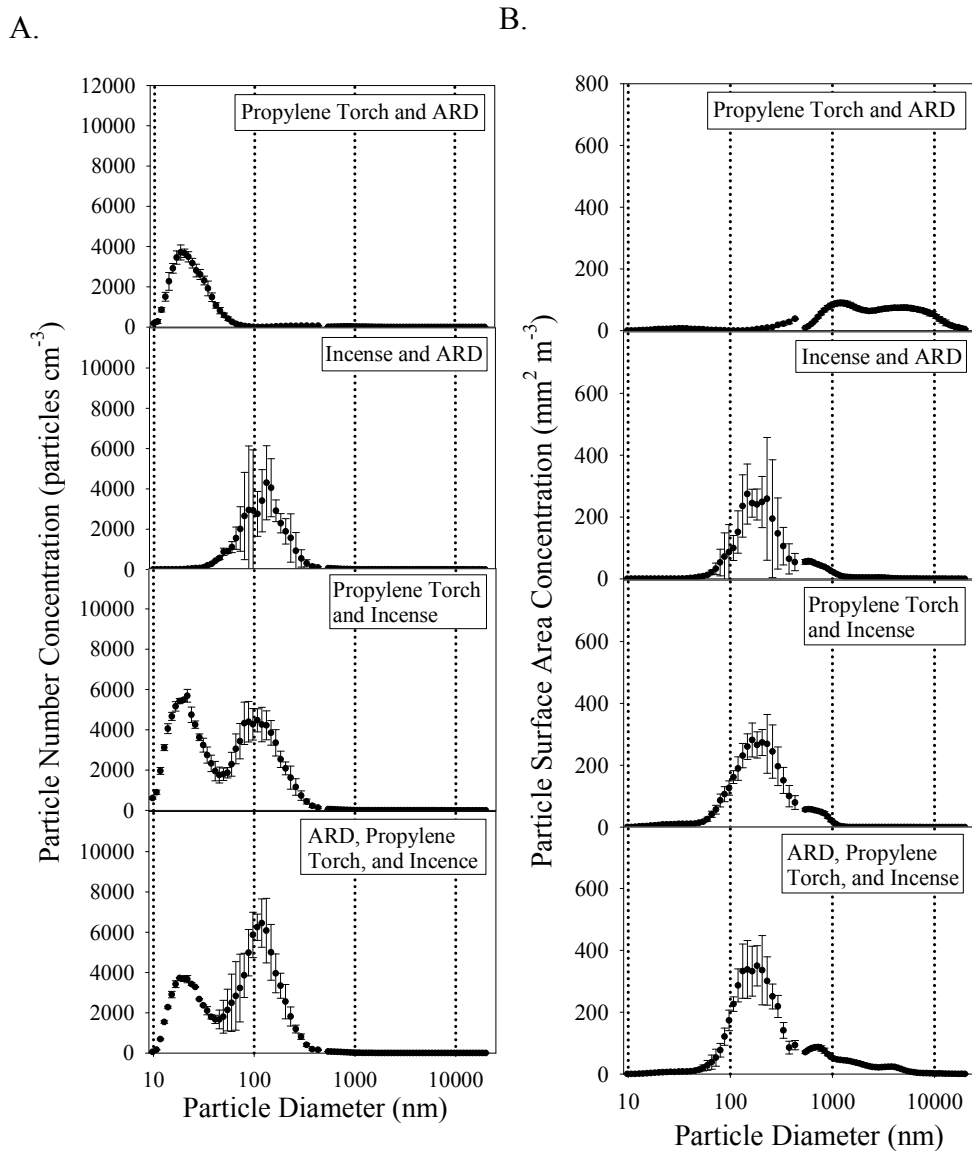


Figure 8. Particle number (A.) and surface area concentrations (B.) by size measured for multimodal polydispersed aerosols.

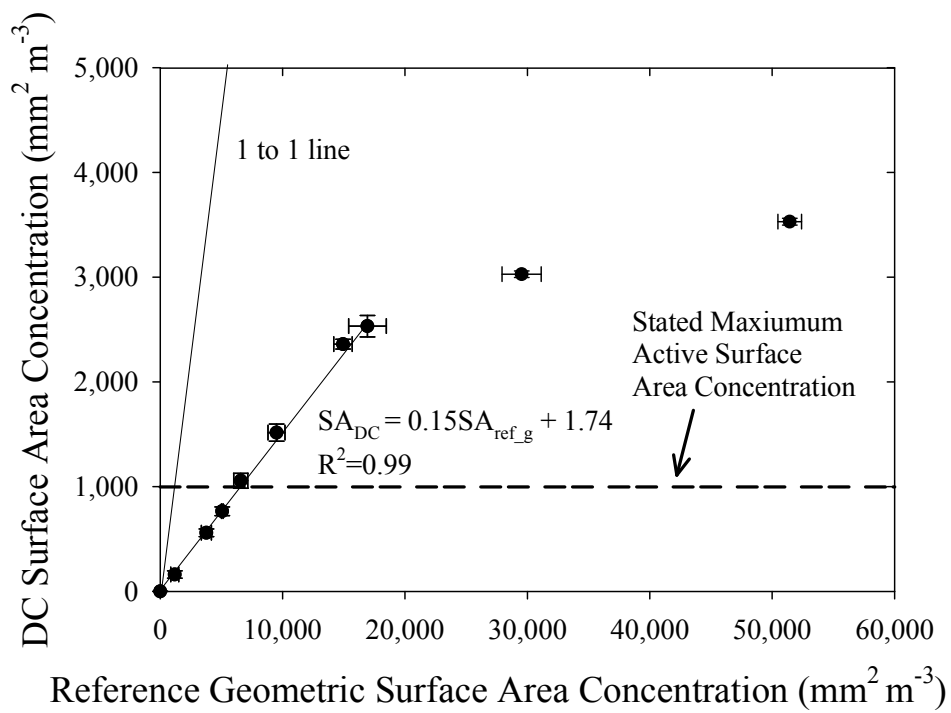
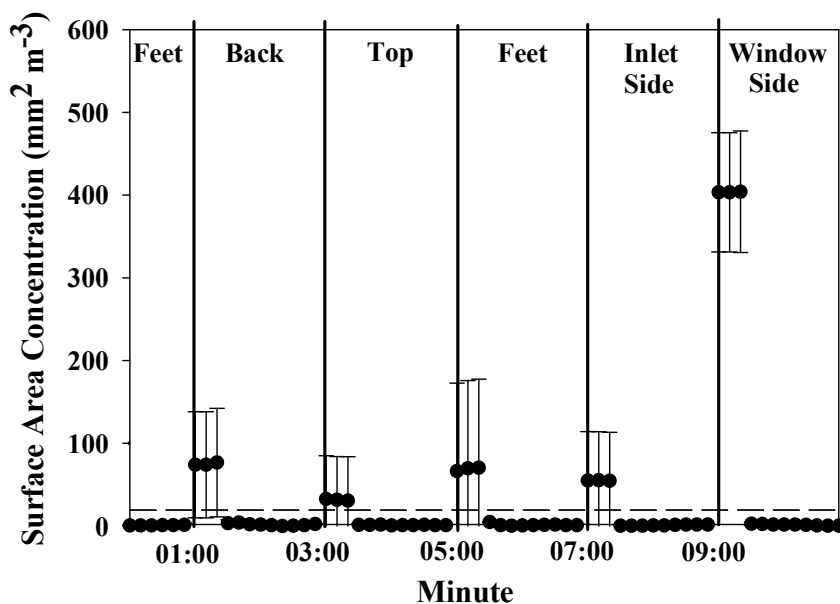


Figure 9. Influence of concentration on DC2000CE response measuring diesel exhaust when concentrations were less and greater than the maximum active surface area concentration stated by the manufacturer.



Abrupt Movement

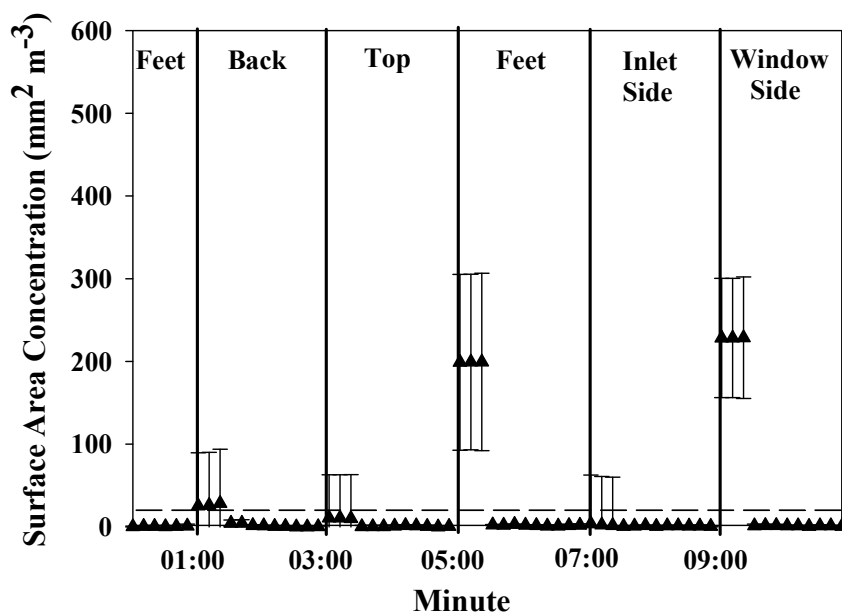


Figure 10. The influence of orientation and movement on DC2000CE measurements. The dotted line is the minimum active surface area concentration stated by the manufacturer of the DC2000CE ($10 \text{ mm}^2 \text{m}^{-3}$).

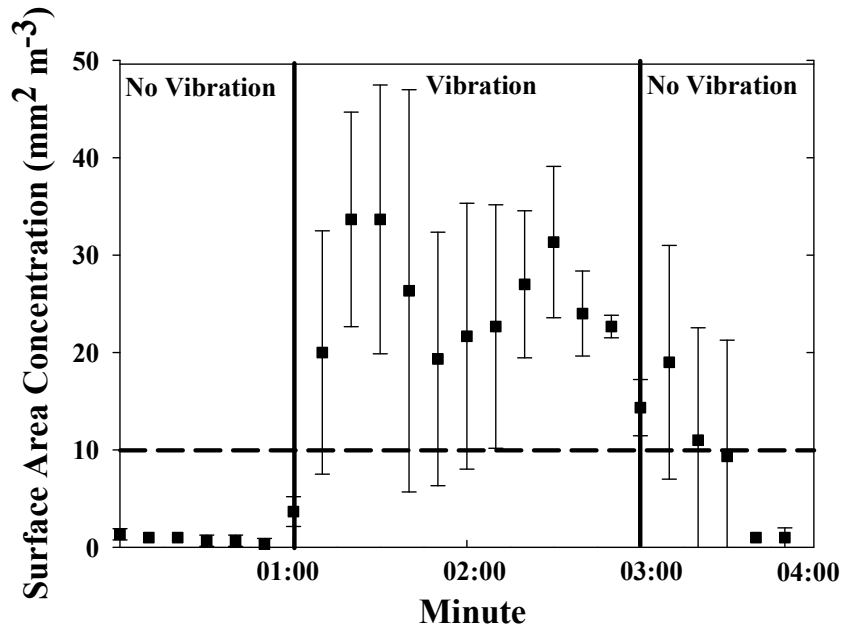


Figure 11. The influence of placing a DC2000CE on a vibrating surface. The dotted line is the minimum active surface area concentration stated by the manufacturer of the DC2000CE ($10 \text{ mm}^2 \text{ m}^{-3}$).

CHAPTER IV
DESIGN AND EVALUATION OF A PERSONAL DIFFUSION
BATTERY

Abstract

A four-stage personal diffusion battery (pDB) was designed and constructed to measure submicron particle size distributions. The pDB consists of a screen-type diffusion battery, a solenoid valve system, and an electronic controller that can be placed in a backpack worn by a worker. A data inversion spreadsheet was created to solve for the number median diameter (NMD), geometric standard deviation (GSD), and particle number concentration of unimodal aerosols using number concentrations of each stage from the pDB combined with a handheld condensation particle counter (pDB+CPC). The inversion spreadsheet included particle entry losses, theoretical penetrations across screens, and detection efficiency of the CPC. The inversion spreadsheet was shown to provide NMD with 90 to 110% accuracy, GSD with 95 to 105% accuracy, and number concentration with 95% to 105% accuracy for aerosols with NMDs that ranged between 17 nm to 286 nm. The penetrations by particle size of each stage of the pDB were found to be lower and shallower than the inversion penetrations that were calculated from theory. The pDB+CPC was evaluated using unimodal propylene torch exhaust and incense exhaust aerosol distributions. The number concentrations for particles with diameters between 9.4 nm to smaller than 100 nm estimated by the pDB+CPC with the inversion spreadsheet were within 86% to 109% of reference instrument results when the inversion did not solve to an inversion constraint. For inversion results that solved to a constraint, the number concentration of particles with diameters between 9.4 nm to 100 nm was 6% to 198%.

Introduction

Airborne nanoparticles—particles with a diameter smaller than 100 nm (ASTM Standard E2456, 2006)—are present in many workplaces. Diffusion causes nanoparticles

to have high rates of deposition in the human respiratory system regardless of age or breathing pattern (Daigle et al., 2003; C. S. Kim & Jaques, 2005). Toxicological studies have found that, depending on their composition, nanoparticles may have increased toxicity compared to larger particles of the same composition (Johnston et al., 2000; Karlsson et al., 2009; Oberdorster et al., 1995).

There are no specific occupational exposure limits in place to protect worker health with regard to nanoparticles. Unless the nanoparticles are of a composition regulated by a permissible exposure limit, airborne particulate matter is measured with a time-weighted average sample measured gravimetrically (National Institute of Occupational Safety and Health, 2003). Gravimetric analysis is not an effective way to measure nanoparticles separately from larger particles that occur in a respirable sample because of negligible mass in nanoparticles (Vincent & Clement, 2000).

Direct-reading instruments that measure particle number or surface area concentration can be a sensitive indicator of airborne nanoparticles (Mohr et al., 2005) but portable direct-reading instruments that measures personal nanoparticle concentrations are unavailable. Nanoparticles coagulate rapidly causing measurements farther from a source to be composed of less, larger particles than were at the source (Hinds, 1999). Depending on the worker's proximity to the source and the direct-reading instrument, the worker's exposure may be different from the airborne nanoparticle concentration measured. Thus, a breathing zone measurement is needed. Some direct-reading instruments using diffusion chargers and condensation particle counters (CPC) are small enough to be carried by a worker but do not provide concentrations by size for submicron particles. Scanning mobility particle sizers or electrical low pressure impactors do provide concentrations by size for submicron particles, but they are too large to be carried by a worker.

A screen-type diffusion battery can be coupled with a low-cost, small direct-reading instrument to obtain submicron size distribution information (Hinds, 1999). In a

screen-type diffusion battery, aerosol is passed through a series of stages that hold screens (Sinclair & Hoopes, 1975). Diffusion causes particles to collect on the screens and not be counted by the detector. The number concentration and particle size collected depending on screen characteristics (Cheng & Yeh, 1980; Cheng, Keating, & Kanapilly, 1980; Cheng, Yeh, & Brinsko, 1985; Yeh, Cheng, & Orman, 1982). A mathematical data inversion algorithm is then required to estimate the distribution of the original aerosol based on the theoretical particle penetrations of the screens, the detection efficiency of the detector compared to the reference instrument used, and particle losses of the aerosol entering the screen-type diffusion battery (Cheng & Yeh, 1984). A data inversion technique that uses an iterative approach increases the accuracy of aerosol distribution estimates (Twomey, 1975). Such an approach was successfully implemented within a spreadsheet to process data from cascade impactors (O'Shaughnessy & Raabe, 2003).

Screen-type diffusion batteries have the potential to be used in a personal nanoparticle direct-reading instrument. Screen-type diffusion batteries have traditionally had many stages and were coupled with large switching valves (Cheng & Yeh, 1984; Gorbunov, Priest, Muir, Jackson, & Gnewuch, 2009). The combined size prohibited them from being used to collect personal measurements. Using only the minimum number of stages and reducing the size of the switching valve, a screen-type diffusion battery could be developed to assess personal nanoparticle exposures by determining number median diameter (NMD), geometric standard deviation (GSD), and number concentration of a submicron aerosol.

The goal of this study was to create a device that could be carried by a worker to determine the amount of a submicron aerosol that was composed of nanoparticles. In this study, we designed and evaluated a personal diffusion battery (pDB) for the purpose of determining the amount of nanoparticles in a submicron aerosol. The pDB consisted of a four-stage screen-type diffusion battery and a solenoid valve system that automatically switched from one pDB stage to the next pDB stage, changing the path of the airflow

through different numbers of screens in the pDB. The pDB unit was combined with a CPC (pDB+CPC) to record number concentrations for each pDB stage, and an inversion spreadsheet was created to estimate the aerosol NMD, GSD, and number concentration. The inversion spreadsheet included experimentally determined penetration through Stage A to adjust for particle losses of the aerosol entering the pDB and the detection efficiency of the CPC compared to the reference instrument to allow for comparisons to the reference instrument. The inversion spreadsheet also included theoretically calculated penetrations through five, 11, and 16 screens. To evaluate the pDB+CPC with inversion, it was challenged with submicron, unimodal, combustion aerosols and results were flagged when the pDB+CPC with inversion distribution NMD, GSD, and/or number concentration estimated differed from the SMPS measured distribution by $\pm 25\%$.

Methods

Personal Diffusion Battery (pDB) Design

As shown in Figure 12A, the pDB consisted of a conductive sampling tube, four-stage screen-type diffusion battery, solenoid valve manifold system, and electronic controller. The weight of the pDB in the backpack, excluding the detector and electrical battery, was 3.2 kg (7 lbs), which allows it to be worn in a backpack. The weight of the battery and detector varied depending on the brands and models chosen. For this study the combined weight of the battery and detector was 4.0 kg (8.8 lbs). A 96-cm sampling tube transports aerosol from the worker's breathing zone into a diffusion battery. The diffusion battery is assembled from a series of 13, 25-mm conductive filter cassette pieces (225-329, SKC Inc., Eighty Four, PA). The distance between the inlet and the first set of screens was 50 mm to allow the airflow to expand to the entire diameter of the cassettes before reaching the screens. The screen-type diffusion battery was sealed with silicone to prevent air leaks.

The diffusion battery had four stages identified as Stage A through D. Each stage is fitted with a 5 mm plastic connector and tubing that is connected to the solenoid valve

manifold (SAM1614-4G2015, Gem Sensors & Controls, New Britain, CT). An electronic controller (custom, TAK, Ind., Muskegon, MI) sequentially opens one of the four solenoid valves so the airflow passes through the different stages of the diffusion battery (Figure 12B). The following repeated sequence was programmed into the controller: Stage A; Stage B; Stage C; Stage D; Stage A; etc. The timing that a solenoid valve remained open was programmed as a variable and two timings were used in this study. The solenoid valves were connected to a common manifold, which was connected to the detector. A handheld CPC (Model 3007, TSI, Inc., Shoreview, MN) was selected as the detector for this work, and the coupled instrument was referred to as the pDB+CPC. The CPC was selected because it measured particle number concentration from 10 nm to approximately 1 μm and had the ability to compensate for changes in inlet pressure to maintain a constant airflow of 0.7 L min^{-3} .

Sets of stainless steel screens (Twill 635 US standard mesh, Dorstener Wire Tech, Spring, TX) were installed at three locations to achieve specific cutoff diameters at an airflow of 0.7 L min^{-3} . The screen fiber wire diameter was 0.02 mm, thickness was 0.04 mm, average weight was 0.0548 g, and density was 8000 kg m^{-3} . The calculated solid volume fraction of each screen was 0.349. The inside diameter of the cassettes was 21.1 mm. The 0.7 L min^{-1} flow rate of the CPC resulted in a superficial velocity of 0.03 m sec^{-1} , within the laminar flow regime (Reynolds number = 46.4).

Stage A of the pDB was operated as a bypass stage without screen media (Figure 12B). Five screens were used in Stage B. Six additional screens were added to Stage C for a total of 11 screens the aerosol passed through. Five additional screens were added to Stage D for a total of 16 screens the aerosol passed through.

Theoretical pDB Stage Pressure Drop and Penetration

The theoretical pressure drops using Cheng, Yeh, and Brinsko (1985) and the theoretical penetrations using Cheng and Yeh (1984) were calculated for each set of screens in Stages B, C, and D. For Stage B the theoretical pressure drop (ΔP_5) and

penetration ($P_{5,d}$) was calculated for five screens. For Stage C theoretical pressure drop (ΔP_{11}) and penetration ($P_{11,d}$) was calculated for 11 screens. For Stage D the theoretical pressure drop (ΔP_{16}) and penetration ($P_{16,d}$) was calculated for 16 screens ($P_{16,d}$). The airflow used for the calculations was 0.7 L min^{-3} , the airflow of the CPC.

The theoretical pressure drop (ΔP_n) was calculated using equation 6:

$$\Delta P_n = (4\pi/k)(U\mu\alpha n h)/(\pi a^2) \quad \text{equation 6}$$

where U equaled the superficial velocity, μ equaled the gas viscosity, α equaled the screen solid volume fraction, n equaled the number of screens, h equaled the screen thickness, a equaled the screen wire radius, and k equaled:

$$k = -0.5\ln(2\alpha/\pi) + (2\alpha/\pi) - 0.75 - ((2\alpha/\pi)^2)/4 \quad \text{equation 7}$$

The theoretical penetration (P_{nd}) was:

$$P_{nd} = 10^{-nm} \quad \text{equation 8}$$

where m equaled:

$$m_d = A_0 Pe^{-2/3} + A_1 R^2 + A_2 Pe^{-1/2} R^{2/3} \quad \text{equation 9}$$

where Pe equaled the peclet number and R equaled the interception parameter. A_0 , A_1 , and A_2 were determined using the theory of Cheng, Yeh, and Orman (1982).

$$A_0 = 1.17B \quad \text{equation 10}$$

$$A_1 = 0.434B/k \quad \text{equation 11}$$

$$A_2 = 0.539B/(k^{1/2}) \quad \text{equation 12}$$

where B equaled:

$$B = 4\alpha h/\pi(1-\alpha)D_f \quad \text{equation 13}$$

and D_f equaled the diffusion coefficient.

Measured pDB Stage Pressure Drop and Penetration

For each stage, the pressure drop was measured with an inclined manometer (Model 400 Red Fluid, Dwyer Instruments, Inc., Michigan City, IN) at a pDB airflow rate of 0.7 L min^{-1} . The stage particle penetration by size was determined using the set up shown in Figure 13A. Two nebulizers (Model AirLife, Cardinal Health, McGaw Park,

IL) were used to generate test aerosol composed of ammonium fluorescein particles of widely varying size. The nebulizers were operated with one containing a solution of 2.5 g fluorescein in 1L of N NH₄OH and the other containing a solution of 0.123 g of fluorescein in 1 L of N NH₄OH. The test aerosol was diverted into a mixing chamber and mixed with HEPA-filtered air.

A scanning mobility particle sizer (SMPS) (SMPS+C model 5.4, Grimm, Ainring, Germany) was used to measure the particle number concentration by size alternately without (WO) or with (W) the pDB inline before the SMPS in the following sequence: WO_{Start}, W_{Stage A}, W_{Stage B}, W_{Stage C}, W_{Stage D}, WO_{End}. The SMPS airflow was only 0.3 L min⁻¹ so a supplemental pump (Model Omni, BGI Incorporated, Waltham, MA) was used to draw additional airflow to obtain 0.7 L min⁻¹ through the pDB. This sequence was repeated four times. The penetration of each stage (P_{Stage}) was calculated for each sequence using equation 14:

$$P_{\text{Stage},d} = W_{\text{Stage},d} / [WO_{\text{Start},d} + WO_{\text{End},d}]/2] \quad \text{equation 14}$$

where d was particle size. TableCurve 2D version 3 (Systat Software, Inc., San Jose, CA) was used to fit an equation to the mean penetration curve of Stage A by particle size (P_{TC,Stage A,d}).

Detection Efficiency

The detection efficiency by particle size (DE_d) of the CPC to the SMPS was needed in the inversion to compare the results of the pDB+CPC with inversion to the SMPS. The CPC does not measure the number concentration of all particles with diameters between 9.5 nm to 1000 nm with the same accuracy as the SMPS. For this study, the DE_d was used to correct for those differences in accuracy to reduce the differences of CPC measurements to ± 20% of the SMPS measurement.

The DE_d was determined using monodispersed ammonium fluorescein particles (Figure 13C). A nebulizer (Model AirLife, Cardinal Health, McGaw Park, IL) generated ammonium fluorescein aerosols from a solution of 2.5 g fluorescein in 1L of 0.01 N

NH_4OH . The resulting aerosol was injected into a mixing chamber, passed through a desiccant dryer, and then passed into an electrostatic classifier (Model 3071, TSI, Inc., Shoreview, MN), which was operated in overpressure mode. The electrostatic classifier was used to select particles with a mean size of 54, 80, 97, 119, 147, 292, 430, 493, and 566 nm. The monodispersed particles were then sent into a chamber where they were diluted with HEPA filtered air and measured with the CPC and SMPS. Three measurements of each particle size were taken using the CPC and SMPS for six minutes each, the time needed for one measurement of the SMPS. The CPC logged data every second and the results were averaged over the six minute SMPS measurement.

An iterative approach using a spreadsheet (Excel 2007, Microsoft Corp., Seattle, WA) was used to compute the DE_d for particle diameters from 9 to 1000 nm. The iterative approach was necessary to adjust for the presence of multiple charged particles in the monodispersed aerosol which caused some of the particles to be of sizes other than the intended size. For each monodispersed particle measurement, the three SMPS number concentration measurements were input in the spreadsheet by particle size bin. The mean of the three monodispersed SMPS number concentration measurements were calculated for each bin. Potential DE_d values for each particle size bin (starting with all DE_d values equal to 1) were then multiplied by the calculated mean number concentration of each bin. The product of the DE_d value and the calculated mean number concentration of each bin were then summed to calculate the SMPS number concentration for each monodispersed particle size. The raw ratio of CPC number concentration divided by the SMPS number concentration was calculated for each monodispersed particle size. The values of DE_d were changed by hand, while retaining a power relationship between DE_d and particle diameters, until the ratios for all monodispersed diameters were between 0.8 to 1.2. A regression line was then fit to the DE_d values from 9.5 nm to 1000 nm.

Inversion Spreadsheet

A data inversion spreadsheet was developed to estimate the number median diameter (NMD), geometric standard deviation (GSD), and number concentration of a lognormal, unimodal aerosol from particle number concentrations measured with the CPC exiting the four stages of the pDB (N_A , N_B , N_C , and N_D). Following Cheng and Yeh (1984), the spreadsheet included theoretical screen penetrations for each stage and experimentally determined particle losses from the aerosol entering the pDB and the DE_d . The inversion was implemented in an Excel spreadsheet (2007, Microsoft Corp., Seattle, WA) using the ‘Inversion Method’ described by O’Shaughnessy and Raabe (2003). A representation of the inversion spreadsheet is shown in Figure 14 and instructions for creating the spreadsheet are in Appendix B.

Initial input values were: NMD = 500 nm; GSD = 2; and number concentration = N_A . The inversion used 100 diameter size bins between 9.5 nm and 1000 nm ($0.991-3 \log_{10}$ diameter by increments of 0.02009 log diameter) and the NORMDIST function to compute the theoretical cumulative fraction values associated with the 100 bins for the log of the beginning NMD and GSD. The number concentration of each bin was determined by calculating the number fraction in each bin and then multiplying it by the input number concentration. Then, for each stage, the number concentration of each bin was multiplied by the penetration of Stage A ($P_{TC,Stage A,d}$)—which adjusted for particle losses of the aerosol entering the pDB—the theoretical penetration through the screens that define the stage (Stage B = $P_{5,d}$, Stage C = $P_{11,d}$, Stage D = $P_{16,d}$), and the DE_d to calculate the bin number concentration that penetrated each stage. The total number concentrations that passed through each stage (Inv_A , Inv_B , Inv_C , and Inv_D) were then calculated by summing the calculated bin number concentrations that penetrated their respective stages. The Microsoft add-in “Solver” adjusted the initial NMD, GSD, and number concentration until the sum of square differences between the total number

concentrations that passed through each and the input number concentrations from the pDB+CPC was minimized (equation 15) .

$$\min = (N_A - \text{Inv}_A)^2 + (N_B - \text{Inv}_B)^2 + (N_C - \text{Inv}_C)^2 + (N_D - \text{Inv}_D)^2 \quad \text{equation 15}$$

Constraints were input into “Solver” to keep it from providing solutions outside of the distribution assumptions. The initial constraints were an aerosol distribution number concentration greater than N_A , NMD between 1 and 500 nm, and GSD between 1.1 and 3. The constraints were updated after the inversion limitations were determined.

pDB+CPC Inversion Spreadsheet Limitations

The lower and upper limits of the distribution NMD that could be distinguished and the minimum number of pDB stages used in the inversion while maintaining the same level of accuracy were theoretically evaluated to identify limitations of the pDB+CPC inversion. The lower and upper limits of the NMDs that could be distinguished with the pDB+CPC inversion were determined using 23 distributions created with the inversion spreadsheet. Values for Inv_A , Inv_B , Inv_C , and Inv_D were calculated by inputting a distribution NMD, GSD, and number concentrations into the spreadsheet. The inversion spreadsheet was then reset and the calculated Inv_A , Inv_B , Inv_C , and Inv_D were then entered in the inversion as N_A , N_B , N_C , and N_D . The inversion was then solved to calculate the distribution NMD, GSD, and number concentration. An NMD was considered below the lower limit or above the upper limit if at least one of the four following occurred: the inversion distribution NMD was more than $\pm 10\%$ different from the original distribution NMD, the inversion distribution GSD was more than $\pm 5\%$ different from the original distribution GSD, the inversion distribution number concentration was more than $\pm 5\%$ different from the original distribution number concentration, and/or the inversion solved to a constraint.

The pDB+CPC inversion was evaluated to determine if less than all four stages could be used without reducing accuracy. Once the lower and upper NMD limits were identified, their distributions were solved with the inversion using less than four stages.

Six configurations of two stages and four configurations of three stages were tested. For both distributions, the four values of N_A , N_B , N_C , and N_D were entered into the data inversion. Then “Solver” was changed to solve for each configuration by only including the stages of the configuration in equation 15. A number of stages was unacceptable if, for either size distribution, at least one of the following occurred: the inversion distribution NMD was more than $\pm 10\%$ different from the original distribution NMD, the inversion distribution GSD was more than $\pm 5\%$ different from the original distribution GSD, the inversion distribution number concentration was more than $\pm 5\%$ different from the original distribution number concentration, and/or the inversion solved to a constraint.

Polydispersed Aerosols

To validate the inversion spreadsheet, the particle number concentration by size estimated with the pDB+CPC with inversion spreadsheet was compared to that measured with the SMPS for two test aerosols: exhaust from a propylene torch (Model MAP-Pro, Worthington Cylinders, Columbus, OH) and a burning incense stick. Those aerosols were chosen to examine different size distributions: the propylene torch exhaust is composed of particles less than 100 nm, and incense exhaust is composed of particles both less than and greater than 100 nm. As shown in Figure 13B, the test aerosol was directed into a mixing chamber and diluted with HEPA-filtered air. The test aerosol was then passed into a sampling chamber where they were measured with the pDB+CPC and then immediately after with the SMPS. A pump (Model Omni, BGI Incorporated, Waltham, MA) was attached to the sampling chamber to keep a constant flow through the chamber. Two pDB solenoid valve timings were used for these tests: 60 seconds a stage for a total time to cycle through the four stages of 240 seconds; and 20 seconds a stage for a total time to cycle through the four stages of 80 seconds. The CPC was set to log particle number concentrations every second. The first ten 1-second measurements of each stage were not included in the stage mean to allow the aerosol to clear the pDB before measuring the

aerosol of the stage. Three runs of alternating pDB+CPC then SMPS measurements were conducted.

The means for each stage of the pDB+CPC were calculated (N_A , N_B , N_C , and N_D) from the one-second measurements logged by the CPC. The times when the pDB+CPC switched to a new stage were recorded by an observer. The N_A , N_B , N_C , and N_D were input into the inversion and the NMD, GSD, and number concentration of each measurement were calculated. The inversion upper NMD limit that was identified during the pDB+CPC inversion spreadsheet limitation tests was input into Solver as a constraint to replace the original constraint of 500 nm; the lower NMD limit remained at 1 nm.

The estimates of NMD, GSD, and number concentration from the pDB+CPC with inversion were compared to those measured by the SMPS. Results were flagged when the pDB+CPC with inversion distribution NMD, GSD, and/or number concentration estimated differed from the SMPS measured distribution by $\pm 25\%$. Number concentration comparisons were not conducted for the aerosols where the SMPS was unable to measure the entire distribution.

The number concentration of particles between 9.4 nm to 100 nm was determined for twelve runs to determine the ability of pDB+CPC with inversion to measure the nanoparticle portion of the aerosols. The ratio ($R_{9.4-100}$) of number concentration of particles between 9.4 nm to 100 nm measured by the pDB+CPC with inversion to number concentration of particles between 9.4 nm to 100 nm measured by the SMPS was calculated for each run using equation 16.

$$R_{9.4-100} = (\text{pDB+CPC estimate } 9.4-100 \text{ nm}) / (\text{SMPS } 9.4-100 \text{ nm}) \quad \text{equation 16}$$

Results

pDB Stage Pressure Drop and Penetration

As shown in Table IX, the observed mean pressure drops across the screens were more than seven times the theorized pressure drops for the screens alone. The mean

observed pressure drops included the screen pressure drop and also the pressure drops across the tubing, connectors, and solenoid valves.

The measured penetrations through each stage of the pDB are shown in Figure 15. Equation 17 was fitted to experimental data to represent the penetration of Stage A

$$P_{TC,Stage A,d} = 1 - 0.033 + (2.99/d) \quad \text{equation 17}$$

where d is the particle diameter in nm. For Stages B, C, and D, the observed penetration did not increase for particles larger than approximately 150 nm, while the inversion penetration curves did not increase for particles larger than approximately 300 nm.

The inversion penetrations used in the inversion spreadsheet for Stages B, C, and D—which are the product of $P_{TC,Stage A,d}$ and the screen theoretical penetrations—were larger than the observed penetrations for particles larger than 30 nm.

Detection Efficiency

Figure 16 shows the iterated DE_d values with the fit regression line represented by Equation 18 where d is the particle diameter in nm. The R^2 value was 0.92.

$$DE_d = 1.22d^{0.07} \quad \text{equation 18}$$

Figure 17 shows how the ratios of CPC number concentration divided by the product of the SMPS number concentration and DE_d changed through the iteration process. When the DE values were equal to 1, the ratio values for the monodispersed diameters of 119 and 292 were not within 0.8 to 1.2. With the DE_d values equal to equation 18, the ratio of CPC number concentration divided by the product of the SMPS number concentration and DE_d was between 0.88 to 1.07 for all monodispersed particle size.

pDB+CPC Inversion Spreadsheet Limitations

The results of the ten aerosol distributions used to determine the inversion lower and upper NMD limits are shown in Table X. The lower and upper limit of the pDB+CPC with inversion was 17 nm and 286 nm, respectively. The inversion distribution for the 16 nm original distribution solved to a constraint with regard to GSD for the original GSD of 1.4. The inversion distribution for the 287 nm original

distribution solved to a GSD of 1.52 for the original GSD of 1.4, which was greater than the 5% difference allowed.

The results of the required stage number evaluation are shown in Table XI. The distribution used to represent the lower limit of the inversion was NMD of 17 nm, GSD of 1.4, and number concentration of 50,000 particles cm^{-3} . The distribution used to represent the upper limit of the inversion was NMD of 286, GSD of 1.4, and number concentration of 50,000 particles cm^{-3} . The combinations that solved for both distributions were: Stages A, B, and C; Stages A, B, and D; and the four stage combination.

Polydispersed Aerosols

The results of measuring exhaust from a propylene torch and incense stick are shown in Table XII, Table XIII, Figure 18, and Figure 19. The 240-second propylene torch distributions measured by the SMPS had a NMD of 15 nm with GSD ranging from 1.42 to 1.49 (Table XII), while the 80-second distributions were slightly larger with a NMD of 17 and GSD ranging from 1.43 to 1.49. The number concentrations for the 240-second distributions were approximately 10,000 particles cm^{-3} less than the 80-second distributions. The NMD and GSD of the 240-second and 80-second distributions measured by the pDB+CPC with inversion ranged from 11 nm to 17 nm with a GSD of 1.30 to 1.71, and 17 nm with a GSD of 1.43 to 1.49, respectively (Table XII and Figure 18). The range of NMD and GSD for the 240-second distributions measured with the pDB+CPC with inversion were greater than the 80-second measurements although the variability in the propylene torch distributions measured by the SMPS for both timings were similar. The number concentrations measured with the pDB+CPC with inversion was larger than measured with the SMPS for the 240-second measurements but were less than the SMPS measured for the 80-second measurements. The only NMD or GSD that exceeded the $\pm 25\%$ criteria for the propylene torch was the third 240-second run (Table XII). The number concentration could not be compared because the entire distribution

was not measured by the SMPS (Figure 18). The $R_{9,4-100}$ was from 0.86 to 1.09 (Table XIII).

The 240-second incense distributions measured by the SMPS had NMD of 97 nm to 107 nm with GSD ranging from 1.74 to 1.82 (Table XII) while the 80-second distributions were slightly narrower with NMD of 97 nm and a GSD ranging from 1.57 to 1.74. The number concentrations of the 240-second distributions were greater than the 80-second distributions (Table XII and Figure 19). The NMD of the 240-second incense distributions measured by the pDB+CPC with inversion ranged from 87 nm to 156 nm and 69 nm to 113 nm for the 80-second distributions. Two of the three 240-second and two of the three 80-second distributions solved to the constraint $GSD = 1.3$. The NMDs and GSDs of the 240-second incense and 80-second distributions that did not solve to a constraint were 87 nm with 1.56 and 94 nm with 1.52, respectively. Three of the incense runs were larger than the $\pm 25\%$ criteria for NMD and two were larger than $\pm 25\%$ for GSD and number concentration (Table XII). All the runs that were larger than $\pm 25\%$ for NMD, GSD, and number concentration had solved to a constraint. Although the last 80-second incense run solved to a constraint, the NMD, GSD, and number concentration estimate were all within $\pm 25\%$. $R_{9,4-100}$ was 0.90 and 0.99 for the runs where the pDB+CPC inversion did not solve to a constraint and was from 0.06 to 1.98 for runs where the pDB+CPC inversion solved to a constraint (Table XIII).

Discussion

A pDB was designed and constructed that can be placed in a backpack to be carried by a worker. When combined with a handheld CPC, the pDB+CPC with a data inversion can be used to determine differences between submicron distributions. When the inversion did not solve to a constraint, the accuracy of the pDB+CPC with inversion compared to the SMPS was acceptable with only the last 240-second propylene torch run NMD falling outside of $\pm 25\%$. The pDB+CPC with inversion was able to place the distribution NMD within 5 nm for the propylene torch and within 50 nm for incense even

with four of the six incense measurements solving to a constraint (Table XII). The SMPS and electrical low pressure impactor (ELPI) are the only instruments commercially available that provide similar information (Baron & Willeke, 2001). Due to their size, both of these instruments are impractical for personal measurements.

The ratio of $R_{9,4-100}$ (Table XIII) being close to one was to be expected for the propylene torch because the portion of the distribution that could be measured by the SMPS was entirely below 100 nm. Thus differences in NMD and GSD were masked. That was not true for the incense $R_{9,4-100}$. Differences in NMD and GSD from the pDB+CPC inversion solving to a constraint caused almost the entire distribution to fall above or below the 100 nm cut off.

The accuracy of the pDB+CPC distribution estimate compared to the distribution measured by the SMPS was not reduced by shortening the valve sequencing to 80 seconds. There was only one 80-second run where the pDB+CPC estimated NMD was more than 25% different than the SMPS measurement while there were three 240-second runs where the NMD was more than 25% different (Table XII). An 80-second measurement was almost five times faster than the six-minute measurement time required for a full scan of the SMPS+C model 5.4 Grimm SMPS used in this study.

The pDB+CPC with inversion estimations of the propylene torch distribution NMDs, GSDs, and number concentrations were not equal to those measured by the SMPS. The difference in NMDs, GSDs, and number concentrations may be due to the propylene torch distributions having had NMDs below or equal to the lower limit of the data inversion (Table XII).

The design of the screen-type diffusion battery in the pDB was different from others used in the past (Cheng & Yeh, 1980; Cheng et al., 1980; Cheng et al., 1985; Yeh et al., 1982). The design of the pDB caused the entire airflow through the screen-type diffusion battery to go through a 90 degree turn before going into the solenoid valve manifold. The majority of the flow in the screen-type diffusion battery used in past

studies went straight through the screen-type diffusion battery with only part of the flow turning 90 degrees. Also, the superficial velocity of the screen-type diffusion battery was lower than those in past studies. The superficial velocity of this study was two-thirds that of the lowest superficial velocity of the past studies, after correcting for differences in atmospheric pressure. The pDB also had a sampling tube and a unique valve switching device. In Table IX, the larger observed pressure drop across the stages compared to the theoretical pressure drop across just the screens illustrates the importance of the other components of the pDB. Their influence on how the pDB will function cannot be ignored.

The inversion spreadsheet was created in a commonly used computer software instead of an inversion computer program as was done by Cheng and Yeh (1984). Due success of the inversion computer program, it served as a guide for the inversion spreadsheet thus the theoretical screen penetrations, DE_d , and $P_{TC,Stage A,d}$ were included the inversion spreadsheet. The use of the observed penetrations in the data inversion spreadsheet instead of the theoretical screen penetrations and the $P_{TC,Stage A,d}$ has not been evaluated: it may improve the estimates because the observed penetrations should account for both the theorized penetrations and the particle losses from entering the pDB. This study found a difference in the observed and inversion penetrations (Figure 15) and it is unknown how the difference would influence inversion spreadsheet distribution estimates.

The upper limit of the pDB+CPC with inversion was not experimentally verified and is a limitation of this study. The upper limit of the pDB+CPC with inversion may be less than the 286 nm determined from the analysis of the pDB+CPC inversion spreadsheet. The observed penetrations were larger than the computed inversion penetrations (Figure 15) with the maximum penetrations occurring at approximately 150 nm for the observed penetrations instead of approximately 300 nm for the inversion penetrations. The lack of penetration distinction between stages for particles larger than

150 nm may have reduced the upper limit of the pDB+CPC with inversion to less than 286 nm. Also, it is unknown if a cyclone or impactor is required on the front of the pDB to remove larger particles before the device can be used in a workplace. A cyclone or impactor was required on the front of the screen-type diffusion battery used by Cheng and Yeh (1984) because their inversion program included only penetration values equal to 1 for particle sizes larger than the maximum penetration particle size. Programming the penetration values to equal 1 required the measured aerosol distributions to fall below the particle size of maximum penetration. The inversion spreadsheet had penetration values for particle sizes up to 1000 nm, which were larger than the particle size of maximum penetration. If a NMD distribution included particles larger than the upper limit of the inversion spreadsheet but smaller than the upper limit of the CPC (1000 nm), it should solve to the NMD upper constraint of 286 nm, but that has yet to be verified.

This study did not test the influence of reducing or increasing the number of stages in the pDB screen-type diffusion battery. The inversion distribution results (Table XI) identified that the pDB should be able to be reduced to three stages, either Stages A, B, and C or Stages A, B, and D, without reducing the range of distribution NMDs that could be estimated. Rearranging the 16-screen configuration across an increased number of stages may be more useful for increasing the accuracy of measuring aerosols compared to the SMPS than adding additional stages with additional screens. The maximum penetration of the inversion penetration was at approximately 300 nm (Figure 15). With 16 screens, the observed penetration maximum only extended to 60% which caused at least 40% of all particles greater than the maximum to be removed without size separation. Adding additional screens would increase the percentage of particles greater than the maximum that would be removed without size separation and eventually there would be no benefit in including the additional screens in the diffusion battery. At 16 screens a benefit has been shown, but the benefit for a greater number of screens is unknown.

There are limitations with use of the pDB+CPC in work environments. The pDB was designed to be carried by a worker with minimal interference in a backpack. Although wearing a backpack has not been found to influence basic mobility (Al-Khabbaz, Shimada, & Hasegawa, 2008; Goh, Thambyah, & Bose, 1998; Hong & Cheung, 2003), backpacks with a load cause a shift in the body's center of gravity which causes the worker to lean forward (Goh et al., 1998). The fact that tilting of the TSI CPC 3007 can cause the optics to flood with condensation fluid (TSI Incorporated, 2004) prevents its use in a backpack. Thus the pDB+CPC is impractical for personal sampling, although exposures could be measured by placing a sampling tube in a worker's breathing zone while having the pDB+CPC stationary near the worker. Future work is needed to identify a robust detector that can be used in a backpack with the pDB, but the pDB has shown promise for measuring worker exposure to nanoparticles.

Conclusions

A four-stage personal diffusion battery was designed to be coupled with a direct-reading instrument to measure the size distributions of aerosols with a NMD from 17 nm to 286 nm. A mathematical data inversion spreadsheet was developed to convert the CPC number concentration to a size-distribution estimate to provide additional information on unimodal submicron aerosols containing nanoparticles. In a theoretical evaluation, the pDB+CPC inversion was found capable of determining the particle size distribution of an aerosol with a NMD between 17 nm to 286 nm with all four pDB stages.

Experiments were conducted and identified that the penetration by size of the particles through each stage of the pDB were less than the calculated inversion penetrations. The NMD measured with the pDB+CPC with inversion was within 5 nm of that measured with a SMPS for propylene torch exhaust and within 50 nm for incense. The ratios of number concentration less between 9.4 nm to 100 nm measured by the pDB+CPC with inversion to that measured by the SMPS was from 86% to 109% when the inversion did not solve to a constraint and from 6% to 198% when the inversion did

solved to a constraint. It is unknown why four of the six inversions for the larger incense aerosols solved to a constraint. Future work is needed to find a detector that can be placed in a backpack, verify the upper limit of the inversion, and determine if a cyclone or impactor is needed on the front of the pDB.

Table IX: Theoretical pressure drops across only screens and observed pressure drops across each stage of pDB at 0.7 L min^{-1} .

Stage	Theoretical Across Screens	Observed Across pDB Stages
	Pressure Drop (inches H ₂ O)	Mean (inches H ₂ O)
A	-	0.42±0.01
B	0.03	0.47±0.01
C	0.07	0.50±0.12
C	0.10	0.73±0.01

Table X: Original distributions and inversion distribution results to determine lower and upper NMD that could be distinguished with the pDB+CPC inversion.

Original Distribution			Inversion Distribution		
NMD (nm)	GSD	Number Concentration (particle cm ⁻³)	NMD (nm)	GSD	Number Concentration (particle cm ⁻³)
16	1.40	50,000	17	1.3*	47,489
16	1.50	50,000	16	1.50	49,980
16	2.00	50,000	16	2.00	49,982
16	2.80	50,000	16	2.80	50,003
17	1.40	50,000	17	1.40	49,997
17	2.00	50,000	17	2.00	49,993
17	2.80	50,000	17	2.80	50,010
50	1.40	50,000	50	1.40	50,000
50	2.00	50,000	50	2.00	50,000
50	2.80	50,000	50	2.80	50,000
200	1.40	50,000	200	1.40	49,997
200	2.00	50,000	200	2.00	49,991
200	2.80	50,000	199	2.80	49,970
250	1.40	50,000	250	1.40	49,995
250	2.00	50,000	248	1.99	49,929
250	2.80	50,000	249	2.79	49,937
286	1.40	50,000	287	1.41	50,010
286	2.00	50,000	281	1.98	49,755
286	2.80	50,000	286	2.80	49,987
287	1.40	50,000	310	1.52	50,343
287	1.50	50,000	287	1.50	50,002
287	2.00	50,000	282	2.00	49,726
287	2.80	50,000	285	2.79	49,851

* Represents inversion results that solved to a constraint.

Results in bold show when one of the following occurred: the inversion distribution NMD was more than $\pm 10\%$ different from the original distribution NMD, the inversion distribution GSD was more than $\pm 5\%$ different from the original distribution GSD, the inversion distribution number concentration was more than $\pm 5\%$ different from the original distribution number concentration, or the inversion solved to a constraint.

Table XI: Inversion distribution results for varying number of pDB+CPC stages to determine minimum number of stages required for the NMD particle size range of 17 nm to 286 nm.

Data Inversion Stages	Lower Limit Distribution NMD = 17 nm, GSD = 1.4 Number Concentration=50,000			Upper Limit Distribution NMD = 286 nm, GSD = 1.4 Number Concentration = 50,000		
	NMD (nm)	GSD	Number Concentration (particle cm ⁻³)	NMD (nm)	GSD	Number Concentration (particle cm ⁻³)
A, B	18	1.31	48,241	272	1.3*	49,847
B, C	500*	3.0*	38,092	304	1.50	50,251
C, D	500*	3.0*	38,092	273	1.3*	49,837
A, C	18	1.3*	47,912	272	1.3*	49,852
B, D	500*	3.0*	38,092	303	1.49	50,247
A, D	19	1.3*	47,675	272	1.3*	49,857
A, B, C	17	1.40	49,996	278	1.34	49,910
B, C, D	500*	3.0*	38,092	273	1.3*	49,847
A, C, D	18	1.31	47,947	272	1.3*	49,852
A, B, D	17	1.40	49,998	281	1.36	49,940
A, B, C, D	17	1.40	49,997	287	1.41	50,010

* Represents inversion results that solved to a constraint.

Results in bold show when one of the following occurred: the inversion distribution NMD was $\pm 10\%$ different from the original distribution NMD, the inversion distribution GSD was $\pm 5\%$ different from the original distribution GSD, the inversion distribution number concentration was $\pm 5\%$ different from the original distribution number concentration, or the inversion solved to a constraint.

Table XII: Polydispersed aerosol distributions measured with the SMPS and pDB+CPC with inversion.

Aerosol	Timing (sec)	SMPS Measured			pDB+CPC with Inversion		
		NMD (nm)	GSD	Number Concentration (particle cm ⁻³)	NMD (nm)	GSD	Number Concentration (particle cm ⁻³)
Propylene Torch	240	15	1.49	31,378**	13	1.67	45,503
Propylene Torch	240	15	1.42	29,302**	14	1.52	31,499
Propylene Torch	240	15	1.42	21,187**	11	1.71	37,025
Incense	240	107	1.75	96,022	156	1.3*	63,046
Incense	240	97	1.74	114,793	87	1.56	102,141
Incense	240	97	1.82	131,986	131	1.3*	105,569
Propylene Torch	80	17	1.43	43,633**	18	1.36	38,101
Propylene Torch	80	17	1.49	42,725**	19	1.32	37,618
Propylene Torch	80	17	1.43	37,955**	18	1.36	35,645
Incense	80	97	1.66	41,968	69	1.3*	45,587
Incense	80	97	1.74	82,325	94	1.52	76,803
Incense	80	97	1.57	72,589	113	1.3*	65,103

* Represents inversion results that solved to a constraint.

** Represents distributions that were not entirely measured by the SMPS therefore number concentration comparison was not able to be done.

Results in bold show when one of the following occurred: the pDB+CPC with Inversion distribution NMD was $\pm 25\%$ different from the SMPS measured distribution NMD, the pDB+CPC with Inversion distribution GSD was $\pm 25\%$ different from the SMPS measured distribution GSD, the pDB+CPC with Inversion distribution number concentration was $\pm 25\%$ different from the SMPS measured distribution number concentration. Number concentration comparisons were not conducted for the aerosols where the SMPS was unable to measure the entire distribution.

Table XIII: Comparison of pDB+CPC with inversion to SMPS with regard to particle number concentrations between 9.4 nm and 100 nm for polydispersed aerosol distributions measured with the SMPS and pDB+CPC with inversion.

Aerosol	Timing (sec)	SMPS 9.4nm-100 nm Number Concentration (particle cm⁻³)	pDB+CPC with Inversion 9.4nm-100 nm Number Concentration (particle cm⁻³)	Ratio pDB+CPC/ SMPS (R_{9.4-100})
Propylene Torch	240	31,378	32,422	1.03
Propylene Torch	240	29,302	26,424	0.90
Propylene Torch	240	21,187	23,191	1.09
Incense	240	46,348	2,640*	0.06*
Incense	240	63,487	63,000	0.99
Incense	240	70,144	15,245*	0.22*
Propylene Torch	80	43,633	37,447	0.86
Propylene Torch	80	42,725	37,363	0.87
Propylene Torch	80	37,955	34,933	0.92
Incense	80	21,115	41,889*	1.98*
Incense	80	46,499	41,817	0.90
Incense	80	38,574	19,920*	0.52*

* Represents inversion results that solved to a constraint.

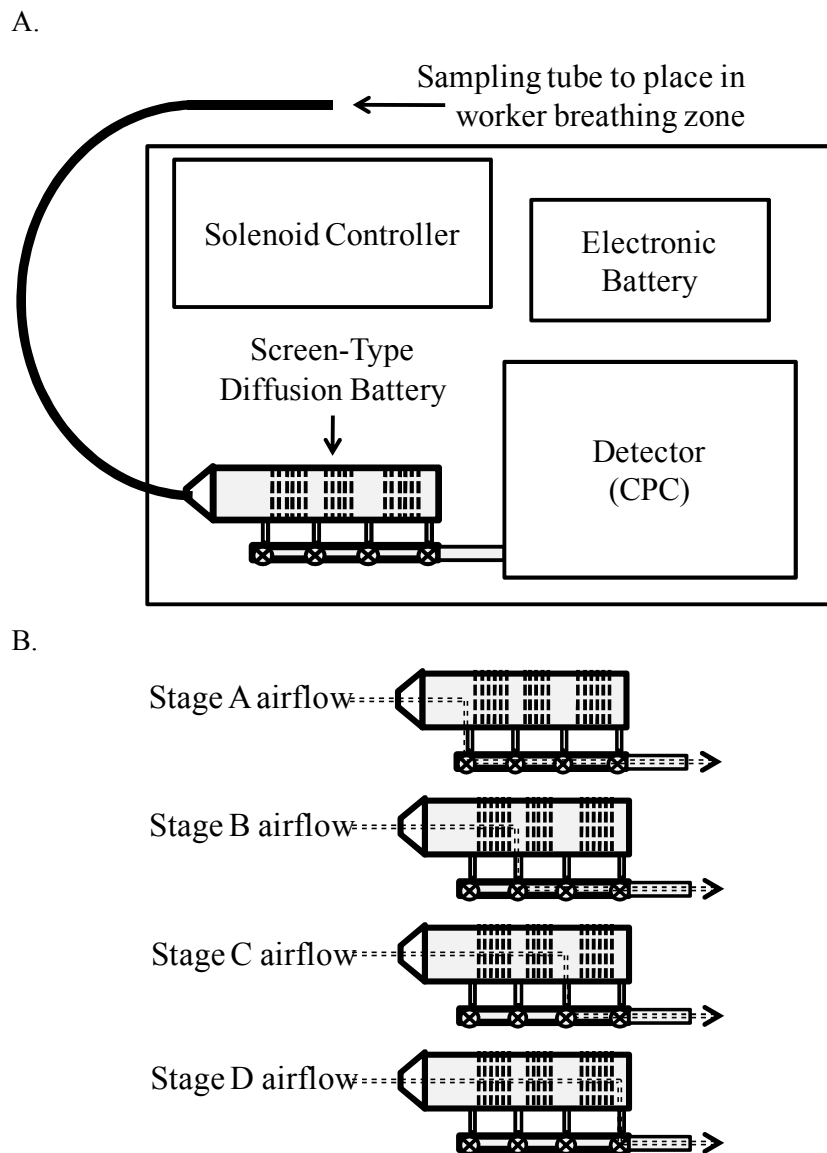
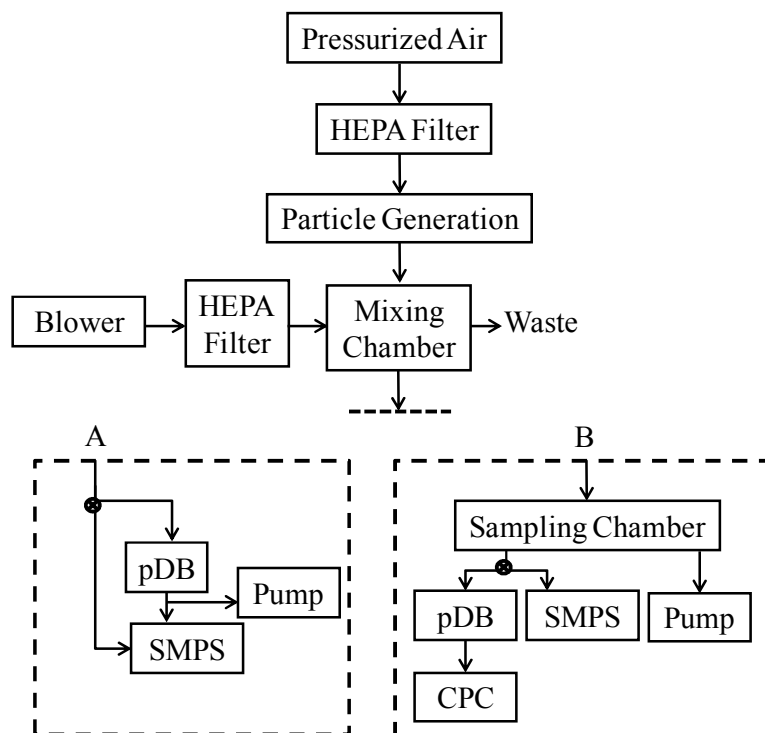


Figure 12: Personal diffusion battery (pDB) (A.) Schematic of the pDB (B.) Airflow through each stage of pDB.

A. and B.



C.

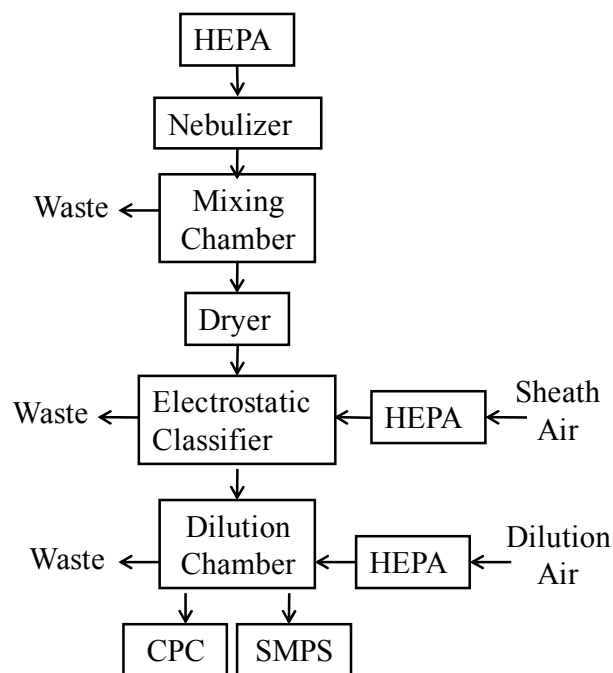


Figure 13: Experimental set ups to (A.) Determine particle penetration across the pDB at 0.7 L min^{-1} (B.) Test pDB+CPC with inversion using combustion aerosols (C.) Determine detection efficiency of CPC to SMPS.

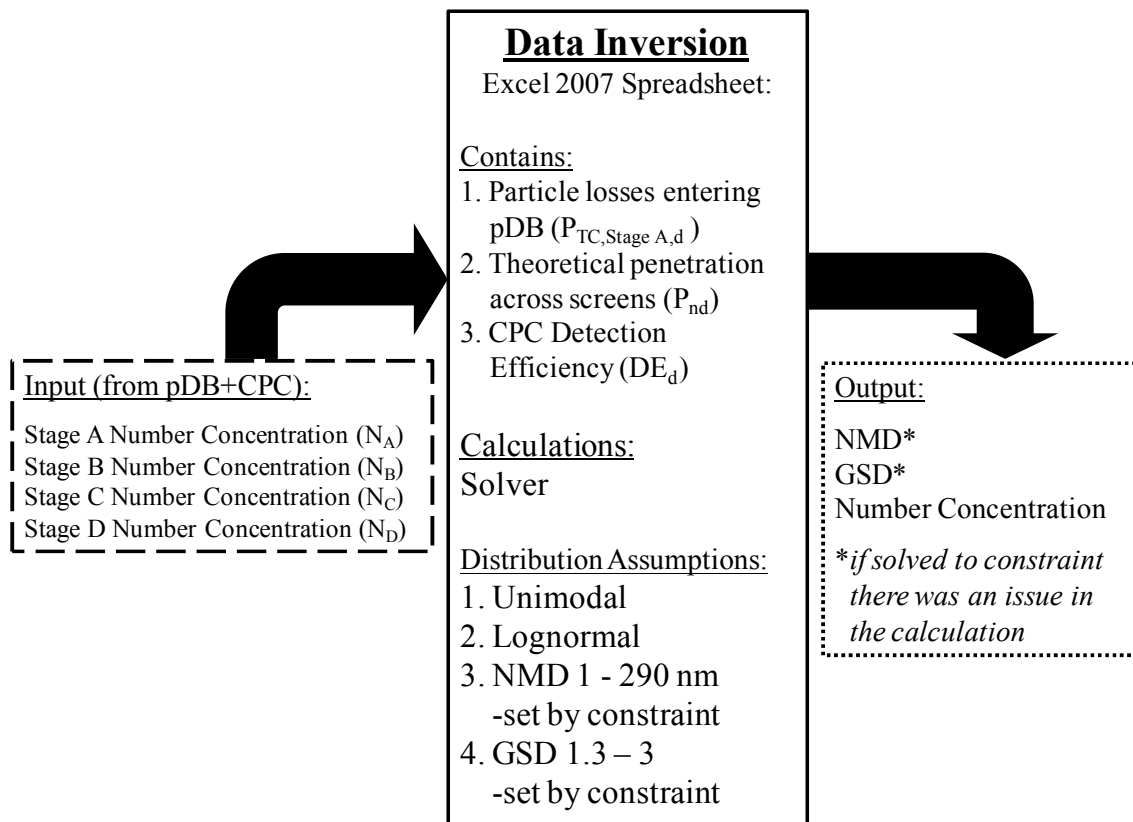


Figure 14: Representation of the inversion spreadsheet specifying the input, output, and required parts of the spreadsheet.

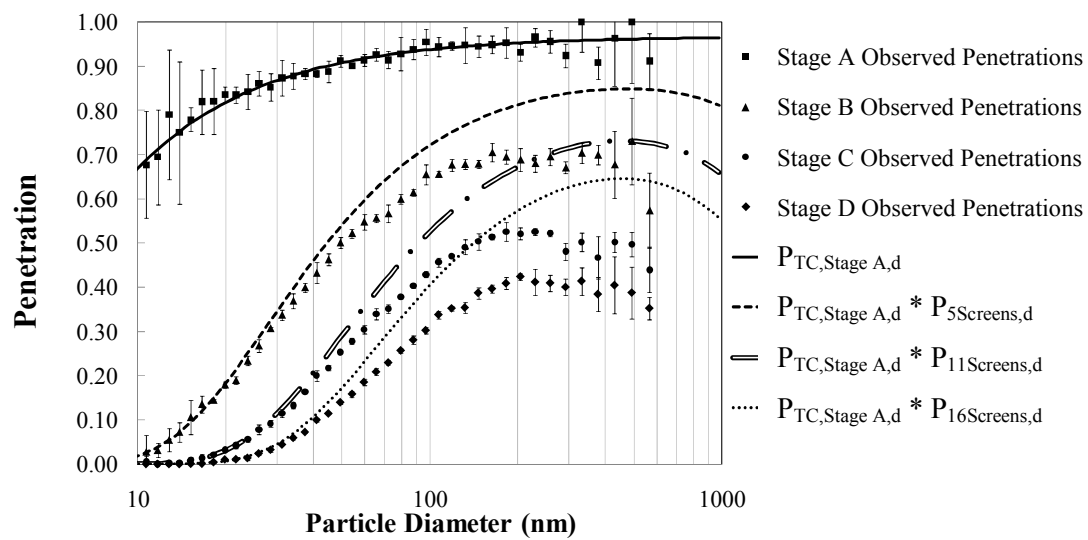


Figure 15: pDB observed and inversion penetrations for airflow of 0.7 L min^{-1} .

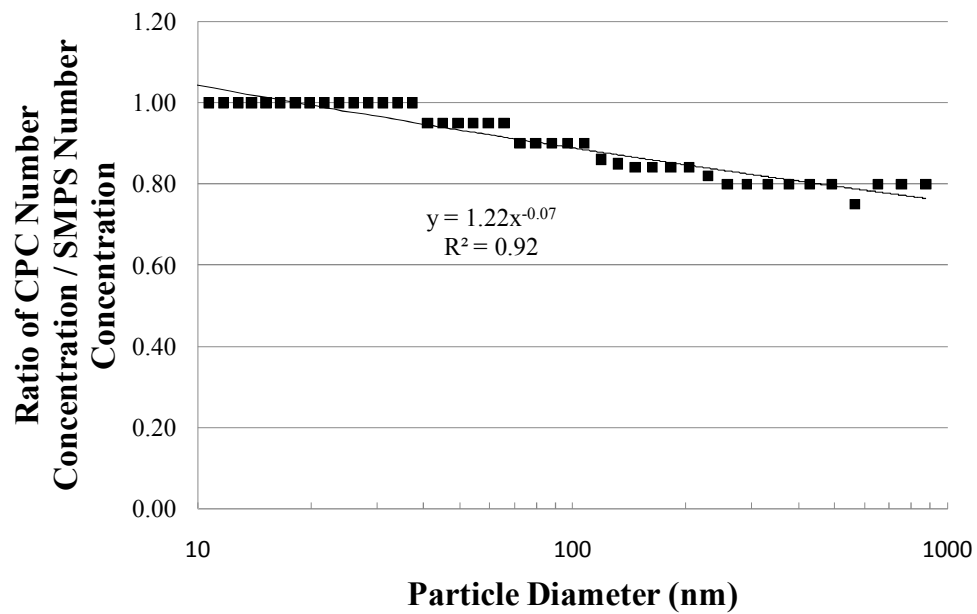


Figure 16: Iterated DE values with the fit regression line.

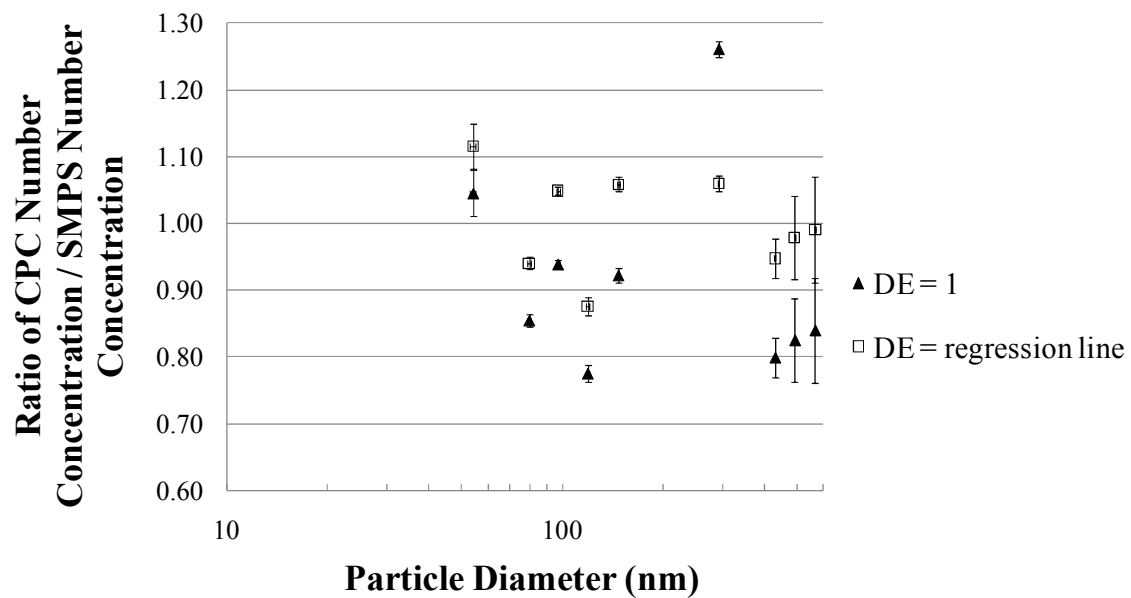
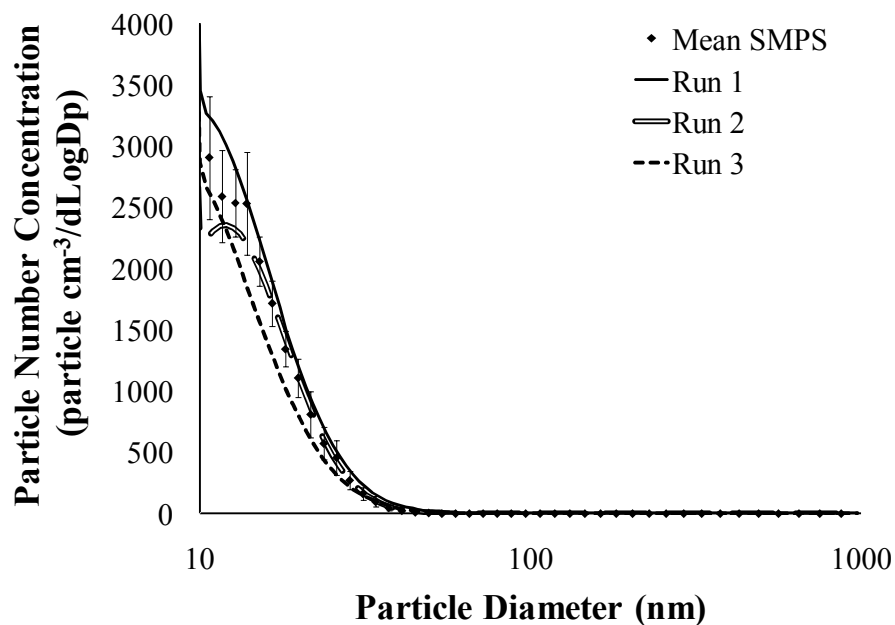


Figure 17: Ratios of CPC number concentration to the product of SMPS number concentration and DE_d when DE_d values equaled 1 and when they equaled the regression line.

A. 240-Second Measurements



B. 80-Second Measurements

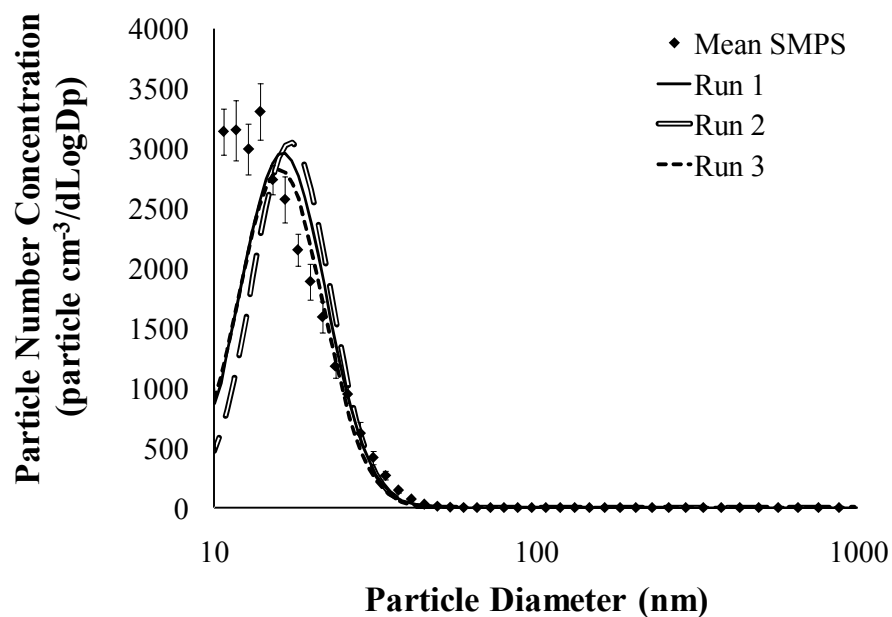
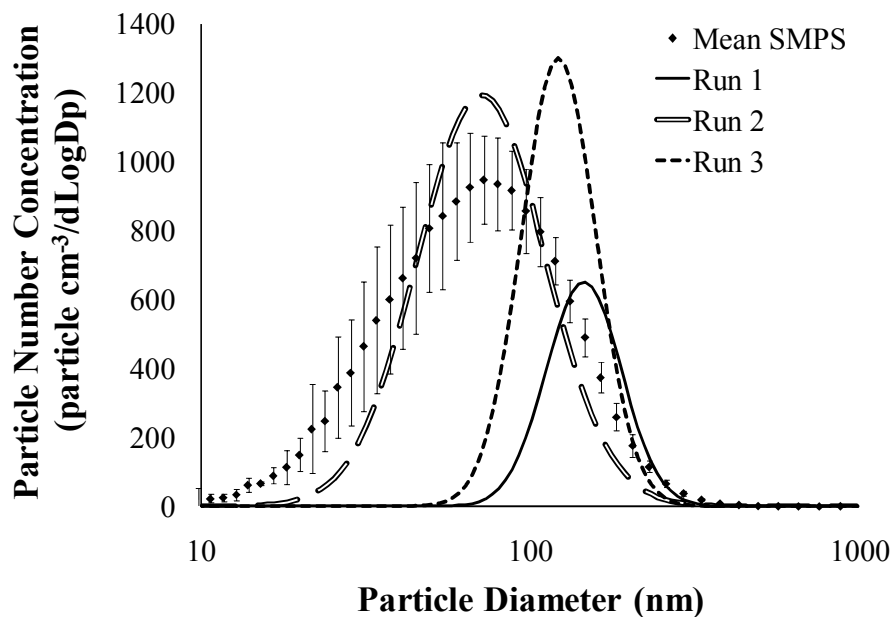


Figure 18: Comparison of the mean propylene torch measured by the SMPS and the results of the three pDB+CPC with inversion runs for the 240-second measurements (A) and 80-second measurements (B).

A. 240-Second Measurements



B. 80-Second Measurements

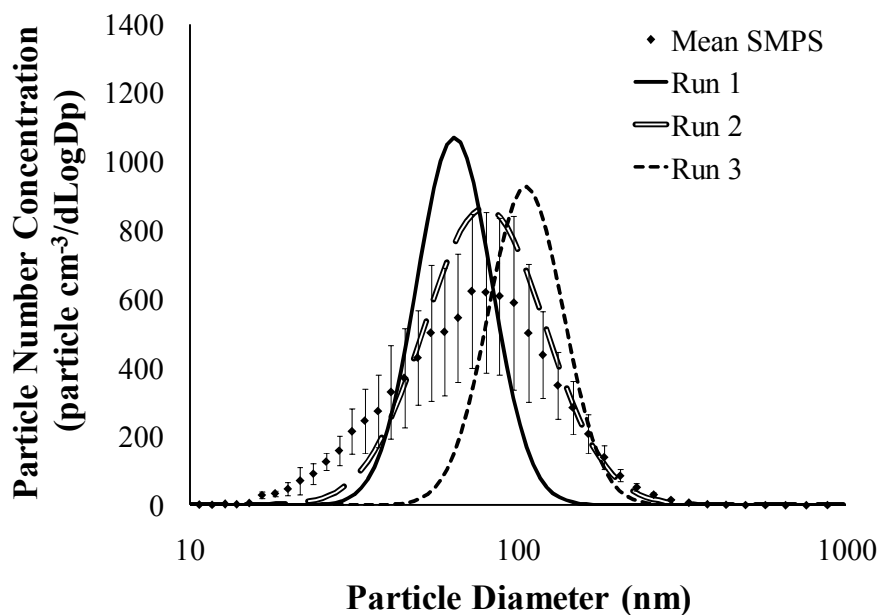


Figure 19: Comparison of the mean incense measured by the SMPS and the results of the three pDB+CPC with inversion runs for the 240-second measurements (A) and 80-second measurements (B).

CHAPTER V

CONCLUSIONS

The three studies reported on in this dissertation provide knowledge on assessing airborne nanoparticle concentrations in the workplace. The first study characterized airborne nanoparticle concentrations with direct-reading instruments in a work environment that had not previously been investigated. The second study evaluated a commercially available direct-reading instrument for measuring airborne nanoparticle concentrations. The third study developed a device to be coupled with a direct-reading instrument to measure personal nanoparticle exposure of a worker.

Evidence presented in Chapter II supports the idea that hot processes produce substantial nanoparticle concentrations even with control measures in place. Nanoparticle number concentrations were found to be substantially greater than background measurements in a facility that produced waterproof, breathable apparel composed of PTFE fabric. The greatest concentrations were found in the breathing zone of workers responsible for sealing sewn seams, a hot process that had not previously been considered a particle generation source of hazard importance. Canopy hoods were ineffective at controlling fume generated by the sealing process. Limitations of canopy hoods when applied to this particular application may explain why they were ineffective.

Chapter III identified limitations of a DC2000CE that restrict its ability to measure airborne nanoparticle concentrations in the workplace. The active surface area concentration measured by the DC2000CE did not equal the geometric surface area concentration measured by the reference instruments and the ratio of the two decreased as particle size increased. The difference between the DC2000CE results and those of the reference instruments were not just a difference of measuring active versus geometric surface area concentration. The design of the DC2000CE also influenced its accuracy with respect to the reference instruments. Thus, the Sp ratio alone cannot be used as a calibration factor. The maximum measurable active surface area of a DC2000CE was

substantially greater than the maximum active surface area concentration stated by the manufacturer. This maximum value translates to a nanoparticle number concentration greater than the maximum number concentration measurable by some handheld CPCs. Care should be taken not to move or vibrate a DC2000CE while it is measuring aerosols in a workplace.

Chapter IV presented a novel four-stage personal diffusion battery (pDB) that was designed to be coupled with a direct-reading instrument to measure the size distributions of particles with a NMD smaller than 286 nm. A data inversion was developed to estimate the NMD, GSD, and number concentration from data measured with the pDB coupled with a handheld CPC (pDB+CPC) for lognormal, unimodal aerosols. In a theoretical evaluation, the pDB+CPC inversion was found capable of determining the particle size distribution of an aerosol with a NMD from 17 nm to 286 nm with all four pDB stages. The penetrations by size of the particles through each stage of the pDB were less than those calculated for the inversion using theoretical penetration across screens and particle losses entering the pDB. The pDB+CPC with inversion was evaluated using unimodal propylene torch exhaust and incense exhaust. For number concentrations of particles with diameters smaller than 100 nm, the pDB+CPC with inversion results were 86% to 109% of reference instrument results when the inversion did not solve to an inversion constraint. For inversion results that solved to a constraint, the number concentration of particles with diameters smaller than 100 nm was 6% to 198%.

Future Studies

Three future studies are envisioned to expand on the work presented in Chapter II. First, the composition of the particles in the facility should be determined to definitively confirm that the sealing process is the source of the nanoparticles. Compositional analysis would also help identify the hazard potential posed by nanoparticles in the facility. Second, the canopy hood at sealing stations should be redesigned to increase fume capture. A hood redesign would likely reduce nanoparticle exposures throughout the

facility. Third, airborne nanoparticle concentrations should be investigated in other industries that rely on work conducted near hot processes.

Future studies are needed before a DC2000CE could be used independently in a workplace to measure nanoparticle surface area concentrations. A calibration factor by size is needed to convert the active surface area concentration measured by the DC2000CE into the geometric surface area concentration measured by the reference instruments. The lower concentration limit of the DC2000CE should be tested to see if it equals with the minimum stated by the manufacturer. Other instruments that use diffusion charging should be evaluated to determine if and how their designs influence their surface area responses compared to a reference instrument. Direct-reading instruments that are designed to be taken into a workplace should be tested for the presence of physical limitations with regard to movement and vibration.

Future studies are needed to refine the pDB. The pDB+CPC with inversion must be tested with aerosols with a NMD between 150 nm to 250 nm to determine if the upper NMD limit of the pDB+CPC with inversion is less than the inversion limit of 286 nm. The pDB+CPC with inversion must also be tested with aerosols with NMD greater than 300 nm to determine if a cyclone or impactor is needed on the inlet. The cause of the reduced observed penetrations through the stages of the pDB compared to the inversion penetrations should be identified. Possible causes to be investigated include: the influence of requiring the aerosol to turn 90° as it goes through the screen-type diffusion battery; a superficial velocity lower than has been used in previous studies; and the influence of charged aerosol particles. For the pDB to truly be personal, a detector that can be placed in the backpack with the pDB must be identified. Once found, the detection efficiency of the detector with respect to the SMPS must be determined and included in the inversion.

APPENDIX A: CALCULATION OF NANOPARTICLE NUMBER
CONCENTRATION AND RESPIRABLE MASS USING A
CONDENSATION PARTICLE COUNTER (CPC) AND OPTICAL
PARTICLE COUNTER (OPC)

The nanoparticle number concentration (N) and respirable mass concentration (M) was estimated during aerosol mapping using measurements taken with a condensation particle counter (CPC) (Model 3007, TSI Incorporated, Shoreview, MN) and an optical particle counter (OPC) (PDM-1108, Grimm, Ainring, Germany). N was calculated by

$$N = (N_{cpc})(DF) - \sum_{i=1}^5 (N_{opc,i}) \quad \text{equation 19}$$

where N_{cpc} was the CPC number concentration, DF was the filter dilution factor of the HEPA filter with a hole that was on the inlet of the CPC, and $N_{opc,i}$ was the OPC number concentration for the given channel i . Equation 7 was used to calculate M where

$$M = \frac{\pi}{6} (dcpc)^3 \rho N(RPM)(dcpc) + \sum_{i=1}^{15} \frac{\pi}{6} (dmid,i)^3 \rho (N_{opc,i})(RPM)(dmid,i) \quad \text{equation 20}$$

$dcpc$ was the assumed midpoint diameter of the CPC (150 nm), ρ was the assumed particle density (1000 kg m^{-3}), RPM was the function of the respirable mass per ACGIH criteria (2007), and $dmid,i$ was the midpoint diameter of the OPC channel i .

APPENDIX B: CREATING THE INVERSION SPREADSHEET

The assumptions of the aerosol that would be measured were that it was unimodal and lognormally distributed with a number median diameter (NMD) between 1 and 1000 nm and a geometric standard deviation (GSD) between 1.3 and 3. The input into the inversion was the particle number concentrations for Stages, A, B, C, and D measured by the personal diffusion battery coupled with a condensation particle counter (Model 3007, TSI Incorporated, Shoreview, MN) (pDB+CPC). The output of the inversion was the NMD, GSD, and number concentration of the measured aerosol.

Steps to create the inversion spreadsheet

1. Define three cells on the spreadsheet where the NMD, GSD, and particle number concentration will be input.
2. Define four cells on the spreadsheet where the particle number concentrations for each stage (N_A , N_B , N_C , N_D) will be input.
3. In a column, create particle size bins in the spreadsheet for 100 diameters between 9.5 nm and 1000 nm ($0.991 \cdot 3 \log_{10}$ diameter by increments of $0.02009 \log$ diameter).
4. In the next column, compute the theoretical cumulative fraction values associated with each of the 100 particle size bins (TCF_{bin}) for a given NMD diameter and GSD using the NORMDIST function. The log of the midpoint diameter of the particle size bins, NMD, and GSD were taken to match the assumption of a lognormal aerosol distribution.

$$TCF_{bin} = \text{NORMDIST}(\text{LOG}(\text{bin}_d, 10), \text{LOG}(\text{NMD}, 10), \text{LOG}(\text{GSD}, 10), \text{TRUE}) \quad \text{equation 21}$$

5. In the next column, calculate the number fractions of each particle size bin (NF_{bin}) by subtracting the theoretical cumulative fraction of the bin smaller than the bin from the theoretical cumulative fraction of the bin.

$$NF_{bin} = TCF_{bin} - TCF_{bin-1} \quad \text{equation 22}$$

6. In the next column, calculate the number concentration of each bin by multiplying the bin number fraction by the given number concentration.

$$NC_{bin} = NF_{bin}(NMD) \quad \text{equation 23}$$

7. In the next column, for each particle size bin, incorporate the Stage A penetration by using equation 17 with d equal to the bin midpoint diameter.
8. In the next column, calculate the number concentration in each bin that penetrates Stage A by multiplying the number concentration of each bin by the bin Stage A penetration.

$$NC_{bin,Stage A} = NC_{bin}(P_{TC,Stage A,d}) \quad \text{equation 24}$$

9. In the next column, for each particle size bin, incorporate the detection efficiency of the CPC (DE_{bin}) by using equation 18 with d equal to the bin midpoint diameter.
10. In the next column, calculate the number concentration that penetrates Stage A in terms of the SMPS ($NC_{bin,Stage A,DE}$) by multiplying the number concentration that penetrates Stage A by the DE for each bin.

$$NC_{bin,Stage A,DE} = NC_{bin,Stage A}(DE_{bin}) \quad \text{equation 25}$$

11. Calculate the total number concentration that penetrates Stage A in terms of the SMPS (Inv_A) by summing the number concentrations that penetrate Stage A in terms of the SMPS over the 100 bins (particle diameters of 9.5 to 1000 nm).
12. In the next column, incorporate the theoretical penetration using equation 26 (Cheng & Yeh, 1984) through five screens ($P_{5,d}$) with d equal to the bin midpoint diameter.

$$P_d = 10^{-nm} \quad \text{equation 26}$$

where n equaled the number of screens and m equaled:

$$m_d = A_0Pe^{-2/3} + A_1R^2 + A_2Pe^{-1/2}R^{2/3} \quad \text{equation 27}$$

where Pe equaled the peclet number and R equaled the interception parameter and A_0 equaled:

$$A_0 = 1.17B \quad \text{equation 28}$$

A_1 equaled:

$$A_1 = 0.434B/k \quad \text{equation 29}$$

A_2 equaled:

$$A_2 = 0.539B/(k^{1/2}) \quad \text{equation 30}$$

where k equaled:

$$k = -0.5\ln(2\alpha/\pi) + (2\alpha/\pi) - 0.75 - ((2\alpha/\pi)^2)/4 \quad \text{equation 31}$$

where α equaled the solid volume fraction of the screen and B equaled:

$$B = 4ah/\pi(1-\alpha)D_f \quad \text{equation 32}$$

where h equaled the screen thickness and D_f equaled the diffusion coefficient.

13. In the next column, calculate the number concentration in each bin that penetrates Stage B in terms of the SMPS by multiplying the number concentration that penetrated Stage A in terms of SMPS by the $P_{5,d}$.

$$NC_{\text{bin,Stage B,DE}} = NC_{\text{bin,Stage A}} DE_{\text{bin}} P_{5,d} \quad \text{equation 33}$$

14. Calculate the total number concentration that penetrates Stage B in terms of the SMPS (Inv_B) by summing the number concentrations that penetrate Stage B in terms of the SMPS over the 100 bins (particle diameters of 9.5 to 1000 nm).
15. In the next column, incorporate the theoretical penetration through 11 screens ($P_{11,d}$) (equation 26) for each bin, with d equal to the bin midpoint diameter.
16. In the next column, calculate the number concentration in each bin that penetrates Stage C in terms of the SMPS by multiplying the number concentration that penetrates Stage A in terms of SMPS by the $P_{11,d}$.
- $$NC_{\text{bin,Stage C,DE}} = NC_{\text{bin,Stage A}} DE_{\text{bin}} P_{11,d} \quad \text{equation 34}$$
17. Calculate the total number concentration that penetrates Stage C in terms of the SMPS (Inv_C) by summing the number concentrations that penetrate Stage C in terms of the SMPS over the 100 bins (particle diameters of 9.5 to 1000 nm).

18. In the next column, incorporate the theoretical penetration through 16 screens ($P_{16,d}$) (equation 26) for each bin, with d equal to the bin midpoint diameter.
19. In the next column, calculate the number concentration in each bin that penetrates Stage D in terms of the SMPS by multiplying the number concentration that penetrates Stage A in terms of SMPS by the $P_{16,d}$.

$$NC_{\text{bin,Stage D,DE}} = NC_{\text{bin,Stage A}} DE_{\text{bin}} P_{16,d} \quad \text{equation 35}$$

20. Calculate the total number concentration that penetrates Stage D in terms of the SMPS (Inv_D) by summing the number concentrations that penetrate Stage D in terms of the SMPS over the 100 bins (particle diameters of 9.5 to 1000 nm).
21. Equation 15 was programmed into the spreadsheet. A screenshot of the top of the spreadsheet is shown in Figure B1. A screenshot of the bottom of the spreadsheet is shown in Figure B2.
22. Input the inversion starting values of $NMD = 500$, $GSD = 2$, and number concentration = N_A .
23. Select “Solver” under the Data tab. In the “Solver” window select the NMD, GSD, and number concentration cells as the cells to change, select the equation 3 cell as the target cell, input the constraints, and select value of 0. A screenshot of the “Solver” window is shown in Figure B3.
24. In the “Solver” window select Solve. A Solver Results window will be displayed with the statement “Solver could not find a feasible solution.” Hit OK and look at the NMD, GSD, and number concentration results. Run “Solver” again until the results for NMD, GSD, and number concentration do not change. Once the results do not change, that is the inversion’s final estimate for the NMD, GSD, and number concentration.
25. Look at the final results for NMD, GSD, and number concentration. If any of the results solved to a constraint note that with the results.

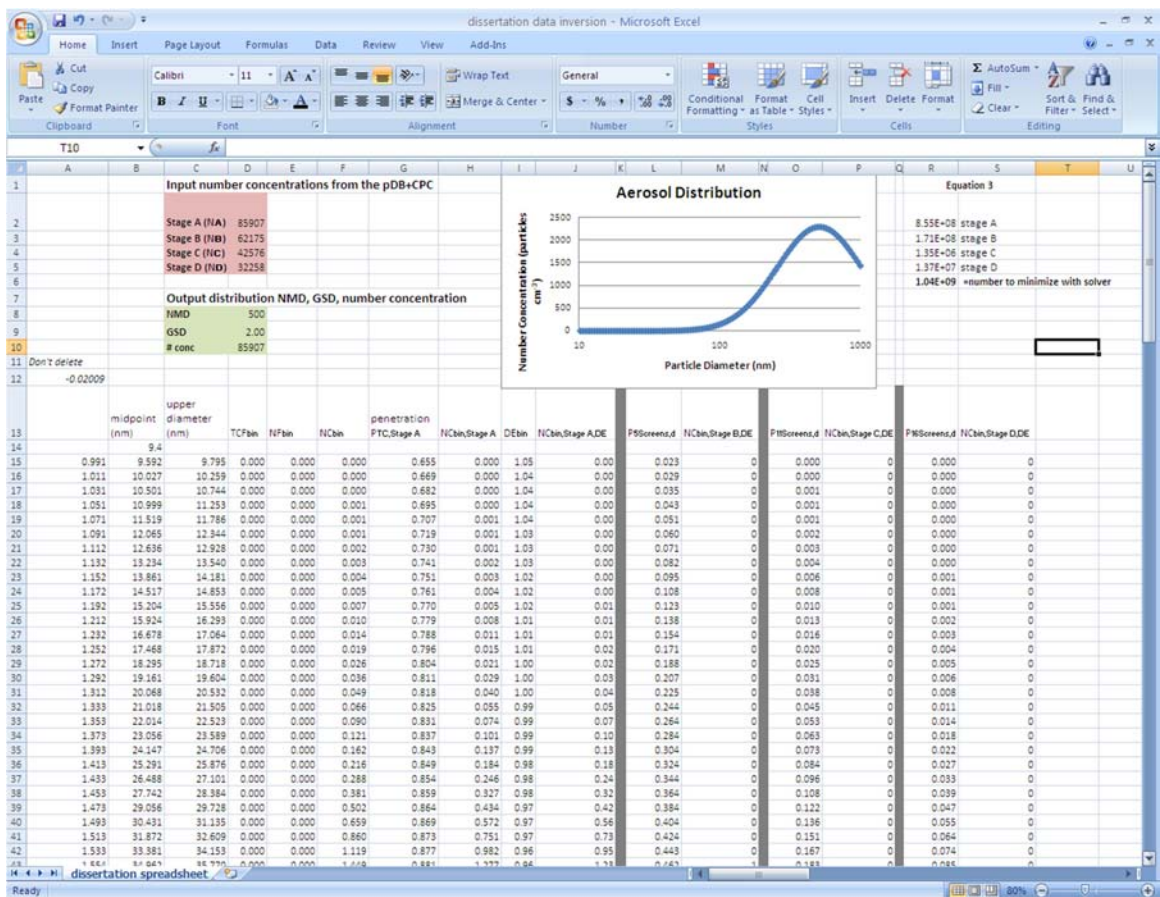


Figure B1: Screenshot of the top of the spreadsheet.

The screenshot displays the bottom portion of an Excel spreadsheet titled "dissertation data inversion - Microsoft Excel". The visible rows range from 70 to 117. Each row contains numerical data across columns A to U. The status bar at the bottom indicates the spreadsheet is ready and zoomed to 80%.

Row	A	B	C	D	E	F	G	H	I	J	K	L	M	N	O	P	Q	R	S	T	U
70	2.096	121.905	124.724	0.793	0.031	3160.787	0.943	2979.147	0.89	2638.88	0.800	2112	0.613	1616	0.490	1294					
71	2.116	127.677	130.629	0.821	0.028	2903.746	0.944	2740.099	0.88	2419.74	0.807	1952	0.623	1508	0.503	1217					
72	2.136	133.721	136.814	0.847	0.026	2638.969	0.945	2493.040	0.88	2194.85	0.813	1784	0.634	1391	0.515	1131					
73	2.156	140.053	143.291	0.870	0.023	2372.588	0.946	2243.789	0.88	1969.39	0.818	1612	0.644	1268	0.527	1037					
74	2.176	146.683	150.076	0.891	0.021	2110.195	0.947	1997.678	0.88	1748.03	0.824	1440	0.653	1142	0.538	941					
75	2.196	153.628	157.181	0.909	0.018	1856.671	0.948	1759.385	0.87	1534.82	0.829	1272	0.662	1016	0.549	842					
76	2.216	160.902	164.623	0.925	0.016	1616.069	0.948	1532.813	0.87	1333.09	0.834	1112	0.671	894	0.559	746					
77	2.237	168.520	172.427	0.939	0.014	1391.544	0.949	1321.025	0.87	1145.40	0.839	960	0.679	777	0.569	652					
78	2.257	176.499	180.580	0.950	0.012	1185.349	0.950	1126.231	0.86	973.53	0.843	821	0.686	668	0.579	563					
79	2.277	184.855	189.120	0.960	0.010	998.668	0.951	949.815	0.86	818.53	0.847	693	0.694	568	0.588	481					
80	2.297	193.607	198.084	0.968	0.008	832.687	0.952	792.405	0.86	680.79	0.851	579	0.701	477	0.596	406					
81	2.317	202.773	207.463	0.975	0.007	686.702	0.952	653.962	0.86	560.14	0.854	479	0.707	396	0.604	338					
82	2.337	212.374	217.285	0.980	0.005	560.231	0.953	533.894	0.85	455.90	0.858	391	0.713	325	0.612	279					
83	2.357	222.429	227.573	0.985	0.004	452.145	0.954	431.177	0.85	367.07	0.861	316	0.719	264	0.619	227					
84	2.377	232.960	238.347	0.988	0.004	360.995	0.954	344.473	0.85	292.36	0.864	253	0.724	212	0.626	183					
85	2.397	243.990	249.632	0.991	0.003	285.126	0.955	272.242	0.85	230.35	0.866	200	0.729	168	0.632	146					
86	2.417	255.541	261.451	0.993	0.002	222.784	0.955	212.841	0.84	179.54	0.869	156	0.734	132	0.638	114					
87	2.437	267.640	273.829	0.995	0.002	172.204	0.956	164.610	0.84	138.43	0.871	121	0.738	102	0.643	89					
88	2.458	280.312	286.794	0.996	0.001	131.679	0.956	125.938	0.84	105.59	0.873	92	0.742	78	0.648	68					
89	2.478	293.583	300.372	0.997	0.001	99.609	0.957	95.315	0.84	79.67	0.875	70	0.746	59	0.652	52					
90	2.498	307.483	314.594	0.998	0.001	74.541	0.957	71.362	0.83	59.47	0.877	52	0.749	43	0.657	39					
91	2.518	322.041	329.488	0.999	0.001	55.183	0.958	52.854	0.83	43.91	0.878	39	0.752	33	0.660	29					
92	2.538	337.288	345.088	0.999	0.000	40.414	0.958	38.725	0.83	32.07	0.880	28	0.754	24	0.663	21					
93	2.558	353.257	361.427	0.999	0.000	29.279	0.959	28.067	0.83	23.18	0.881	20	0.756	18	0.666	15					
94	2.578	369.982	378.538	1.000	0.000	20.985	0.959	20.124	0.82	16.57	0.882	15	0.758	13	0.668	11					
95	2.598	387.500	396.461	1.000	0.000	14.879	0.959	14.274	0.82	11.71	0.882	10	0.759	9	0.670	8					
96	2.618	405.846	415.231	1.000	0.000	10.436	0.960	10.016	0.82	8.19	0.883	7	0.760	6	0.671	6					
97	2.638	425.061	434.891	1.000	0.000	7.241	0.960	6.952	0.82	5.67	0.883	5	0.761	4	0.672	4					
98	2.658	445.186	455.481	1.000	0.000	4.971	0.960	4.774	0.81	3.88	0.883	3	0.761	3	0.672	3					
99	2.679	466.263	477.046	1.000	0.000	3.375	0.961	3.243	0.81	2.63	0.883	2	0.761	2	0.672	2					
100	2.699	488.339	499.632	1.000	0.000	2.267	0.961	2.179	0.81	1.76	0.883	2	0.760	1	0.671	1					
101	2.719	511.459	523.287	1.000	0.000	1.507	0.961	1.448	0.81	1.17	0.882	1	0.759	1	0.670	1					
102	2.739	535.675	548.062	1.000	0.000	0.991	0.961	0.952	0.80	0.77	0.882	1	0.758	1	0.668	1					
103	2.759	561.037	574.011	1.000	0.000	0.644	0.962	0.620	0.80	0.50	0.881	0	0.756	0	0.666	0					
104	2.779	587.599	601.188	1.000	0.000	0.415	0.962	0.399	0.80	0.32	0.879	0	0.753	0	0.662	0					
105	2.799	615.419	629.651	1.000	0.000	0.264	0.962	0.254	0.80	0.20	0.878	0	0.750	0	0.659	0					
106	2.819	644.557	659.462	1.000	0.000	0.166	0.962	0.160	0.79	0.13	0.876	0	0.747	0	0.654	0					
107	2.839	675.074	690.685	1.000	0.000	0.103	0.963	0.100	0.79	0.08	0.874	0	0.743	0	0.649	0					
108	2.859	707.035	723.386	1.000	0.000	0.064	0.963	0.061	0.79	0.05	0.871	0	0.738	0	0.643	0					
109	2.879	740.510	757.635	1.000	0.000	0.039	0.963	0.037	0.79	0.03	0.868	0	0.733	0	0.636	0					
110	2.900	775.570	793.506	1.000	0.000	0.023	0.963	0.023	0.78	0.02	0.865	0	0.727	0	0.629	0					
111	2.920	812.280	831.075	1.000	0.000	0.014	0.963	0.013	0.78	0.01	0.861	0	0.720	0	0.620	0					
112	2.940	850.748	870.422	1.000	0.000	0.008	0.964	0.008	0.78	0.01	0.857	0	0.712	0	0.611	0					
113	2.960	891.028	911.693	1.000	0.000	0.005	0.964	0.005	0.78	0.00	0.853	0	0.704	0	0.600	0					
114	2.980	933.214	954.795	1.000	0.000	0.003	0.964	0.003	0.77	0.00	0.848	0	0.695	0	0.589	0					
115	3.000	977.397	1000.000	1.000	0.000	0.002	0.964	0.002	0.77	0.00	0.842	0	0.685	0	0.577	0					
116																					
117																					

Figure B2: Screenshot of the bottom of the spreadsheet.

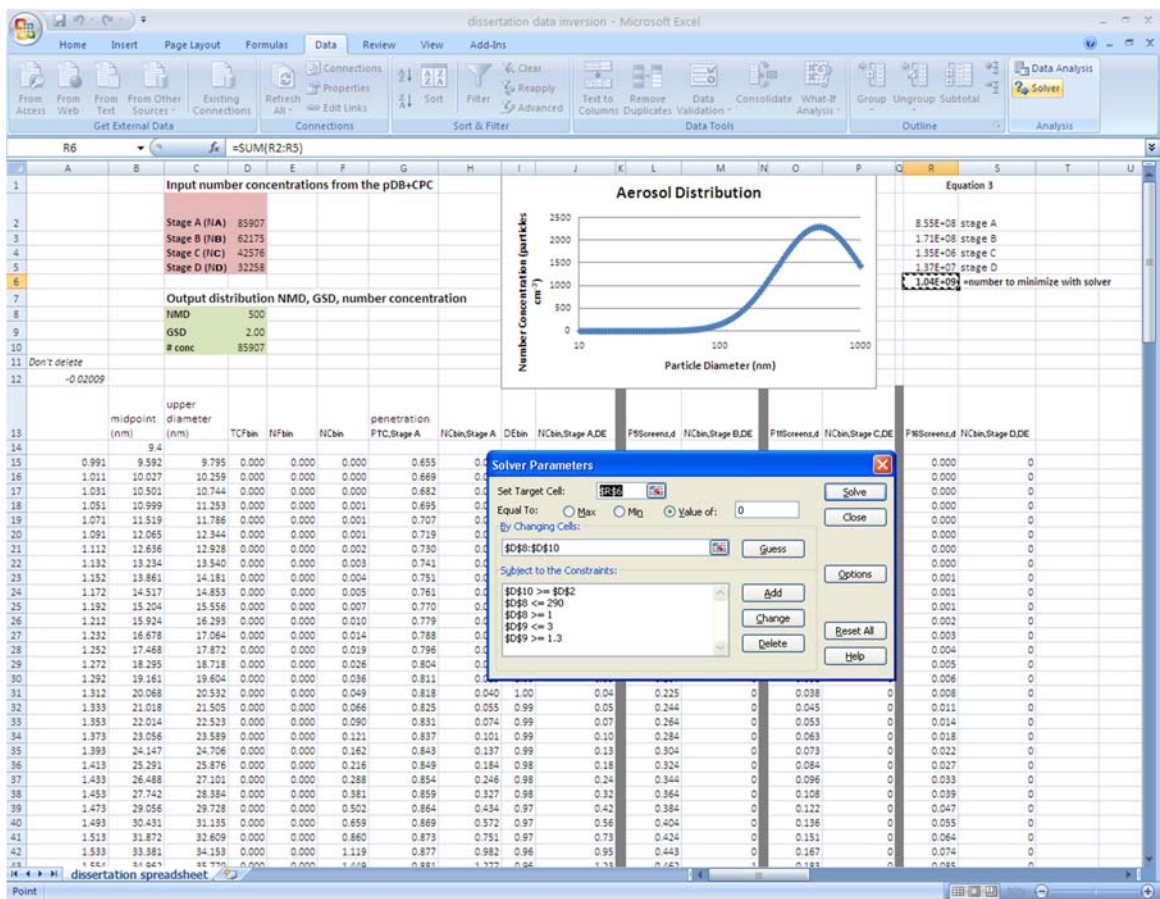


Figure B3: Screenshot of the “Solver” window.

APPENDIX C: INPUT INTO THE INVERSION SPREADSHEET

The input into the inversion spreadsheet was average number concentration measured by the CPC for each stage of the pDB. The output of the inversion was the distribution NMD, GSD, and number concentration. Table C1 has the input for the six propylene torch runs (three 240-second measurements and three 80-second measurements) and the six incense runs (three 240-second measurements and three 80-second measurements).

Table C1: Input number concentrations and inversion spreadsheet output.

Aerosol	Timing (sec)	pDB+CPC Stage Number Concentrations				pDB+CPC with Inversion		
		Stage A (particle cm ⁻³)	Stage B (particle cm ⁻³)	Stage C (particle cm ⁻³)	Stage D (particle cm ⁻³)	NMD (nm)	GSD	Number Concentration (particle cm ⁻³)
Propylene Torch	240	25,188	4,156	896	286	13	1.67	45,503
Propylene Torch	240	20,555	3,376	655	204	14	1.52	31,499
Propylene Torch	240	17,913	2,765	575	178	11	1.71	37,025
Incense	240	50,665	44,780	36,078	25,869	156	1.3*	63,046
Incense	240	85,907	62,175	42,576	32,258	87	1.56	102,141
Incense	240	86,797	72,406	54,759	42,902	131	1.3*	105,569
Propylene Torch	80	27,819	5,458	1,059	354	18	1.36	38,101
Propylene Torch	80	30,004	6,370	1,276	430	19	1.32	37,618
Propylene Torch	80	29,893	6,042	1,205	405	18	1.36	35,645
Incense	80	37,014	30,633	14,293	10,890	69	1.3*	45,587
Incense	80	64,476	47,949	33,691	25,946	94	1.52	76,803
Incense	80	54,236	42,215	34,443	23,120	113	1.3*	65,103

* Represents inversion results that solved to a constraint.

REFERENCES

- ACGIH. (2007). *2007 TLVs and BEIs Based on the Documentation of the Threshold Limit Values for Chemical Substances and Physical Agents and Biological Exposure Indices*. Cincinnati, OH: American Conference of Governmental Industrial Hygienists.
- ASTM Standard E2456 (2006) Standard Terminology Relating to Nanotechnology. ASTM International, West Conshohocken, PA: www.astm.org
- Alessandrini, F., Beck-Speier, I., Krappmann, D., Weichenmeier, I., Takenaka, S., Karg, E., et al. (2009). Role of oxidative stress in ultrafine particle-induced exacerbation of allergic lung inflammation. *American Journal of Respiratory and Critical Care Medicine*, *179*, 984-991.
- Al-Khabbaz, Y. S., Shimada, T., & Hasegawa, M. (2008). The effect of backpack heaviness on trunk-lower extremity muscle activities and trunk posture. *Gait & Posture*, *28*, 297-302.
- Alonso, M., Alguacil, F. J., Santos, J. P., Jidenko, N., & Borra, J. P. (2007). Deposition of ultrafine aerosol particles on wire screens by simultaneous diffusion and image force. *Journal of Aerosol Science*, *38*, 1230-1239.
- Asbach, C., Fissan, H., Stahlmecke, B., Kuhlbusch, T. A., & Pui, D. Y. (2009). Conceptual limitations and extensions of lung-deposited nanoparticle surface area monitor (NSAM). *Journal of Nanoparticle Research*, *11*, 101-109.
- Baron, P. A., & Willeke, K. (Eds.). (2001). *Aerosol measurement: Principles, techniques and applications* (2nd ed.). New York: John Wiley and Sons, Inc..
- Bastian, S., Busch, W., Kühnel, D., Springer, A., Meibner, T., Holke, R., et al. (2009). Toxicity of tungsten carbide and cobalt-doped tungsten carbide nanoparticles in mammalian cells in vitro. *Environmental Health Perspectives*, *117*, 530-536.
- Bekyarova, E., Thostenson, E. T., Yu, A., Kim, H., Gao, J., Tang, J., et al. (2007). Multiscale carbon nanotube-carbon fiber reinforcement for advanced epoxy composites. *Langmuir*, *23*, 3970-3974.
- Boffetta, P., Dosemeci, M., Gridley, G., Bath, H., Moradi, T., & Silverman, D. (2001). Occupational exposure to diesel engine emissions and risk of cancer in Swedish men and women. *Cancer Causes and Control*, *12*, 365-374.
- Braydich-Stolle, L. K., Schaeublin, N. M., Murdock, R. C., Jiang, J., Biswas, P., Schlager, J. J., et al. (2009). Crystal structure mediates mode of cell death in TiO₂ nanotoxicity. *Journal of Nanoparticle Research*, *11*, 1361-1374.
- Brubaker, R. E. (1977). Pulmonary problems associated with the use of polytetrafluoroethylene. *Journal of Occupational Medicine*, *19*, 693-695.
- Cheng, Y. S., Keating, J. A., & Kanapilly, G. M. (1980). Theory and calibration of a screen-type diffusion battery. *Journal of Aerosol Science*, *11*, 549-556.

- Cheng, Y. S., & Yeh, H. C. (1980). Theory of a screen-type diffusion battery. *Journal of Aerosol Science*, *11*, 313-320.
- Cheng, Y. S., & Yeh, H. C. (1984). Analysis of screen diffusion battery data. *American Industrial Hygiene Association Journal*, *45*, 556-561.
- Cheng, Y. S., Yeh, H. C., & Brinsko, K. J. (1985). Use of wire screens as a fan model filter. *Aerosol Science and Technology*, *4*, 165-174.
- Daigle, C. C., Chalupa, D. C., Gibb, F. R., Morrow, P. E., Oberdörster, G., Utell, M. J., et al. (2003). Ultrafine particle deposition in humans during rest and exercise. *Inhalation Toxicology*, *15*, 539-552.
- DiNardi, S. R. (Ed.). (2003). *The occupational environment: Its evaluation, control and management*. Fairfax, VA: AIHA Press.
- EcoChem Analytics. (2005). *User's guide photoelectric aerosol sensor (PAS 2000CE) diffusion charger (DC 2000CE)* (4th ed.). [Brochure]. League City, TX: EcoChem Analytics.
- Elihn, K., & Berg, P. (2009). Ultrafine particle characteristics in seven industrial plants. *Annals of Occupational Hygiene*, *53*, 475-484.
- Evans, E. A. (1973). Pulmonary edema after inhalation of fumes from polytetrafluoroethylene (PTFE). *Journal of Occupational Medicine*, *15*, 599-601.
- Evans, D. E., Heitbrink, W. A., Slavin, T. J., & Peters, T. M. (2007). Ultrafine and respirable particles in an automotive grey iron foundry. *Annals of Occupational Hygiene*, *52*, 9-21.
- Evans, D. E., Ku, B. K., Birch, M. E., & Dunn, K. H. (2010). Aerosol monitoring during carbon nanofiber production: Mobile direct-reading sampling. *Annals of Occupational Hygiene*, *54*, 514-531.
- Figler, B., Sahle, W., Krantz, S., & Ulfvarson, U. (1996). Diesel exhaust quantification by scanning electron microscope with special emphasis on particulate size distribution. *Science of the Total Environment*, *193*, 77-83.
- Fissan, H., Neumann, S., Trampe, A., Pui, D. Y., & Shin, W. G. (2007). Rationale and principle of an instrument measuring lung deposited nanoparticle surface area. *Journal of Nanoparticle Research*, *9*, 53-59.
- Fitzmaurice, G. M., Laird, N. M., & Ware, J. H. (2004). *Applied Longitudinal Analysis*. Hoboken, NJ: John Wiley & Sons, Inc..
- Fujita, K., Morimoto, Y., Ogami, A., Myojyo, T., Tanaka, I., Shimada, M., et al. (2009). Gene expression profiles in rat lung after inhalation exposure to C60 fullerene particles. *Toxicology*, *258*, 47-55.
- Fujitani, Y., Kobayashi, T., Arashidani, K., Kunugita, N., & Suemura, K. (2008). Measurement of the physical properties of aerosols in a fullerene factory for inhalation exposure assessment. *Journal of Occupational and Environmental Hygiene*, *5*, 380-389.

- Goh, J. H., Thambyah, A., & Bose, K. (1998). Effects of varying backpack loads on peak forces in the lumbosacral spine during walking. *Clinical Biomechanics*, *13*, 26-31.
- Goodfellow, H. D., & Bender, M. (1980). Design considerations for fume hoods for process plants. *American Industrial Hygiene Association Journal*, *41*, 473-484.
- Gorbunov, B., Priest, N. D., Muir, R. B., Jackson, P. R., & Gnewuch, H. (2009). A novel size-selective airborne particle size fractionating instrument for health risk evaluation. *Annals of Occupational Hygiene*, *53*, 225-237.
- Hämeri, K., Koponen, I. K., Aalto, P. P., & Kulmala, M. (2002). The particle detection efficiency of the TSI-3007 condensation particle counter. *Journal of Aerosol Science*, *33*, 1463-1469.
- Harris, D. K. (1951). Polymer-fume fever. *Lancet*, *2*, 1008-1011.
- Heitbrink, W. A., Evans, D. E., Ku, B. K., Maynard, A. D., Slavin, T. J., & Peters, T. M. (2009). Relationships among particle number, surface area, and respirable mass concentrations in automotive engine manufacturing. *Journal of Occupational and Environmental Hygiene*, *6*, 19-31.
- Hinds, W. C. (1999). *Aerosol technology* (2nd ed.). New York: John Wiley & Sons, Inc..
- Holmes, D. A. (2000). Waterproof breathable fabrics. In A. R. Horrocks & S. C. Anand (Eds.), *Handbook of technical textiles* (pp. 282-315). Boca Raton, FL: CRC Press LLC.
- Hong, Y., & Cheung, C. K. (2003). Gait and posture responses to backpack load during level walking in children. *Gait & Posture*, *17*, 28-33.
- ICRP. (1994). *Human respiratory tract model for radiological protection* (Publication 66). Oxford: International Commission on Radiological Protection.
- Imhof, D., Weingartner, E., Vogt, U., Dreiseidler, A., Rosenbohm, E., Scheer, V., et al. (2005). Vertical distribution of aerosol particles and NO_x close to a motorway. *Atmospheric Environment*, *39*, 5710-5721.
- Intra, P., & Tippayawong, N. (2009). Progress in unipolar corona discharger designs for airborne particle charging: A literature review. *Journal of Electrostatics*, *67*, 605-615.
- Jenkins, N., Pierce, W., & Eagar, T. (2005). Particle size distribution of gas metal and flux cored arc welding fumes. *Welding Journal*, *84*, 156-163.
- Jeong, W. Y., & An, S. K. (2004). Mechanical properties of breathable waterproof fabrics with seaming and sealing processes. *Fibers and Polymers*, *5*, 316-320.
- Johnston, C. J., Finkelstein, J. N., Mercer, P., Corson, N., Gelein, R., & Oberdörster, G. (2000). Pulmonary effects induced by ultrafine PTFE particles. *Toxicology and Applied Pharmacology*, *168*, 208-215.
- Jung, H., & Kittelson, D. B. (2005). Characterization of aerosol surface instruments in transition regime. *Aerosol Science and Technology*, *39*, 902-911.

- Karlsson, H. L., Gustafsson, J., Cronholm, P., & Möller, L. (2009). Size-dependent toxicity of metal oxide particles—A comparison between nano- and micrometer size. *Toxicology Letters*, *188*, 112-118.
- Keller, A., Fierz, M., Siegmann, K., Siegmann, H. C., & Filippov, A. (2001). Surface science with nanosized particles in a carrier gas. *Journal of Vacuum Science & Technology*, *19*, 1-8.
- Kim, C. S., & Jaques, P. A. (2005). Total lung deposition of ultrafine particles in elderly subjects during controlled breathing. *Inhalation Toxicology*, *17*, 387-399.
- Kim, Y. S., Kim, J. S., Cho, H. S., Rha, D. S., Kim, J. M., Park, J. D., et al. (2008). Twenty-eight-day oral toxicity, genotoxicity, and gender-related tissue distribution of silver nanoparticles in sprague-dawley rats. *Inhalation Toxicology*, *20*, 575-583.
- Kittelson, D. B., Watts, W. F., Savstrom, J. C., & Johnson, J. P. (2005). Influence of a catalytic stripper on the response of real-time aerosol instruments to diesel exhaust aerosol. *Journal of Aerosol Science*, *36*, 1089-1107.
- Korczynski, R. E. (2000). Occupational health concerns in the welding industry. *Applied Occupational and Environmental Hygiene*, *15*, 936-945.
- Ku, B. K. (2010). Determination of the ratio of diffusion charging-based surface area to geometric surface area for spherical particles in the size range of 100–900nm. *Journal of Aerosol Science*, *41*, 835-847.
- Ku, B. K., & Maynard, A. D. (2005). Comparing aerosol surface-area measurements of monodisperse ultrafine silver agglomerates by mobility analysis, transmission electron microscopy and diffusion charging. *Journal of Aerosol Science*, *36*, 1108-1124.
- Lai, J. K., Lai, M. B., Jandhyam, S., Dukhande, V. V., Bhushan, A., Daniels, C. K., et al. (2008). Exposure to titanium dioxide and other metallic oxide nanoparticles induces cytotoxicity on human neural cells and fibroblasts. *International Journal of Nanomedicine*, *3*, 533-45.
- LeVan, T. D., Koh, W. P., Lee, H. P., Koh, D., Yu, M. C., & London, S. J. (2006). Vapor, dust, and smoke exposure in relation to adult-onset asthma and chronic respiratory symptoms the Singapore Chinese Health Study. *American Journal of Epidemiology*, *163*, 1118-1128.
- Lewis, C. E., & Kerby, G. R. (1965). An epidemic of polymer-fume fever. *The Journal of the American Medical Association*, *191*, 375-378.
- Li, S. Q., Zhu, R. R., Zhu, H., Xue, M., Sun, X. Y., Yao, S. D., et al. (2008). Nanotoxicity of TiO₂ nanoparticles to erythrocyte in vitro. *Food and Chemical Toxicology*, *46*, 3626-3631.
- Matson, U., Ekberg, L. E., & Afshari, A. (2004). Measurement of ultrafine particles: A comparison of two handheld condensation particle counters. *Aerosol Science and Technology*, *38*, 487-495.

- Maynard, A. D., Baron, P. A., Foley, M., Shvedova, A. A., Kisin, E. R., & Castranova, V. (2004). Exposure to carbon nanotube material: Aerosol release during the handling of unrefined single-walled carbon nanotube material. *Journal of Toxicology and Environmental Health*, *67*, 87-107.
- Maynard, A. D., & Maynard, R. L. (2002). A derived association between ambient aerosol surface area and excess mortality using historic time series data. *Atmospheric Environment*, *36*, 5561-5567.
- McDermott, H. J. (2001). *Handbook of ventilation for contaminant control* (3rd ed.). Cincinnati: American Conference of Governmental Industrial Hygienists.
- Methner, M. M., Birch, M. E., Evans, D. E., Ku, B. K., Crouch, K., & Hoover, M. D. (2007). Case study: Identification and characterization of potential sources of worker exposure to carbon nanofibers during polymer composite laboratory operations. *Journal of Occupational and Environmental Hygiene*, *4*, 125-130.
- Methner, M. M., Hodson, L., & Geraci, C. (2010). Nanoparticle emission assessment technique (NEAT) for the identification and measurement of potential inhalation exposure to engineered Nanomaterials—Part A. *Journal of Occupational and Environmental Hygiene*, *7*, 127-132.
- Mohr, M., Lehmann, U., & Rutter, J. (2005). Comparison of mass-based and non-mass-based particle measurement systems for ultra-low emissions from automotive sources. *Environmental Science & Technology*, *39*, 2229-2238.
- Moshhammer, H., & Neuberger, M. (2003). The active surface of suspended particles as a predictor of lung function and pulmonary symptoms in Austrian school children. *Atmospheric Environment*, *37*, 1737-1744.
- Mukhopadhyay, A., & Midha, V. K. (2008). A review on designing the waterproof breathable fabrics part II: Construction and suitability of breathable fabrics for different uses. *Journal of Industrial Textiles*, *38*, 17-41.
- National Institute of Occupational Safety and Health. (2003). *NIOSH manual of analytical methods* (NIOSH Publication No. 2003-154). Washington, DC: U.S. Government Printing Office.
- Neumeyer-Gromen, A., Razum, O., Kersten, N., Seidler, A., & Zeeb, H. (2009). Diesel motor emissions and lung cancer mortality—results of the second follow-up of a cohort study in potash miners. *International Journal of Cancer*, *124*, 1900-1906.
- Ntziachristos, L. (2007). Application of a diffusion charger for the measurement of particle surface concentration in different environments. *Aerosol Science and Technology*, *41*, 571-580.
- Nygaard, U. C., Hansen, J. S., Samuelsen, M., Alberg, T., Marioara, C. D., & Lovik, M. (2009). Single-walled and multi-walled carbon nanotubes promote allergic immune responses in mice. *Toxicological Sciences*, *109*, 113.
- Oberdorster, G., Celein, R. M., Ferin, J., & Weiss, B. (1995). Association of particulate air pollution and acute mortality: Involvement of ultrafine particles? *Inhalation Toxicology*, *7*, 111-124.

- Oberdoerster, G., Oberdoerster, E. & Oberdoerster, J. (2005). Nanotoxicity: An emerging discipline evolving from studies of ultrafine particles. *Environmental Health Perspectives*, 7, 823-839.
- O'Shaughnessy, P. T., & Raabe, O. G. (2003). A comparison of cascade impactor data reduction methods. *Aerosol Science and Technology*, 37, 187-200.
- Peters, T. M., Elzey, S., Johnson, R., Park, H., Grassian, V. H., Maher, T., et al. (2009). Airborne monitoring to distinguish engineered nanomaterials from incidental particles for environmental health and safety. *Journal of Occupational and Environmental Hygiene*, 6, 73-81.
- Peters, T. M., Heitbrink, W. A., Evans, D. E., Slavin, T. J., & Maynard, A. D. (2006). The mapping of fine and ultrafine particle concentrations in an engine machining and assembly facility. *Annals of Occupational Hygiene*, 50, 249-257.
- Phillips, J. I., Green, F. Y., Davies, J. C., & Murray, J. (2010). Pulmonary and systemic toxicity following exposure to nickel nanoparticles. *American Journal of Industrial Medicine*, 53, 763-767.
- Pinkerton, L. E., Hein, M. J., & Stayner, L. T. (2004). Mortality among a cohort of garment workers exposed to formaldehyde: An update. *British Medical Journal*, 61(3), 193-200.
- Pui, D. Y. (1976). *Experimental study of diffusion charging of aerosols* (No. COO-1248-49). Minneapolis, MN: University of Minnesota Particle Technology Lab.
- Pui, D. Y., Qi, C., Stanley, N., Oberdörster, G., & Maynard, A. (2008). Recirculating air filtration significantly reduces exposure to airborne nanoparticles. *Environmental Health Perspectives*, 116, 863-866.
- Racette, B. A., McGee-Minnich, L., Moerlein, S. M., Mink, J. W., Videen, T. O., & Perlmutter, J. S. (2001). Welding-related Parkinsonism: Clinical features, treatment, and pathophysiology. *Neurology*, 56, 8-13.
- Ramachandran, G., Paulsen, D., Watts, W., & Kittelson, D. (2005). Mass, surface area and number metrics in diesel occupational exposure assessment. *Journal of Environmental Monitoring*, 7, 728-735.
- Samuelsen, M., Nygaard, U. C., & Lovik, M. (2009). Particle size determines activation of the innate immune system in the lung. *Scandinavian Journal of Immunology*, 69, 421-428.
- Shimizu, M., Tainaka, H., Oba, T., Mizuo, K., Umezawa, M., & Takeda, K. (2009). Maternal exposure to nanoparticulate titanium dioxide during the prenatal period alters gene expression related to brain development in the mouse. *Particle and Fibre Toxicology*, 6, 20-28.
- Sinclair, D., & Hoopes, G. S. (1975). A novel form of diffusion battery. *American Industrial Hygiene Association Journal*, 36, 39-42.
- Song, Y., Li, X., & Du, X. (2009). Exposure to nanoparticles is related to pleural effusion, pulmonary fibrosis and granuloma. *European Respiratory Journal*, 34, 559-567.

- Stephenson, D., Seshadri, G., & Veranth, J. M. (2003). Workplace exposure to submicron particle mass and number concentrations from manual arc welding of carbon steel. *AIHA Journal*, *64*, 516-521.
- Teli, K., Mutalik, S., & Rajanikant, G. K. (2010). Nanotechnology and nanomedicine: Going small means aiming big. *Current Pharmaceutical Design*, *16*, 1882-1892.
- Tsai, P., Guo, Y., Chen, J., & Shieh, H. (2000). An integrated approach to initiative preventive strategies for workers exposed to teflon pyrolytic gases in a plastic industry. *Journal of Occupational Health*, *42*, 297-303.
- TSI Incorporated. (2004). *Model 3007 condensation particle counter operation and service manual* [Brochure]. Shoreview, MN: TSI Incorporated.
- Twomey, S. (1975). Comparison of constrained linear inversion and an iterative nonlinear algorithm applied to the indirect estimation of particle size distributions. *Journal of Computational Physics*, *18*, 188-200.
- Vincent, J. H., & Clement, C. F. (2000). Ultrafine particles in workplace atmospheres. *Philosophical Transactions: Mathematical, Physical and Engineering Sciences*, *358*, 2673-2682.
- Wang, B., Feng, W., Zhu, M., Wang, Y., Wang, M., Gu, Y., et al. (2009). Neurotoxicity of low-dose repeatedly intranasal instillation of nano- and submicron-sized ferric oxide particles in mice. *Journal of Nanoparticle Research*, *11*, 41-53.
- Wang, J., Chen, C., Liu, Y., Jiao, F., Li, W., Lao, F., et al. (2008). Potential neurological lesion after nasal instillation of TiO₂ nanoparticles in the anatase and rutile crystal phases. *Toxicology Letters*, *183*, 72-80.
- Weytjens, K., Labrecque, M., Malo, J. L., & Cartier, A. (1999). Asthma to latex in a seamstress. *Allergy*, *54*, 290-291.
- Yeh, H. C., Cheng, Y. S., & Orman, M. M. (1982). Evaluation of various types of wire screens as diffusion battery cells. *Journal of Colloid and Interface Science*, *86*, 12-16.
- Zhu, M. T., Feng, W. Y., Wang, Y., Wang, B., Wang, M., Ouyang, H., et al. (2009). Particokinetics and extrapulmonary translocation of intratracheally instilled ferric oxide nanoparticles in rats and the potential health risk assessment. *Toxicological Sciences*, *107*, 342-351.